POLITECNICO DI MILANO

Department of Aerospace Science and Technology DAER

Multidisciplinary Approach of Small Air Launched Rocket Preliminary Design

Master Degree in Space Engineering

Academic year: 2019-2020

Candidate:
Daniele Pilori
ID: 898460

Supervisor:
Prof. Michèle Lavagna

October 2, 2020

Abstract

Air Launch to orbit is an interesting launch strategy nevertheless rarely used. It has advantages from the flexibility point of view and the overall efficiency, however interfaces with the carrier aircraft restrict the size of the launcher dramatically. This opens the possibility of designing a small air launched rocket designed to timely inject one nanosatellite at a time, nanosatellites whose market is expected to increase in the incoming years. This concept can broaden Europe and Italy launch capabilities to a new payload range, and can open the opportunity of launching directly from Europe, opportunity nowadays unfeasible.

Multidisciplinary approach is a kind of design method specifically thought for complex architectures where the subsystems are highly coupled among each others. This approach has been widely used in the space and launcher industry showing good results and faster design time.

Such a method is used to the preliminary design phase of a small air launched rocket thought to take service in a few years, this rocket would have the capability of launching specifically and individually one nanosatellite.

Some innovative tools are developed to enhance the design process of launchers and propose solutions for future upgrades. An novel multiconfiguration staging design is sized and used to create multiple configurations of the rocket in order to extend its market without increasing the costs. Another solution regards the usage of an innovative hybrid rocket engine configuration for improving the upper stage performances.

Finally a novel guidance control strategy is proposed for the rocket ascent trajectory, this solution is based on a Model Predictive Control strategy.

Prefazione

Il metodo dell'aviolancio è una delle strategie di lancio più interessanti e promettenti, tuttavia poco utilizzata. Possiede vantaggi dal punto di vista della flessibilità di lancio e dell'efficienza complessiva del lanciatore, tuttavia l'interfaccia con l'aereo che lo trasporta riduce considerevolmente la taglia massima. Questa strategia apre alla possibilità di progettare un piccolo lanciatore aviolanciato pensato per lanciare un nanosatellite alla volta, nanosatelliti il cui mercato è previsto espandersi nei prossimi anni. Questa idea può ampliare le capacità di lancio Europee ed Italiane ad una nuova classe di satellite, e inoltre apre alla possibilità di lanciare direttamente da territorio Europeo, possibilità ad oggi irrealizzabile.

L'approccio Multidisciplinare è un tipo di progettazione pensato specificatamente per architetture complesse i cui sottosistemi sono intrinsicamente interconnessi tra loro. Questo tipo di approccio è stato ampiamente utlizzato nell'industria aerospaziale e dei lanciatori, fornendo ottimi risultati anche dal punto di vista del tempo di progettazione.

Questo metodo è usato per una progettazione preliminare di un piccolo lanciatore aviolanciato pensato per prendere servizio in pochi anni, tale lanciatore avrà la capacità di lanciare specificatamente e individualmente un nanosatellite alla volta.

Infine, alcune soluzioni innovative sono sviluppate per migliorare la progettazione dei lanciatori e alcune idee proposte per un futuro aggiornamento del progetto. Una nuova stadiazione multiconfigurazione è stata ideata per creare una seconda configurazione del lanciatore al fine di allargare il potenziale mercato senza aumentare i costi. Un'altra soluzione riguarda l'uso di un motore ibrido per l'ultimo stadio al fine di aumentarne le prestazioni.

Infine una strategia di controllo innovativa per la traiettoria di ascesa è proposta, questa strategia è basata su un metodo di controllo adattivo (Model Predictive Control).

"Look again at that dot. That's here. That's home. That's us.
On it everyone you love, everyone you know, everyone you ever heard of, every human being who ever was, lived out their lives. The aggregate of our joy and suffering, thousands of confident religions, ideologies, and economic doctrines, every hunter and forager, every hero and coward, every creator and destroyer of civilization, every king and peasant, every young couple in love, every mother and father, hopeful child, inventor and explorer, every teacher of morals, every corrupt politician, every "superstar," every "supreme leader," every saint and sinner in the history of our species lived there–on a mote of dust suspended in a sunbeam."

Carl Sagan

To my family, my friends and everyone who brought me here

Contents

List of Figures

List of Tables

List of Symbols

α Angle of Attack

α_w Wing Angle of Attack

$\alpha_{x,y,z}$ Small Euler Angle

β TVC Angle

χ Thrust Deflection Angle

δ TVC Angle

$\dot{m}$ Mass Flow Rate

ϵ Nozzle Expansion Ratio

ϵ_s Structural Mass Ratio

η_v Ratio between propellant volume and case volume

γ Flight Path Angle

$\mathbf{A}_{B/N}$ Attitude Matrix

$\mathbf{A}_{eul}$ Eulerian Attitude Matrix

$\mathbf{A}_{lin}$ Linearized Attitude Matrix

μ Gravitational Parameter

Ω Orbit Right Ascension of the Ascending Node

$\omega_{x,y,z}$ Angular Velocity

ϕ Euler Attitude Angle

ψ Euler Attitude Angle

ρ Density

θ Euler Attitude Angle

θ_{cn} Convergent angle of the nozzle

θ_{dv} Divergent angle of the nozzle

$\underline{F}_{aero}$ Aerodynamic Forces Vector

$\underline{F}_{thrust}$ Thrust Forces Vector

ξ Structural Mass Index

a Orbit Semi-Major Axis

A_e Exit Area

A_r Aspect Ratio

A_t Throat Area

BC Ballistic Coefficient

C Equivalent exhaust Velocity

c Cross-range

C^* Characteristic Velocity

C_D Drag Coefficient

C_L Lift Coefficient

c_{mac} Mean Chord Length

D Drag Force

d Diameter

$D0$ Zero Lift Drag Force

E Energy

e Orbit Eccentricity

g Gravity accelleration

G_f Fuel Mass Flux

G_{ox} Oxidizer Mass Flux

G_{tot} Total Mass Flux

h Altitude

I Moment of Inertia

i Orbit Inclination

I_{sp} Specific Impulse

J	Cost Function
J_2	Earth Oblateness
k	Specific Heat Ratio
K_d	Derivative Coefficient
K_p	Proportional Coefficient
L	Lift Force
l	Lenght
l_N	Nose Lenght
l_{aero}	Distance between center of gravity and aerodynamic center
l_{TVC}	Distance between center of gravity and thrust application point
m	Mass
M_p	Propellant Mass
M_s	Inert Mass
M_0	Initial Mass
M_{case}	Case Mass
M_{ign}	Igniter Mass
M_{ins}	Insulator Mass
M_{misc}	Miscellaneous Mass
M_{noz}	Nozzle Mass
M_{pay}	Payload Mass
M_{tvc}	Thrust Vector Control Mass
$M_{x,y,z}$	Moment
Ma	Mach Number
N_i	Mass Ratio
$N_{x,y,z}$	Normal Force
P_a	Ambient ressure
P_c	Combustion Chamber Pressure
P_e	Exit Pressure

q	Dynamic Pressure
q_i	Quaternions
r	Radius
r_b	Regression Rate
R_E	Earth Radius
s	Downrange
S_{ref}	Reference Surface
T	Thrust
t	time
t_{mac}	Mean Chord Thickness
$Temp$	Temperature
u	Control Vector
V	Velocity
v	Volume
v_{port}	Central Port Volume
X_{AC}	Aerdoynamic Center Position
X_{cg}	Center of Gravity Position
y	Output Vector

List of Acronyms

2BP 2 Body Problem

ADN Ammonium DiNitramide

Al Aluminum

AP Ammonium Perchlorate

CEA Chemical Equilibrium with Applications

CFD Computational Fluid Dynamics

CO Cooperative Optimization

DCM Direction Cosine Matrix

DOF Degrees Of Freedom

EA Euler Angles

ESA European Space Agency

GA Genetic Algorithm

GOX Gaseous OXygen

HRE Hybrid Rocket Engine

HTPB Hydroxyl-Terminated PolyButadiene

LEO Low Earth Orbit

LOX Liquid OXygen

LQR Linear Quadratic Regulator

LRE Liquid Rocket Engine

MDO Multidisciplinary Design Optimization

MOO MultiObjective Optimization

MOPSO MultiObjective Particle Swarm Optimization

MPC Model Predictive Control

O/F Oxidizer over Fuel Ratio

ODE Ordinary Differential Equations

PD Proportional Derivative

PID Proportional Integral Derivative

QP Quadratic Programming

RAAN Right Ascension of the Ascending Node

RCS Reaction Control System

SLS Space Launch System

SSO Sun Synchronous Orbit

SRB Solid Rocket Booster

SRM Solid Rocket Motor

T/W Thrust over Weight Ratio

TRL Technology Readiness Level

TVC Thrust Vector Control

VCLS Venture Class Launch Services

VFP Vortex Flow Pancake

VSVO Variable Step Variable Order

Chapter 1

Introduction

Air Launched Rocket is a kind of launch vehicle that it is deployed by an aircraft instead of lifting off vertically from a launch pad like every other classical rockets. Maybe the most important advantage of this strategy regards the flexibility than can be achieved. Air to orbit launch vehicles do not need a launch pad, therefore they can reach orbit in a more wide variety of ways and different launch locations; this strength is given by the high maneuverability of the aircraft.

Another aspect regards the efficiency of such a launch strategy: sometimes the aircraft itself is considered to be the first stage of this kind of launcher which is more efficient than a rocket in terms of specific impulse (around an order of magnitude higher), and furthermore it is fully reusable. The rocket nozzle of the first stage also operates at low ambient pressure, increasing its efficiency.

The altitude at which the rocket is released plays an important role as well, being above 10 Km avoid the launcher flying inside the most dense layers of the atmosphere, this reduces significantly the drag losses as well as the gravity losses since the trajectory is not required to be as vertical as the one of a classical launcher.

The drawbacks are mainly represented by the presence of an aircraft, the launcher must respect the limits in terms of dimensions, weight and interfaces. Thus, the micro-launcher is the most interesting class of launch vehicle for this kind of solution. Furthermore, payload integration and propellant loading are performed before the aircraft takes off, this can introduce problems from the propellant boil off point of view.

On the other hand, small satellite's market is currently growing very fast, in particular satellites below 10 Kg, also called nanosatellites, are expected to increase more and more in the upcoming years as can be noticed in figure 1.1. Improvements in electronics and miniaturization techniques, have lead to the possibility of achieving good scientific and Earth observation results from satellites with a fraction of its original mass. In a few decades the standard satellite mass has decreased by order of magnitudes, making the nanosatellite class one of the most interesting from both the

scientific and the economic point of view.
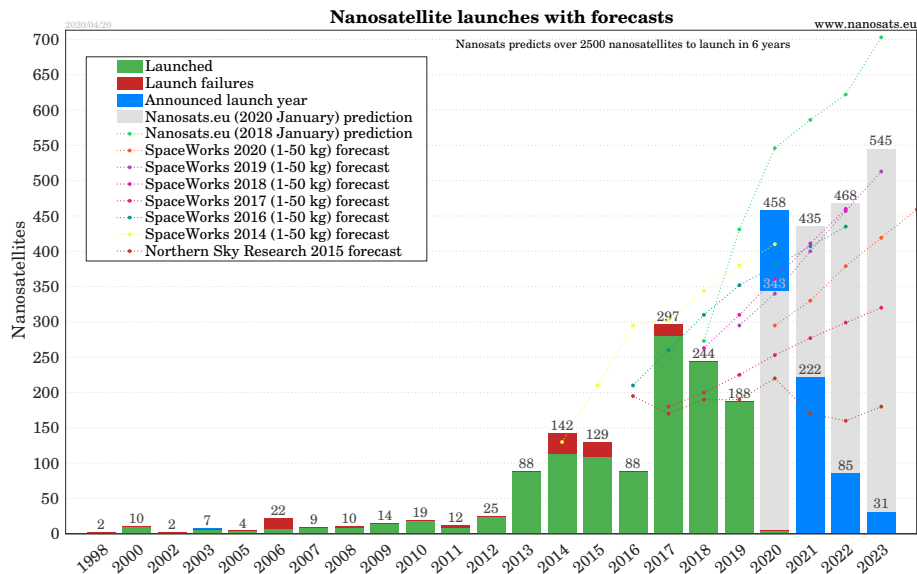
Figure 1.1: Nanosatellite Forecast [1]

Nowadays, those kind of small satellites are usually launched as secondary payloads of a primary spacecraft, thus they must share the same launch date and orbit. Currently operational small launch vehicles do not have an high launch frequency, therefore a small satellite with an highly time-dependent mission would probably be injected in a not optimal orbit for its purpose. Furthermore, as can be seen in figure 1.2, small launchers currently have the highest specific launch price among every other rockets, in particular the Pegasus-XL, which is the only air launched vehicle present in that figure, is far above the fitting curve.

Nowadays small satellites are usually launched in clusters mainly due to cost reduction, this is the case of Starlink satellites that are being launched by SpaceX, and the European SSMS (Small Spacecraft Mission Service) used by the VEGA launcher. The aim of this works goes in the opposite direction, since an air launched rocket has the advantage of a short time-to-orbit which has a key importance for particular Earth observation missions. This means that the target payload of this launcher is not part of a satellite constellation (again, like Starlink), but is a single built payload for Earth observation with an highly time dependent mission.

A small air launched rocket would surely be a Europe-first, and moreover due to its very narrow capability would be the world first launch vehicle to put into orbit specifically and individually one nanosatellite at a time. If the cost per kilogram of the rocket would be lower than the fitting curve shown in 1.2 together with a simple and reliable design, this launch solution would surely see a lot of markets.
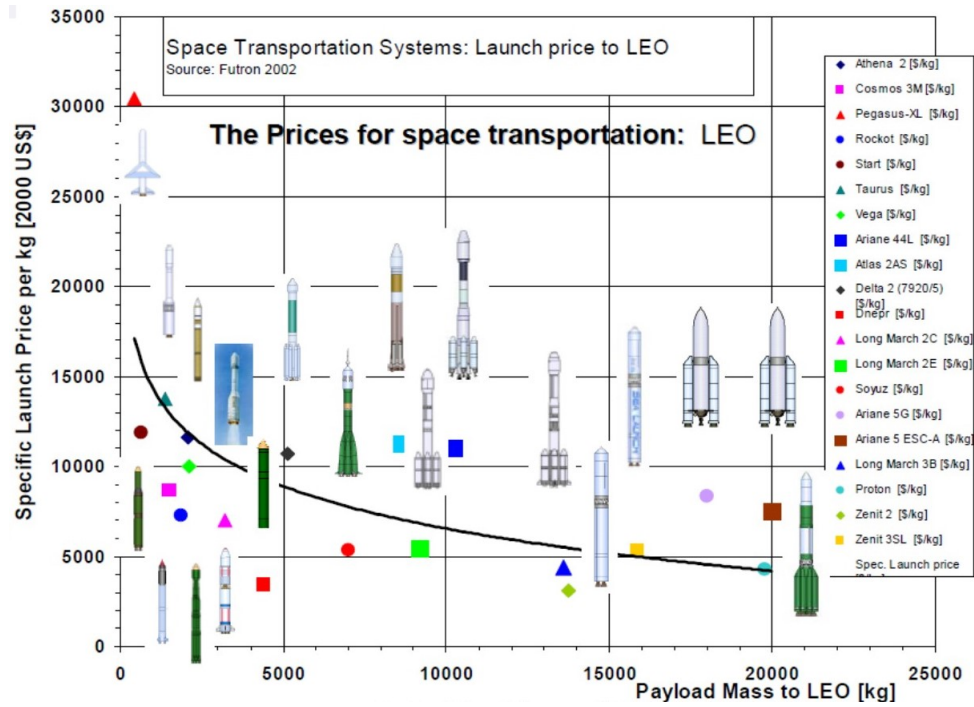
Figure 1.2: Launch Cost LEO [2]

The aim of this master thesis is to perform a preliminary design of a small air launched rocket, capable of inserting a nanosatellite into Low Earth Orbit (LEO), this work is based on a multidisciplinary approach as required by the topic itself. The models used in this thesis are not particularly complex, this must be intended as a preliminary analysis to prove the feasibility of such a concept and provide rough budgets of mass, trajectory, launch location and ascent control. Tools are developed for each sector and interconnected by the others through a hierarchic multidisciplinary design, then some topics are deepened more proposing innovative solutions to improve the design not only on air to orbit launch vehicles but launchers in general.

The thesis is structured as follows:

- **Chapter 1: Introduction**
  Here a brief overview of the work is pointed out. At first the research motivation is expressed and explained in details, focusing in particular on the meaning of the air to orbit solution and the choice of the payload class. After that some preliminary analysis are performed regarding the carrier aircraft, the multidisciplinary workflow and the deployment conditions.

- **Chapter 2: Staging Design**
  In this chapter the selection of the stages configuration is performed, first using available theories and then showing a multi-configuration solution developed by the candidate.

- **Chapter 3: Propulsion System Design**
  Here the propulsion system is chosen and designed, focusing on the overall configuration of the launcher and proposing some innovative solutions as well. Budgets of mass and dimensions are the outcomes.

- **Chapter 4: Trajectory and Launch Location**
  In this chapter using the data coming from the previous sections, the rocket dynamic is integrated using a simplified model to ensure the feasibility of the choices done so far and computing a reference trajectory for the next parts. Then some consideration are presented on the stages re-entry and the definition on the launch location.

- **Chapter 5: 6DOF Rocket Model**
  A full 6 degrees of freedom rocket model is implemented to simulate the ascent trajectory from the deployment to the payload orbit insertion. This is another important benchmark of the design.

- **Chapter 6: Ascent Control Law**
  The control law used to follow the desired trajectory is shown in this chapter, first a simple PD controller is used and then compared with another solution based on an MPC controller.

- **Chapter 7: Conclusions**
  This chapter summarizes the most relevant points risen from the development research and addresses the work in terms of future steps to follow.

1.1 Air Launch to Orbit State of the Art

In this section the state of the art regarding air launched rockets, and small launchers is presented. The state of the art regarding each subsystem is addressed at the beginning of the respective chapter.

Air launch to orbit has an history that is present since the dawn of the space era, in fact 1958 was the year of the NOTSNIK rocket, this was a US project part of the Pilot program developed to be a small air launched rocket and anti-satellite weapon. It's a very simple launcher made of 5 solid rocket motors stages with a payload capability of 1 Kg to LEO, during the 1958 it performed 10 flight resulting in 10 failures therefore the project was abandoned. Nowadays only one air launched rocket is operational, the Pegasus from Northrup Grumman; it's a 3 stages solid rocket motors launcher capable of inserting 250 Kg into LEO in its XL configuration [7]. It becomes operational in 1990 and since then it accomplished 39 successful launches many of them in the XL configuration, making it one of the most used launchers in the history despite an high specific cost per kilogram. Pegasus has also the possibility of using a fourth stage powered by hydrazine based monopropellant in order to increase its orbit insertion accuracy.

There's another launcher that will be operational in a few months, the LauncherOne from Virgin Orbit that performed its maiden flight on May 2020 but resulted in a failure after few seconds from its deployment [11]. Its architecture is quite different from the Pegasus, it is a 2 stages vehicle powered by NewtonThree and NewtonFour engines both working using RP-1 and LOX; it is capable

of inserting 300 Kg into LEO [12].

Figure 1.3: From left to right: Pegasus XL, LauncherOne, NOTSNIK

For what concerns the small launch vehicles market, as reported previously, there are no launchers capable of inserting a single 1 nanosatellites into LEO, but the research in this field is growing fast. For this purpose NASA launched in 2015 the so-called VCLS (Venture Class Launch Services), a contract to finance space companies in order to develop small launch vehicles dedicated specifically for nanosatellites [13]. The 3 companies awarded are:

- Virgin Galactic with its LauncheOne rocket

- Firefly Space System with its Firefly Alpha rocket

- RocketLab with its Electron rocket

The LauncherOne has just been discussed, Firefly Alpha is a 2 stages rocket powered by the Raver and Lightning engines both using RP-1 and liquid oxygen, the LEO payload capability is around 600 kg but the maiden launch has not yet happened. The Electron instead flew many times in this years, it uses the Rutherford engine for both first and second stage which again works on RP-1 and LOX, and it is able to bring 150 Kg into LEO [14] [15]. However all those rockets are used not to launch just a single nanosatellite, but a bunch of those; this implies that some of them may not have the perfect launch date, or target orbit, therefore they would work in a slightly off-nominal condition.

It is worth spending a few words regarding this 3 rockets; it can be noticed that the propulsion system is basically the same, 2 stages working with RP-1 and LOX as propellant couple. The choice is not surprising because RP-1 is a very reliable fuel used since the dawn of the space era, it allows to build simple engines and, more importantly, it has the highest density with respect to other classical liquid fuels, thus making the rocket smaller.

1.2 Motivation

The absence of any sort of air launched vehicle in national and European territory motivates the work here presented, the availability of such kind of vehicles to access space would increase Eu-

ropean independence from American small launchers and moreover it would introduce a class of launch vehicles (extra-small) that is a world-first. Another important aspect that is worth mentioning is that currently operational European launchers (e.g. VEGA, Ariane) have their launch pad in Kurou French Guyana, so each satellites must be shipped oversea before launch, an air to orbit launch vehicle like the one considered in this master thesis would avoid such a transportation since it can be launched above the European territory.

The possibility of launching specifically and individually one nanosatellite at a time is something unique up to now, and as already explained it would be key for satellites with highly time-dependent mission that do not want to share the same launch with a bunch of other satellites.

Looking at the current trend of the launch market, it can be noticed a spread in the capability. If in the past a launcher in the medium class (payload $\approx$ 5-20 tons to LEO) was able to accomplish the vast majority of the missions, nowadays the trend is moving towards dedicated launches for each class of payload.

Heavy and super-heavy rockets are being developed for Moon and Mars missions (e.g. SLS, Starship, New Glenn) and big space telescopes, while on the other hand, small launchers already cited are being designed for LEO applications of nano and micro satellites. Therefore, there is a very high meaning of developing micro launchers with high flexibility in this particular period.

1.3 Multidisciplinary Approach

A launch vehicle is a very complex and highly coupled system, it is composed by many subsystems implying different subjects such as structural mechanics/dynamics, propulsion, fluid-dynamics, control laws.

Usually such design is addressed using a Multidisciplinary Design Optimization (MDO), this method takes advantage of those coupling effects to find out the global optimal design of a launch vehicle, moreover it results in faster design time. Many different methods can be used in a MDO process, the most used are certainly CO (Cooperative Optimization) and MDF (Multi Discipline Feasible) [16] [17] [18].

The design strategy used in this master thesis, is not properly a full MDO, since it is not the aim of this work. Nevertheless it is possible to get some properties of the MDO method adopting a multidisciplinary approach. In this case there is no global optimization of the entire process, nevertheless a global overview of all the subsystems involved in the design has been kept.

Particularly important is the work done by Francesco Castellini with his PhD thesis [19], where he designed a Multidisciplinary Design Optimization for an expendable launch vehicle; here many different Multidisciplinary approaches are shown including the one adopted in this master thesis.

The choice here is mainly driven by simplicity and the presence of a well defined direction of proceeding in the design. Therefore it is possible to create a design path from requirements to outcomes that passes through different subsystems. This is something currently done by in tactical missile design as can be seen in figure 1.4. The workflow of this master thesis follows a similar path, but the order of the subsystem and the back iterations are different.

The decomposition in this case is called "hierarchic", meaning that it is worth designing some sub-

systems before others using its outputs as inputs of the followings.
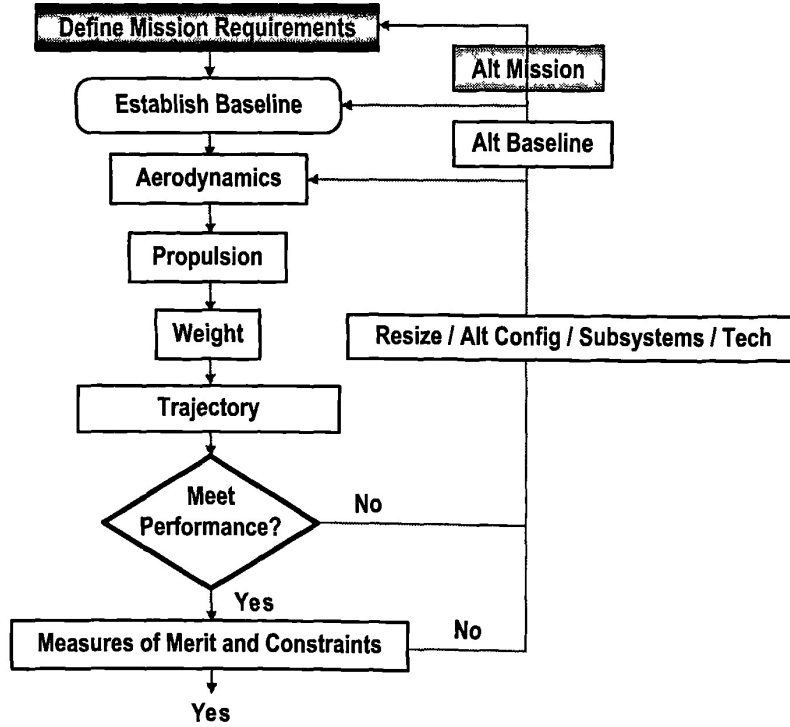
Figure 1.4: Tactical Missile Design Process [3]

In figure 1.5 the hierarchic design workflow selected for this master thesis can be seen.

The first block is the **High Level Requirements** which introduces basically requirements of Payload kind, orbit required, total cost of the launch etc; all those requirements come from customer surveys and market analysis. Another critical input comes from the **Carrier Aircraft Specification**, as already explained an air launched rocket must be compliant with its carrier aircraft that is way more restrictive than a common launch pad; those specification are the mechanical/electrical interfaces as well as the initial conditions which should be optimal for the launcher but must be compliant with the aircraft capabilities.

The outcome of the design process is a set of mass and dimension budgets of the air launched vehicle, validated using a complete rocket model.

The first design block is the **Propulsion System Choice**, where a first selection of the propulsion system is performed based upon the high level requirement and already existing solutions. The

output is a set of typical values of specific impulses (I_{sp}) and structural mass indexes (ξ) coming from literature.

The next step is the **Staging Design** that computes the staging configuration using the values found in the previous block; the results are the propellant M_{p_i} and structural masses M_{s_i} for each stage.

Then, one of the most important block in this diagram is the **Propulsion System Design**, in this block a more refined propulsion analysis is done using the propellant masses just computed. Here the dimensions of each stage are computed L, D, as well as the thrust profile T, the grain configuration (in the case of solid rocket motors), the propulsion performances like specific impulse I_{sp}, characteristic velocity C^* and burning time t_b.

Connected to this last subsystem is the **3DOF Trajectory Design**, here a simple point mass 3 degrees of freedom is implemented in order to test what has been done so far. The ascent trajectory is integrated and a back iteration to the propulsion system design block is performed in case the rocket is not able to reach the desired orbit; often the problem is identified in the thrust profile which is very difficult to model.

When the trajectory is compliant with all the requirements, another back iteration is done to re-compute the staging using this time specific impulses and structural mass indexes not from literature but computed in the propulsion system design block, this passage gives better values of the staging and therefore a more optimal solution at the end. When the difference between those values is near zero the procedure can go on; the overall output is the final configuration of the launcher and a reference trajectory computed using the simplified model.

The final step is to integrate the launch trajectory using a more refined **6DOF Rocket Model**, this model takes into account also the attitude of the vehicle and therefore a **Control Law** is required to follow the reference trajectory. The final results of this Multidisciplinary workflow are the masses breakdown of each stage, the launch location, propulsion performances, and finally the trajectory simulation done in order to prove the feasibility of all the design done so far.
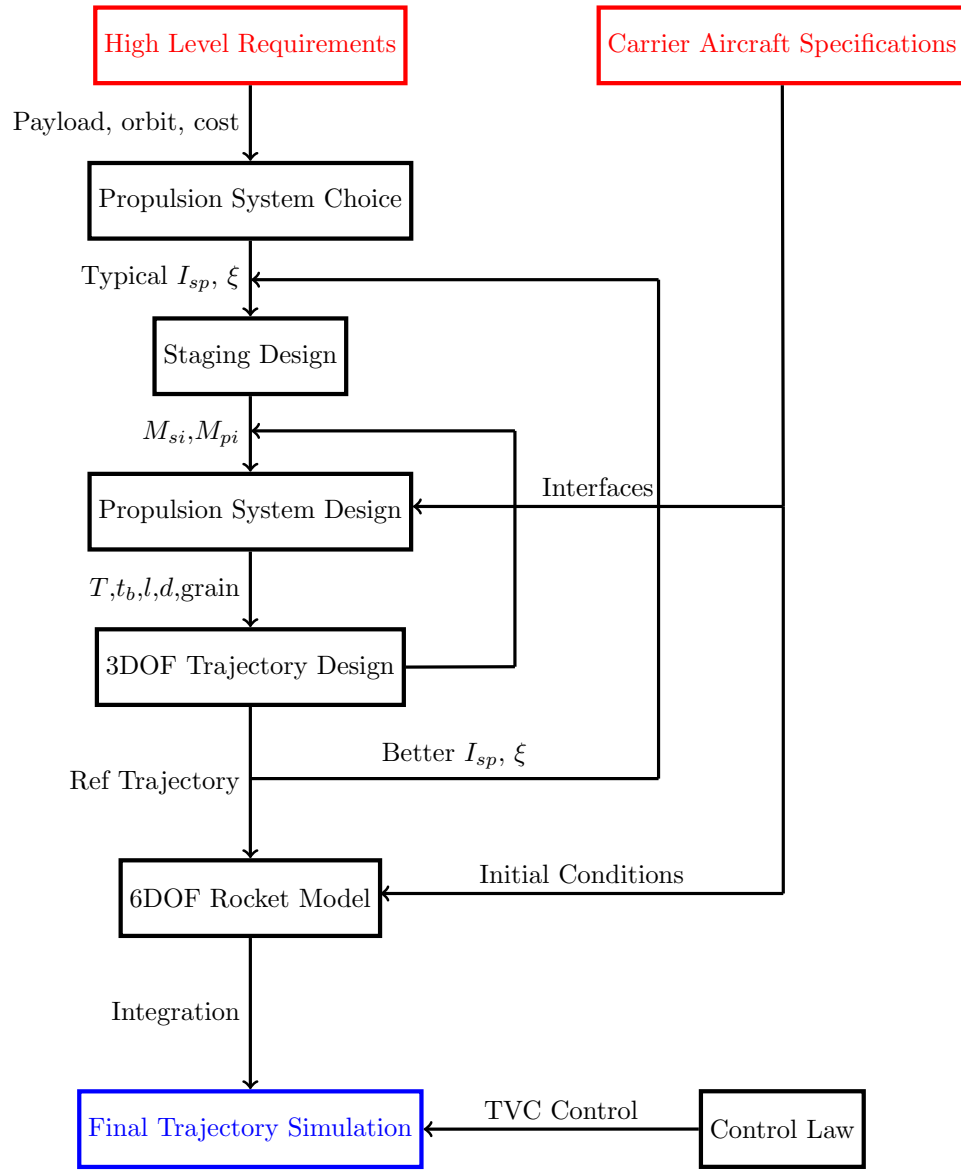
Figure 1.5: Multidisciplinary Workflow Scheme

1.4 Scenario Definition

Before starting with the first block of the multidisciplinary approach, it is worth discussing some preliminary considerations about which kind of payload is considered, what are the initial conditions and why, and finally which carrier aircraft has been selected for launcher.

1.4.1 Payload and Orbit Definition

As expressed in the introduction, the mass of the payload target is around few kilos, satellites in that range are often called *CubeSats*. Cubesat is a small satellite made by multiple units of 10cmx10cmx10xcm each as dimensions. Regarding the mass, each unit has a mean mass of 1.33 kg, however not every satellite has the exact same structure, so a variation is made between 1 and 1.5 kg for each unit. The nominal mass for each unit has been selected as the higher limit (1.5 Kg), to account for lighter CubeSats, the launcher can be deployed at lower velocity or lower altitude. This fact stresses again the importance of the flexibility that an air launched rocket can exploit. The mass distribution for each CubeSat is shown in figure 1.6.
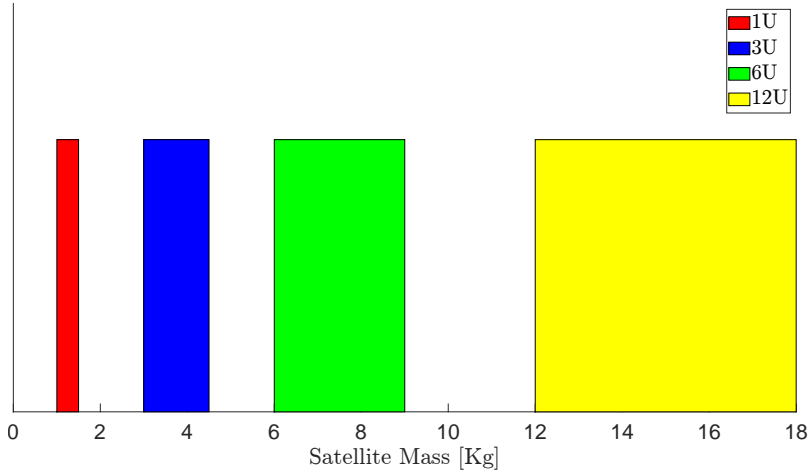
Figure 1.6: Satellite Mass

The overall payload mass that is be considered from here on is not simply the satellite mass, but it includes also deployer, fairing and the margins.

The way to compute it is the following:

$$M_{pay} = ((M_{sat} + M_{deployer})\,1.1 + M_{fair})\,1.2 \tag{1.1}$$

Regarding the orbit, as explained CubeSats are usually placed into LEO, in particular in an altitude

between 400 and 600 Km. Since many of those satellites are thought for Earth observation, the most used orbit for this purpose is the Sun Synchronous Orbit (SSO), this particular orbit exploit the J_2 perturbation of the Earth to make observation with the same Sun aspect angle along its whole mission. [20]

The variation of the Right Ascension of the Ascending Node (RAAN) due to keplerian parameters is given by the following equation:

$$\frac{d\Omega}{dt} = -\frac{3}{2} J_2 \left(\frac{R_e}{a(1-e^2)}\right)^2 \sqrt{\frac{\mu_e}{a^3}} \cos i \tag{1.2}$$

Fixing the semi-major axis to 500 Km, the eccentricity to 0 and the RAAN rate to 360 degrees per year, the resulting orbit inclination is: $i = 97.4°$.

The orbital velocity is immediately computed using the 2BP equations.

$$V_{orbit} = \sqrt{\frac{\mu_e}{a}} \tag{1.3}$$

Considering a launch location at 45 degrees latitude (Italy), the Earth's rotational velocity to be considered is 329 m/s in east direction. So the required launch velocity is 7666 m/s at an inclination of 99 degrees from east.

1.4.2 Fairing and Deployer

As expressed in the previous section, both fairing and deployer concur to the overall payload mass, a simple way to estimate them is by means of regression lines from existing hardware.

Satellites deployer is a mechanism that separate the satellite from the rocket upper stage by means of a spring; it also provides mechanical interfaces between satellite and launcher, so it acts as a common payload adapter. Adapters are usually designed based on the launcher's specifications and customer requirements, CubeSats deployers instead can be used on every launcher since they have standardized dimension like CubeSats are. The regression line is made considering the CubeSats adapter from ISIS Space [21].

$$M_{deployer} = 0.6967 M_{sat} + 0.2868 \tag{1.4}$$

Fairings instead are very complex structures, there are no available hardware off-the-shelf but it is designed for each launcher specifically. A full design of the fairing is useless at this current point, but a simple way to estimate its mass can be implemented. Looking at some existing fairings like the ones developed by RUAG Space (for Ariane, VEGA, Atlas), it is possible to estimate the thickness of the fairing shells [22]. Two major assumptions must be done, the first is assuming a

constant density throughout the whole structure while the second imposes a shape made up by a semi-spherical shell above an hollow cylinder with the same thickness overall. With those assumptions it is possible to compute the thickness of the existing fairings, and then use it to compute the mass of the fairing in this case based on the dimension of the launcher and the satellite. This procedure follows a simplified approach, since the fairing is made up by many materials and elements and the shape is not described by the shape discussed previously; however, the major role of this piece of hardware, is to protect the payload from environmental stresses and since an aero-launcher usually feels lower dynamic pressure with respect to traditional rockets, this procedure somehow overestimates the thickness of the fairing therefore introducing more margins.

Without reporting all the computations, this rough estimation leads to the following relation.

$$M_{fair} = \frac{4}{15} \left(M_{sat} + M_{dep} \right) \tag{1.5}$$

Despite being considered as part of payload mass, the fairing is deployed after the first stage burn, when the launcher is basically outside the atmosphere.

Masses	M_{sat}	M_{dep}	M_{fair}	M_{pay}
Units	Kg	Kg	Kg	Kg
1U	1.5	1.13	0.70	4.31
3U	4.5	1.99	1.73	10.64
6U	9	3.28	3.27	20.14
12U	18	5.86	6.36	39.13

Table 1.1: CubeSats masses breakdown

1.4.3 Carrier Aircraft

The selection of the carrier aircraft is a critical point in the design of an air launched rocket, this choice inevitably influences the design because it introduce limits in the deployment conditions as well as the maximum mass of the rocket. The carrier aircraft for the Pegasus rocket is a Lockheed L-1011 TriStar, which is an airplane commonly used for commercial lines, the launcher is placed below the fuselage. The LauncherOne is deployed by a Boeing 747-400 aircraft named Cosmic Girl, like the L-1011 is usually used in commercial flights and the rocket is placed below one wing, since the airplane was thought to have 2 more engines that it now has.

The carrier aircraft selected for this rocket is the Eurofighter Typhoon, a military fighter used by many European air forces.

The Eurofighter Typhoon is a military aircraft which is operational since 2003 in many European airforces, it has two turbojet EJ200 engines that provides 180 kN thrust in total and around 2000 s of specific impulse [4]. Looking at its armament it can bring the rocket both under the fuselage and below the wing like a missile, the choice of where put the launcher, the electro-mechanical

interfaces between the aircraft and the rocket are all topics for a further development. In Italy there are few military bases where the Eurofighter can be prepared for flight, this can restrict the launch locations to a few around Italy. This topic is pointed out in more details in chapter 4.

Figure 1.7: EuroFighter Typhoon [4]

1.4.4 Deployment Conditions

Looking again at existing air launched vehicles, it is possible to infer some insights about typical velocity, altitude and pitch of the carrier aircraft at the deployment of the rocket. PegasusXL is deployed at an altitude of almost 12 Km, a velocity of Mach 0.82 and a pitch not defined in its manual but looking at some videos it can be fixed at no more than 20 degrees [7]. The LauncherOne is released at an altitude of around 11 Km, the velocity is not specified but should be around Mach 0.8 like the Pegasus, the pitch angle in this case is 27.5 degrees.

Up to this point, it is impossible to fix precise values of deployment conditions, but some typical values can be get from literature and existing technologies like the ones just pointed out above. Since the carrier aircraft is designed for air supremacy applications, there are no very stringent boundaries to respect, but at this point is better taking standard values and, if a later design find out how much is feasible to push those limit, it is possible to get more optimal deployment conditions for the rocket trajectory.

The deployment altitude is fixed to 11 Km and the velocity of Mach 0.8, that, using the standard atmospheric model explained in chapter 5 and the perfect gas hypothesis, corresponds to a speed of 236.1 m/s.

For what concerns the initial pitch angle, a work done by Sarigul-Klijn [23] shows how much is important the initial angle for the ΔV gain of an air launched rocket with respect to a classical one. Increasing the initial angle provides a better performance up to 30 degrees, and after that the gain remains almost constant for higher angles. However that model only takes into account the energetic gain but not other factors like the TVC required, analysis has been done on this topic in chapter 4 and it turns out that a good initial pitch is around 50 degrees.

Chapter 2

Staging Design

The stage configuration is one of the most important feature in a launcher design, a good staging can lead to efficient orbit insertion while minimizing the overall initial mass. The aim of this chapter is to find the best solution for this purpose and study new tools for designing the configuration of small launch vehicles.

The preliminary propulsion selection, according to what explained in section 1.3, leads to a solid choice for every stage. The values of I_{sp} and ξ (defined as inert mass over propellant mass) considered for the staging design can be seen in table 2.1.

Parameters	I_{sp}	ξ
Units	s	-
1st Stage	279	0.09
2nd Stage	290	0.1
3rd Stage	293	0.16

Table 2.1: Propulsion Hypothesis for Staging Design

A detailed analysis on the propulsion system is done in chapter 3, where those values are validated and discussed.

2.1 Preliminary Hypothesis

Before beginning, it is worth spending a few words about the hypothesis involved in this chapter. First of all, the following theories are based upon the Tsiolkovsky Equation.

$$\Delta V_i = I_{sp_i} g_0 \log(N_i) \tag{2.1}$$

Where N_i is the mass ratio of the i-th stage.
This equation defines the ΔV value given the specific impulse of the stage, a parameter which

defines the efficiency of the engine, and the mass ratio which gives information about how much of the stage mass is propellant.

The Tsiolkovsky equation is based on two major assumptions, the former is constant specific impulse and the latter is the absence of gravity and drag losses. Constant specific impulse is not a big issue, its variations are due mainly to changes in ambient pressure or in engine parameters (O/F, Pc ...). Drag and gravity losses have instead a more important contribution and must be taken into account, the former is higher for classical launchers while an air launched rocket feels lower drag losses being released at high altitude.

To take those contributions into account the required orbital ΔV has been margined by a factor of 1.22, in the following chapters models that takes into consideration those losses are explained, and the losses are estimated in more details.
In this section the mass of each stage is considered as made by two contributions:

$$M_{0_i} = M_{p_i} + M_{s_i} \tag{2.2}$$

Where M_{p_i} represent the whole propellant mass of the i-th stage, and M_{s_i} the inert mass, so: engines, TVC, structures...
So the Tsiolkovsky equation for each stage can be re-written as:

$$\Delta V_i = I_{sp_i} g_0 \log \left(\frac{M_{0_i}}{M_{0_i} - M_{p_i}} \right) \tag{2.3}$$

2.2   Optimal Staging Theory

A first guess can be done according to the Optimal staging theory, this method makes use of the Lagrangian multipliers to minimize the initial mass given the payload mass and the total ΔV as constraint.
The mass ratio of the i-th stage can be written in the following way.

$$N_i = \frac{M_{s_i} + M_{p_i} + M_{s_{i+1}} + M_{p_{i+1}} + ...M_{pay}}{M_{s_i} + M_{s_{i+1}} + M_{p_{i+1}} + ...M_{pay}} = \frac{M_{0_i} + M_{0_{i+1}} + ...M_{pay}}{M_{0_i} \epsilon_{s_i} + M_{0_{i+1}} + ...M_{pay}} \tag{2.4}$$

The constraint is imposed by the required ΔV.

$$\Delta V = \sum_{i=1}^{n} C_i \ln N_i \tag{2.5}$$

Where n is the number of stages and C is the equivalent exhaust velocity.
The function to minimize is the overall launcher wet mass, but for demonstration reasons it is normalized by the payload mass. M_R represents the initial mass not including the payload.

$$M_R = \sum_{i=1}^{n} M_{0_i} \tag{2.6}$$

$$\frac{M_R + M_{pay}}{M_{pay}} = \frac{M_{0_1} + M_{0_2} + ...M_{pay}}{M_2 + ...M_{pay}} \frac{M_{0_2} + ...M_{pay}}{M_{0_3} + ...M_{pay}} ... \frac{M_{0_n} + M_{pay}}{M_{pay}} \tag{2.7}$$

Re-arranging the terms, the cost function can be written as:

$$\frac{M_R + M_{pay}}{M_{pay}} = \prod_{i=1}^{n} \frac{(1 - \epsilon_{s_i})N_i}{1 - N_i \epsilon_{s_i}} \tag{2.8}$$

Considering that:

$$\epsilon_{s_i} = \frac{M_{s_i}}{M_{s_i} + M_{p_i}} \tag{2.9}$$

Now, taking the logarithm of the cost function and exploiting the logarithm properties.

$$\ln\left(\frac{M_R + M_{pay}}{M_{pay}}\right) = \sum_{i=1}^{n} \left[\ln(N_i) + \ln(1 - \epsilon_{s_i}) - \ln(1 - N_i \epsilon_{s_i})\right] \tag{2.10}$$

Taking the partial derivatives according to Lagrange multipliers optimization method, the procedure ends up with a system of equations to be solved numerically. An analytical solution can be found under the hypothesis of constant parameters C_i, ϵ_{s_i}, but this is not the purpose of this analysis.

$$\begin{cases} \frac{1}{N_i} + \frac{\epsilon_{s_i}}{1 + N_i \epsilon_{s_i}} - \lambda \frac{C_i}{N_i} = 0 & i = 1...n \\ \Delta V - \sum_{i=1}^{n} C_i \ln N_i = 0 \end{cases} \tag{2.11}$$

The result of this system is a set of mass ratios N_i for each stage from which it is possible to compute the initial rocket mass as well as the breakdown of each stage.

$$M_0 = M_{pay} \prod_{i=1}^{n} \frac{1 - \epsilon_{s_i} N_i}{1 - N_i \epsilon_{s_i}} \tag{2.12}$$

$$M_{p_i} = M_{0_i}(N_i - 1)/N_i \qquad i = 1...n \tag{2.13}$$

$$M_{s_i} = M_{p_i}(\epsilon_{s_i} - 1)/\epsilon_{s_i} \qquad i = 1...n \tag{2.14}$$

$$M_{0_{i+1}} = M_{0_i} - M_{p_i} - M_{s_i} \qquad i = 1...n - 1 \tag{2.15}$$

An important aspect that this theory does not account for, and it is worth spending a few words about, is the interstage mass. Usually rockets have 2 to 4 stages and, of course, the presence of more stages allows the launcher to be more mass efficient and each engine nozzle can be optimized at the right altitude. However, there are some inevitable mass additions due to interstages, separation mechanisms, and moreover, the structural mass indexes become higher for smaller stages.
For those reasons, the maximum number of stages considered for this preliminary design has been fixed to 3.

2.3 Multi-Configuration Design

From the optimal staging theory is quite easy to get the stage subdivision and then proceed with the design of the launcher, but as can be seen in equation (2.12) the initial mass depends a lot on the payload mass; this opens the question on which kind of CubeSat should be selected as target payload and why. One solution could be to look at CubeSats already launched and planned, and then infer which may get the largest market in the future.
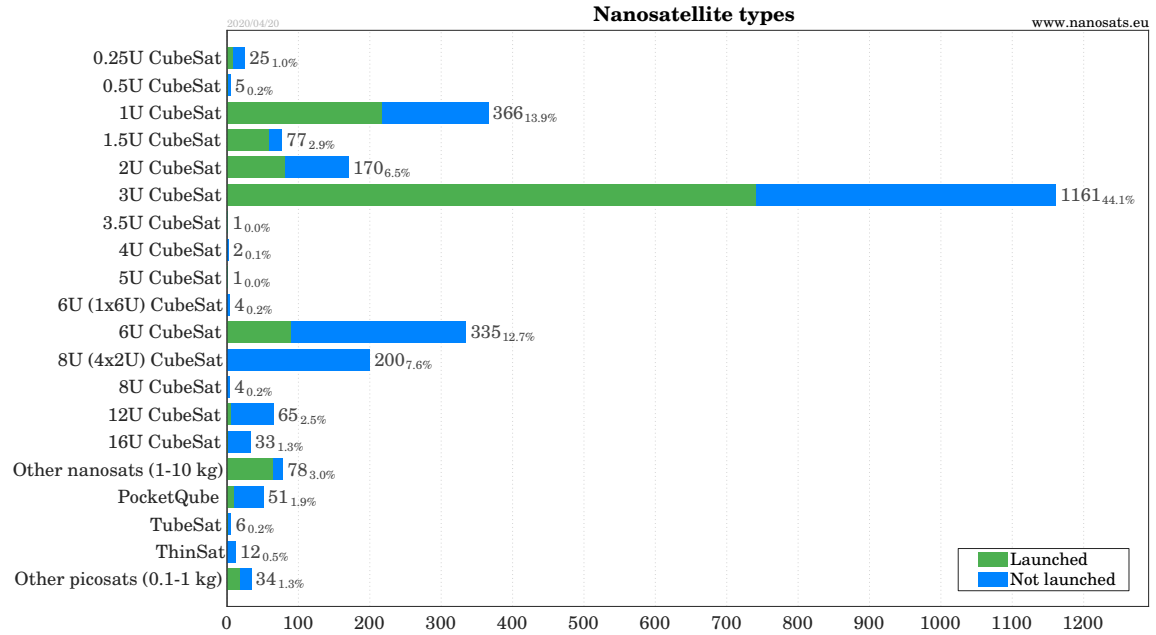

Figure 2.1: Nanosatellite Type [1]

31

Looking at figure 2.1, it's easy to notice that 3U CubeSat will be a perfect candidate as target payload, however 6U is still very important due to its possibility of using heavier instruments while being quite small at the same time. So, designing the rocket for the 3U makes impossible launching a 6U, while designing for the 6U constrains the rocket to launch two 3U at a time, therefore loosing the capability of dedicated launches.

One interesting alternative is to make different configurations of the same rocket for different classes of payloads, this is currently being done by launchers such as Ariane6 with its 2/4 SRB configurations and Atlas V that could use 0 to 5 strap-on boosters. This solution leads to the possibility of increasing the payload mass range designing only few more rocket motors, thus keeping the costs lower.

For this purpose a novel approach is proposed. A first staging design is made for the lighter payload (M_{pay}^{I}), then one of the stages is enhanced or one more is added to make the rocket capable of launching the heavier one (M_{pay}^{II}). This approach can be applied to any couple of payloads and any orbit, the value considered in this chapter are taken from section 1.4. Several solutions are possible, and are shown in the list below.

1 2 Stage Rocket with an Enhanced First Stage

2 2 Stage Rocket with an Enhanced Second Stage

3 2 Stage Rocket with the addition of a Third Stage

4 3 Stage Rocket with an Enhanced First Stage

5 3 Stage Rocket with an Enhanced Third Stage

6 2 Different 2-Stage Rockets both Optimal

7 2 Different 3-Stage Rockets both Optimal

Solution **1** means a 2 stage rocket capable of launching M_{pay}^{I}, then a second configuration of the first stage is created, such that using the same second stage as before, the rocket can launch M_{pay}^{II} into orbit. This creates two configurations of the rocket.

Solution **2** does basically the same procedure, but in this case the first stage is kept constant and a second configuration of the second stage is created.

Starting from the same 2 stage rocket for M_{pay}^{I}, solution **3** does not change those two stages, but instead adds a third one on top such that this 3 stage rocket is able to launch M_{pay}^{II} into orbit.

Solution **4** is basically the same as **1** but in this case the rocket has 3 stages, and again only the first stage is enhanced keeping the same second e third stage.

Similar to this latter, solution **5** starts with a 3 stage rocket for M_{pay}^{I} and a second configuration of the third stage this time is created for M_{pay}^{II}.

Finally, solution **6** is composed by a two stage rocket fully optimized for M_{pay}^{I} using the just derived optimal staging theory, and by another two stage rocket optimized this time for M_{pay}^{II}.

Solution **7** does basically the same procedure like this latter, but in this case both rockets have 3 stage each.

Those 7 different solutions basically create two configurations of the rocket changing one or more stages doing so. Figure 2.2 helps understanding better all those solutions.
Now it is worth asking which of them provides the best solution, and to do so a cost function to discriminate better and worse solutions must be found.
Like the optimal staging theory, a good cost function could be the initial wet mass of the rocket. But two launchers are present here, the rocket in the first and in the second configuration. If the initial wet mass of the first configuration is chosen as cost function, the final result would be optimal for M_{pay}^{I} and sub-optimal for M_{pay}^{II} and vice versa.

Since at this stage is not meaningful benefiting one payload class more than the other, a result as wide as possible should be left for a further development. Detailed market analysis and customer surveys can address this question in a future work.
A MultiObjective Optimization (MOO) is suitable for this kind of problem, since it optimize both the initial wet masses of the two configurations at the same time. And a Pareto-Front result can provide a wide set of dominant solutions including the optimal values for the two payload classes.
Moreover, another important parameter is the total number of different stages (or better, motors) to be developed. This value is strictly linked to the overall cost and complexity of the project, therefore this must be considered in the cost function.

This discussion leads to the following cost function vector:

$$\underline{J}_{MOO} = \begin{bmatrix} M_0^I & M_0^{II} & n_{motors} \end{bmatrix} \tag{2.16}$$

To compute those initial wet masses, a procedure must be implemented.
Table 2.2 shows which variables are needed by each solution process, and also the n_{motors} value.

Solution	Independent Variables	n_{motors}
1	M_{s_2}	3
2	M_{s_1}	3
3	M_{s_2}	3
4	M_{s_2}, M_{s_3}	4
5	M_{s_1}, M_{s_2}	4
6	-	4
7	-	6

Table 2.2: Staging Solutions
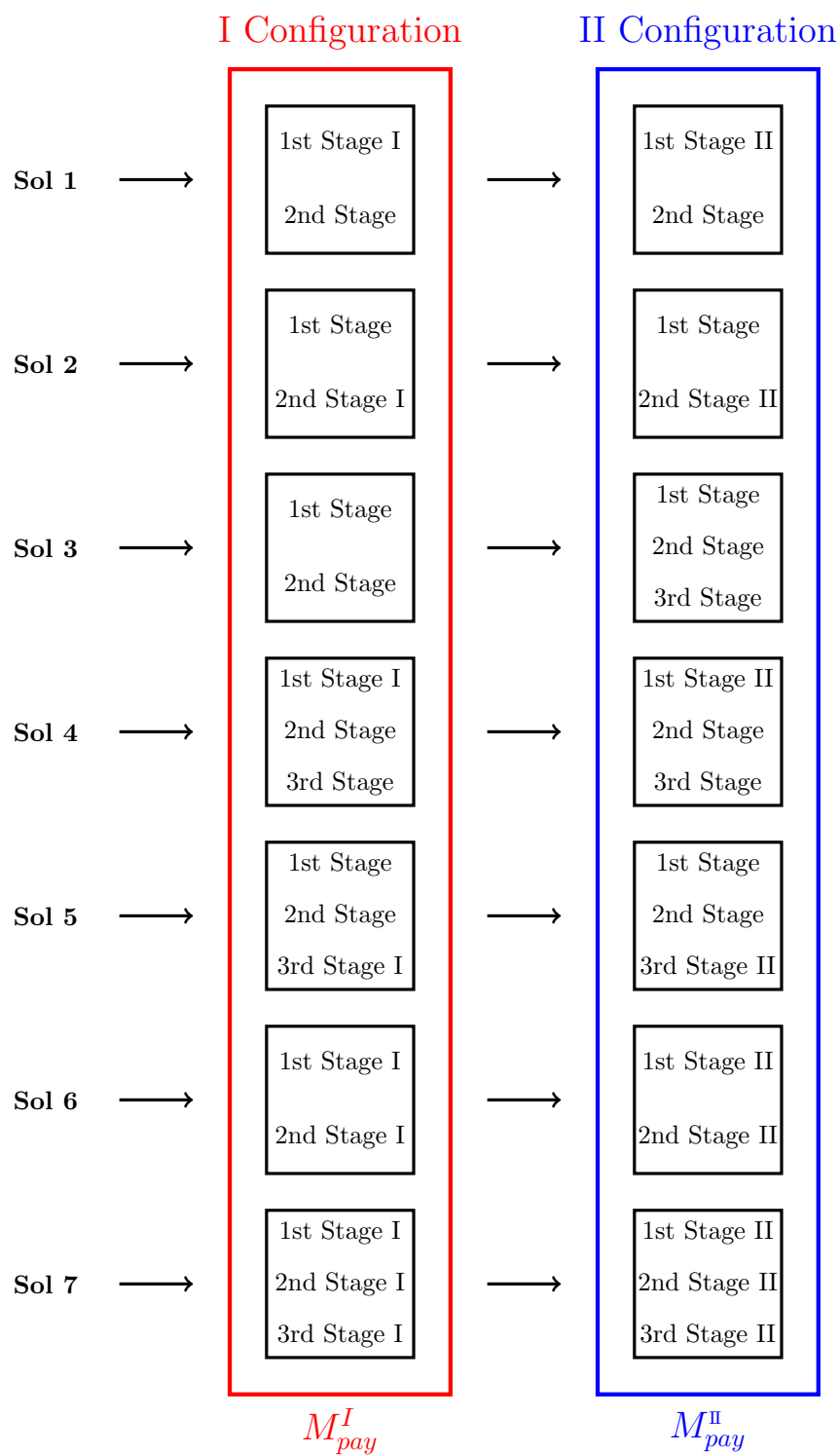
Figure 2.2: Multi-configuration Solutions Breakdown

Therefore, the independent variables vector is chosen to be made by the inert masses of the 3 stages; also the propellant masses can be used since are linked through the structural mass indexes ξ_i already assumed. However the 3 inert masses have values closer one to each other with respect to the propellant ones, this gives meaning for such a choice.

Figure 2.3 gives another point of view of the 7 solutions, dividing the ones implying a 2 stage design rocket to a 3 stage one. Moreover it also introduces the problem on how to compute the cost functions M_0^I and M_0^{II}. Some of them require a numerical solution while others can be solved analytically. The solutions that express an enhancement of the first stage, can be computed analytically since only the first mass ratio depends on the first stage elements. While the replacement or the addition of an upper stage must be solved numerically, because every mass ratio is function of the upper stage values.
The following list summarizes the solving procedure.

- Solutions **6** and **7** are computed using the optimal staging theory, expressed by system of equations (2.12).

- Solutions **1** and **4** can be computed using an analytical approach.

- Solutions **2**, **3** and **5** are found using a numerical process.

Figure 2.3: Multi-configuration staging, solution methods

2.3.1 Analytical Solution
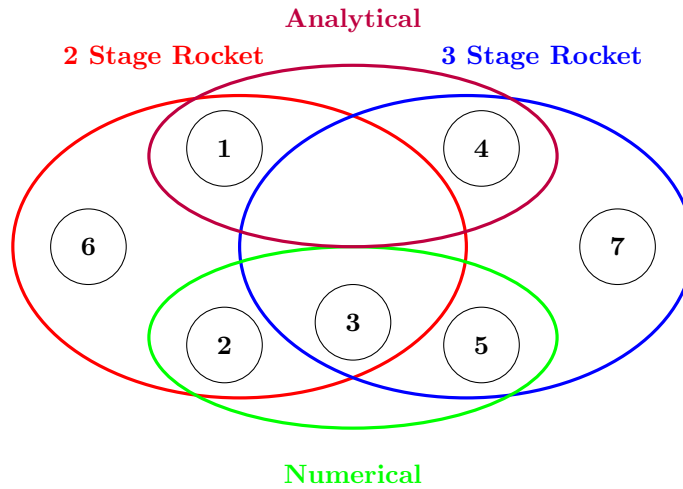
As figure 2.3 shows, solutions **1** and **4** can be computed analytically since they are dealing with the enhancement of a first stage. Solution **4** is more general, therefore the passages to compute its wet masses are shown here, while solution **1** can be solved in the same way just neglecting the presence of a third stage.

Given M_{s2} and M_{s3} as independent variables, as first step the propellant masses M_{p_2}, M_{p_3} are computed simply dividing respectively by the structural mass index ξ. Then, the second and the third stage mass ratios of the first configuration are computed.

$$M_{s_i} = M_{p_i} \xi_i \tag{2.17}$$

$$\begin{cases} N_2^I = \frac{M_{s_2} + M_{p_2} + M_{s_3} + M_{p_3} + M_{pay}^I}{M_{s_2} + M_{s_3} + M_{p_3} + M_{pay}^I} \\ N_3^I = \frac{M_{s_3} + M_{p_3} + M_{pay}^I}{M_{s_3} + M_{pay}^I} \end{cases} \tag{2.18}$$

The remaining mass ratio is immediately found from the ΔV constraint.

$$N_1^I = \exp\left(\frac{\Delta V - C_2 \log(N_2^I) - C_3 \log(N_3^I)}{C_1}\right) \tag{2.19}$$

And from it the propellant mass of the first stage, consequently its structural mass by means of ξ_1 is found as well.

$$M_{p_1}^I = \frac{M_{s_2} + M_{p_2} + M_{s_3} + M_{p_3} + M_{pay}^I}{1 + \xi_1 - N_1^I \xi_1}(N_1^I - 1) \tag{2.20}$$

The initial mass of the launcher in its first configuration is then computed:

$$M_0^I = M_{p_1}^I + M_{s_1}^I + M_{p_2} + M_{s_2} + M_{p_3} + M_{s_3} + M_{pay}^I \tag{2.21}$$

Regarding M_0^{II}, the same procedure from (2.18) to (2.21) can be done using in this case M_{pay}^{II} as payload mass.

As already explained, solution **1** follows a very similar procedure, the only independent variable is M_{s_2}, therefore the same analytical equations are followed but in this case, each variable referring to the third stage is not considered.

2.3.2 Numerical Solution

Solutions **2**, **3** and **5** must be solved numerically since they are dealing with the replacement or the addition of an upper stage.

In this subsection, it is worth focusing on one solution in particular and showing the procedure to solve it. Then it can be proved that the other two solutions can be solved in a very similar way. The solution solved in this section is number **3**.

In case of this solution, the independent variable is M_{s_2}. The first step is to compute the first stage that allows the 2 stage rocket of launching M_{pay}^I. This is done in the same way of solution **1** already explained in the previous section (eq (2.18) to (2.21)).

Once the first and second stage are computed, the complex part is to calculate a third stage such as, if placed on top of the existing two stages, the resulting 3 stage launcher is capable of launching M_{pay}^{II}.
This can be simply done by numerically solving equation (2.22) as a function of the propellant mass of the third stage (or the inert mass, is the same).

$$\Delta V = C_1 \ln(N_1^{II}) + C_2 \ln(N_2^{II}) + C_3 \ln(N_3^{II}) \tag{2.22}$$

A better way to do so, is to switch from a non-linear solving problem, to an optimization process. It is very important to point out that this optimization is **NOT** the MultiObjective optimization explained before, this is another way to numerically solve equation (2.22), everything in this subsection that deals with an optimization is referred to this one, and not the MOO.
The meaning of this switch comes after a few passages. The cost function in this case is J, that is clearly equal to 0 when equation (2.22) is solved.

$$J = \left(\Delta V - C_1 \ln(N_1^{II}(M_{p3})) - C_2 \ln(N_2^{II}(M_{p3})) - C_3 \ln(N_3^{II}(M_{p3}))\right)^2 \tag{2.23}$$

A question that is important to answer, is if any value of the independent variable M_{s_2} can lead to a zero of J, and consequently to a feasible value of M_{p3}.
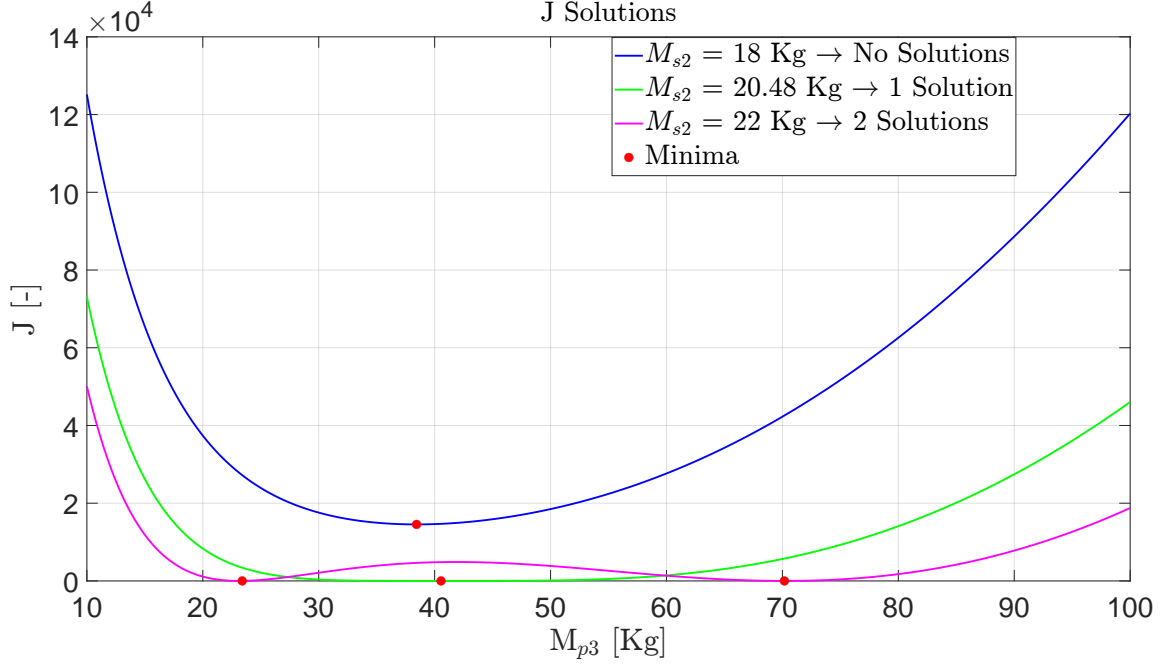
Figure 2.4: J Possible Solutions

Figure 2.4 can answer to this question, for M_{s_2} lower than a certain threshold J does not have a zero which means no solution. At that threshold there is only one solution of the equation, but for higher values two solutions appear and start spreading out for increasing value of M_{s_2}.

Now it is worth asking which of those 2 solutions leads to a lower value of M_0^{II}, while clearly M_0^I does not depend on which of the two solutions is picked up, but instead only on M_{s_2}.
As can be seen in figure 2.5, the higher solution tends to increase almost linearly with M_{s_2}, the lower solution instead has a small decrease and then has a linear increment but with a less stiff slope.

An important aspect that can be inferred from figure 2.5 is that the lower solution provides always better results than the higher one, this fact has a key importance when defining the initial condition of the gradient based optimization without recurring to global one.
Regarding the values of M_{s_2} smaller than the threshold, as explained previously they do not provide any feasible solution, however for continuity purposes, M_0^{II} has been penalized by the value of the minimum J shown in equation (2.23). This explains the choice of using an optimization process instead of a non-linear solver. So, in case of available solutions, the penalty is simply 0.
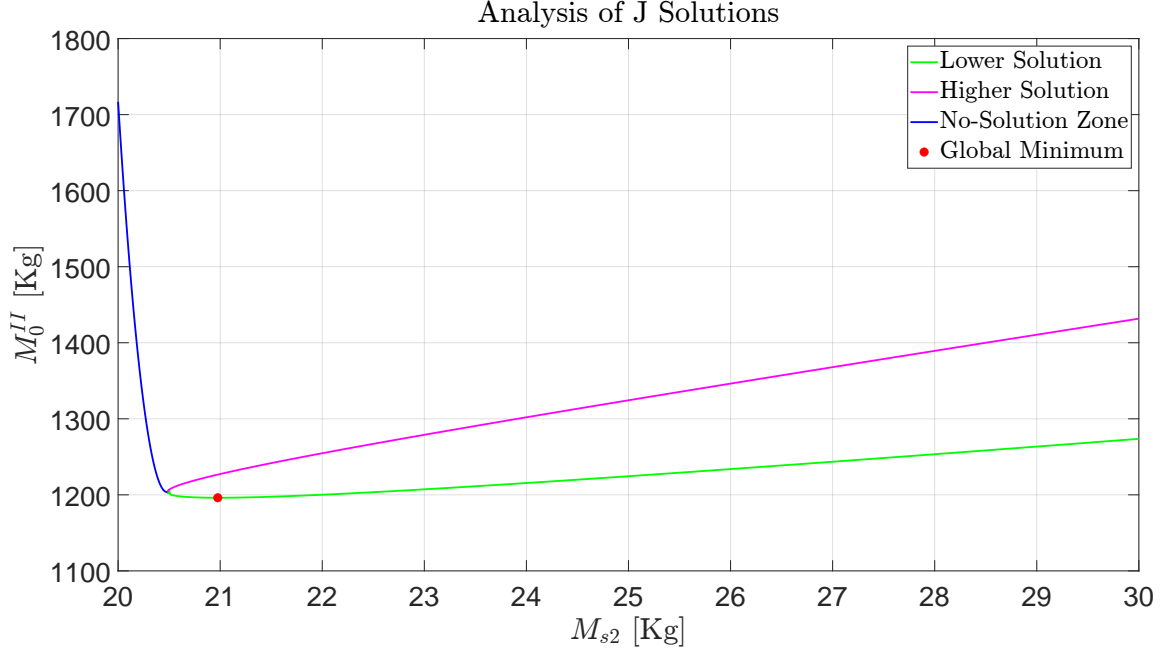
Figure 2.5: Analysis of the 2 J Solutions

Regarding the other solutions, number **2** is solved by doing the same optimization twice. In this case M_{s_1} is the independent variable, and the optimization outcomes are $M_{p_2}^{I}$ and $M_{p_2}^{II}$ for the two classes of payloads respectively.

Finally, solution **5** is slightly more complex. The independent variables are M_{s_1} and M_{s_2} while the optimization outcomes are $M_{p_3}^{I}$ and $M_{p_3}^{II}$. Again the same optimization is done twice.

The optimization algorithm chosen for this numerical solution, is a gradient-based method that depends on the initial conditions. This gives further meaning to the analysis of the 2 J solutions just done, because depending on the initial value of the optimization the algorithm can converge on the higher or lower solutions shown in figure 2.5.

2.3.3   MultiObjective Optimization

Finally it is possible to set up the whole MultiObjective Optimization process. The independent variable vector is the following:

$$\underline{X}_{MOO} = \begin{bmatrix} M_{s_1} & M_{s_2} & M_{s_3} & n_{sol} \end{bmatrix} \tag{2.24}$$

Where n_{sol} is an integer number ranging from 1 to 7 that identifies the solutions proposed previously.

The multiobjective algorithm chosen is an heuristic MultiObjective Particle Swarm Optimization (MOPSO), this is chosen mainly for the availability of this algorithm in the coding environment where this process is implemented. The same optimization has been performed using this case a Genetic Algorithm (GA) multiobjective, however it results with a slightly worse outcome and a slower computational time.

2.4 Results
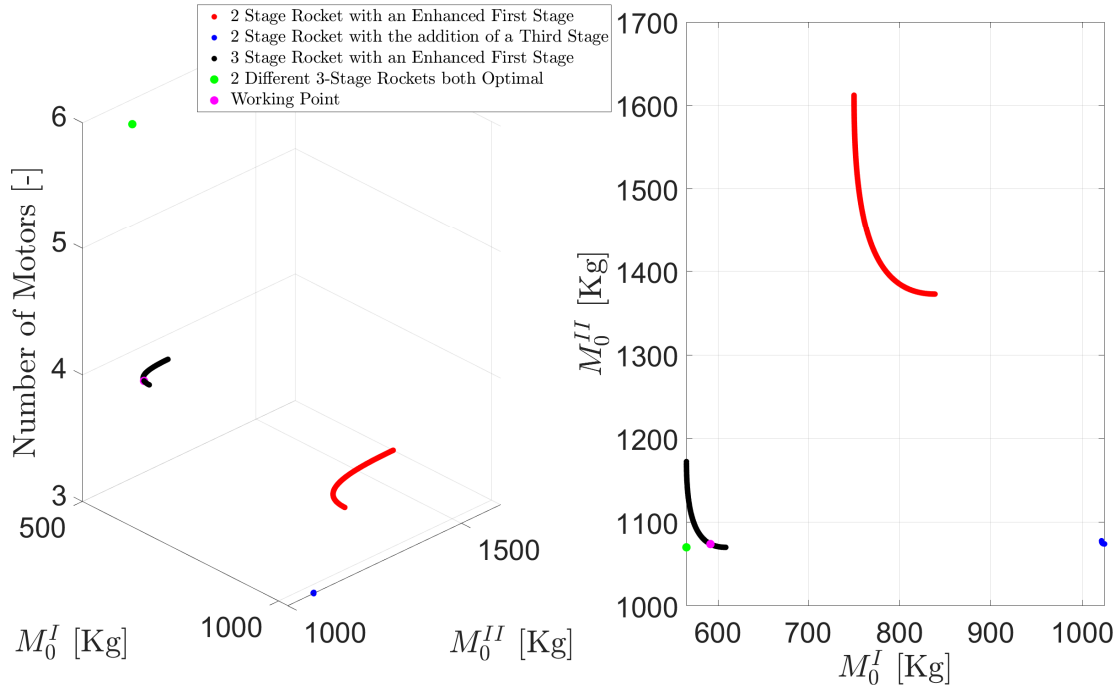
Figure 2.6: 3D Pareto-Front Solution

What can be seen from figure 2.6 is that the best solution for both M_0^I and M_0^{II} is number **7**, this is not surprising because that solution is basically made of 2 different rockets both optimized for their respective payload class. Solutions **2**, **5** and **6** do not appear meaning that there are solution with the same number of engines which are more mass efficient.

It is worth discussing also of solutions **1** and **3**, with the same number of motors they lead to different design both optimal depending which payload class is worth benefiting. Up to this point there is not reason to favor one payload class with respect to the other, a wide choice is left to a further design only neglecting the sub-optimal solutions.

Finally, solution **4** is the most interesting one. Using 4 different motors it gets very close to the optimal solution given by **7** saving also 2 motors, then, among the Pareto-Front solutions, the closest to the origin has been selected as working point from now on.

What can also be noticed of that solution, is that the two outermost points of that front, correspond to the optimal value expressed by solution **7** in the two classes. For instance, the top point of that front, has the same M_0^I as the optimal solution, while the other outermost point (to the right) has the same M_0^{II} of the optimum. A future work may find out which one of the two classes is worth optimizing the rocket for, and one of the solutions belonging to that front may be selected. Table 2.3 shows all the outcomes resulting from this optimization.

Parameters	$\mathbf{M_p}$	$\mathbf{M_s}$	$\mathbf{M_{tot}}$
Units	Kg	Kg	Kg
1st Stage I	346.8	31.2	378
1st Stage II	778.9	70.1	849
2nd Stage	156.3	15.6	172
3rd Stage	27.7	4.5	32
Full Rocket I	531	51.3	593
Full Rocket II	963	90.2	1073

Table 2.3: Staging Results

2.5   Validation

Even if the computations are quite clear and the results can be verified just looking at the resulting ΔV, a very brief validation can be interesting also to understand better the results.

A very simple way to prove the optimal staging theory is by means of a so-called grid search analysis. As explained, if the payload mass and the total ΔV are fixed, a 3 stage rocket has 2 degrees of freedom that can be expressed in various different ways. The ones selected are the inert masses of the second and the third stage, having those values it is possible to compute the rest of the launcher and estimate its total wet mass. The choice over those two inert masses has been made since the first stage can be computed analytically and not numerically as the last sections explained. The same analysis can be done using any two masses of the rocket, even using two propellant masses of any two stages.

This has been done for varying values of those two independent elements, and a contour has been made to show the total initial mass of the launcher in both configurations.
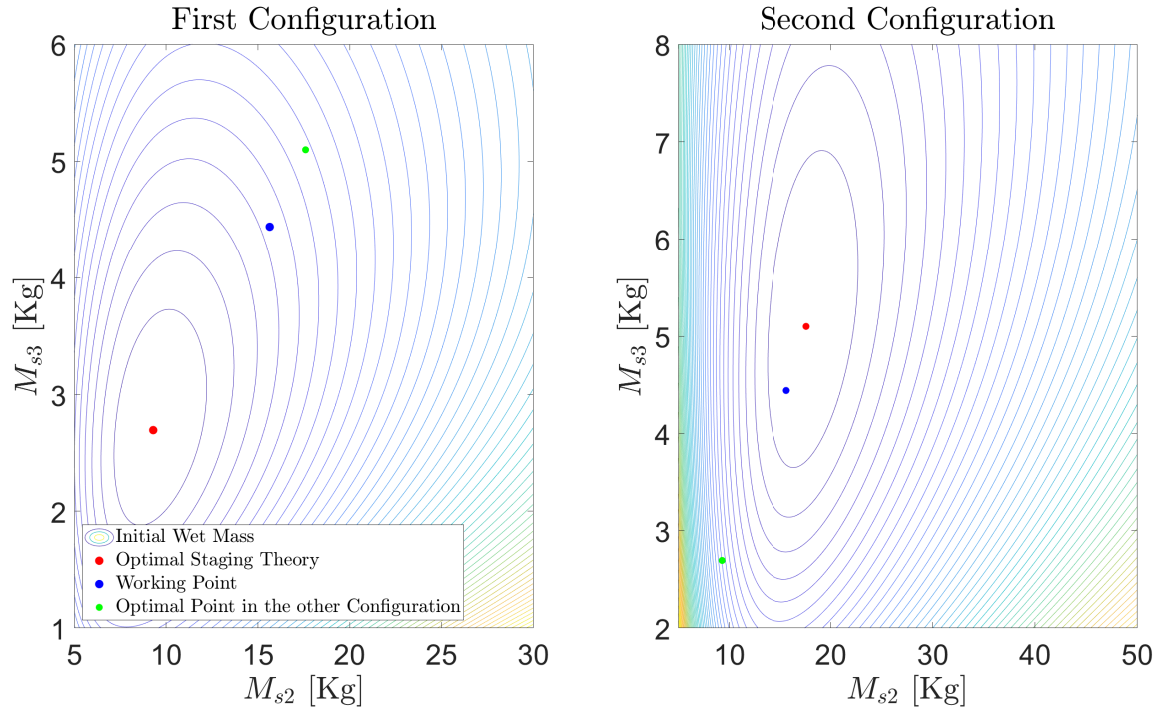
Figure 2.7: Staging Validation

Looking at figure 2.7, it is easy to notice that the results from the optimal staging theory (red dots) match perfectly the minima of both configurations, the green dot represent the optimal value in the other configuration and the blue one shows the solution selected for this work. The blue dot in fact is somewhere in between the two optimal results which is an expected outcome. It can be proved that the solutions of the Pareto front analysis shown in figure 2.6, identified by the black line, are part of an hypothetical curve joining the two minima.

Chapter 3

Propulsion System Design

The propulsion system is a key part in the design of a launch vehicle, maybe the most important one. A good propulsion selection can lead to high engine efficiency, that is strictly linked to the initial mass of the launcher. Many different propulsion choices are available, from liquid to solid passing from hybrid, each one has its own advantages and drawbacks. In this chapter the propulsion system is selected and designed, the guesses used in chapter 2 are checked and at the end, an interesting solution is proposed for further development. The multidisciplinary workflow can be seen in figure 1.5.

3.1 Propulsion System Choice

As expressed in chapter 1, the market of air launched rockets and small launchers usually adopts simple propulsion solutions like solid rocket motors or liquid rocket engines powered by RP-1 and LOX for their simplicity, reliability and energy density.
The first important design choice, is the propellant couple selection.
The driving aspects for this choice are shown in the following list:

- **Simplicity**
  Since the size of the launcher is very small, a simple design is highly desirable. Simplicity can also mean cost effective, and it is also desirable from the aircraft interfaces point of view.

- **Storability**
  A standard launcher is usually fueled up a few minutes before lift off directly on the launch pad. An air launched rocket instead is fueled up and then integrated on the aircraft several hours before its ignition depending on the launch location. This may induce a lot of issues from both the thermal control and the propellant boil-off point of view. A storable solution is therefore desirable.

- **Low Toxicity**
  The usage of hazardous propellants is always not advisable. In particular in air launched

rockets, having a very dangerous fluid stored a few meters from the pilot is definitely a big issue. The world is currently moving towards the removal of hydrazine-based fuel from in-space activities, for instance ESA Clean Space Office is dealing with that problem [24]. Nowadays the only launcher operational that works with toxic propellants is the Russian Proton [25].

- **Efficiency**
  Efficiency is always desirable in a space launcher. An high efficiency can lead to a low initial wet mass as explained in chapter 2. The efficiency for a launcher can be seen in terms of engine efficiency (Specific Impulse I_{sp}) and stage efficiency (Structural mass index ξ).

- **Throttlability**
  The absence of the possibility of controlling the thrust magnitude, especially for the upper stage, can lead to a low orbit insertion precision. Nanosatellites usually do not have any primary propulsion system onboard, this means that correcting a wrong orbit is harder if not impossible. Moreover since the lifetime of those satellites is actually very short, a poor orbit insertion can jeopardize the entire mission.

- **Heritage**
  The heritage of existing air launched rockets must be considered as well.

Table 3.1 shows the list of propellant couples taken into consideration for this analysis [1].

Propellant Couple	ξ	I_{sp}	Toxicity	Storability	Throttlability
$CH_4 + LO_2$	-	380 s	Low	Both Cryo	Yes
$RP-1 + LO_2$	0.07-0.09	340 s	Low	LO_2 Cryo	Yes
$LH_2 + LO_2$	0.08-0.12	420 s	Low	Both Cryo	Yes
Solid	0.05-0.07	290 s	Low	Room Temp	No
$MMH + N_2O_4$	0.05-0.07	310 s	High	Room Temp	Yes

Table 3.1: Propellant Couple Choice [5] [8]

Liquid Rocket Engines (LREs) are more efficient than solid propulsion in terms of specific impulse, moreover all of them have the throttling capability. The drawbacks are due to higher complexity, and storability issues. The only LRE that is storable at room temperature is based on hydrazine, which is highly toxic.

In terms of structural mass index and overall simplicity Solid Rocket Motors are way more efficient, they can also grant higher structural resistance, thus the rocket can withstand higher accelerations

---

[1]MethaLox couple does not have any ξ since there is no rocket that ever used that couple. However it would be in line with the other liquid couples

improving its trajectory-related efficiency. Moreover they can be stored for a long period of time at room temperature. As regarding the heritage, the Pegasus launcher uses a 3 stage solid rocket motors as explained in section 1.1.

For the reasons just pointed out, the propulsion system of every stage is a solid architecture.

More considerations are done regarding precision orbit insertion and possible future different architectures in section 3.4.

3.2   Propulsion Performances

The propellant composition choice is the first step to go through. Several solutions exist but many currently used solid rocket motors adopt a mixture of Ammonium Perchlorate (AP) as oxidizer, a binder and some energetic additives.

The propellant composition selected for this study is based on AVIO technology, the mixture is named HTPB 1912. It uses AP as oxidizer, Hydroxyl-Terminated PolyButadiene (HTPB) as a binder and Aluminum (Al) as energetic additive, the mass percentage of such a mixture is the following [26]:

$$\begin{cases} AP = 69\% \\ HTPB = 12\% \\ Al = 19\% \end{cases} \tag{3.1}$$

As expressed in figure 1.5, the propulsion system design provides engine parameters that are needed for the incoming trajectory design explained in chapter 4. The propulsion parameters to be derived or assumed in this section are the following:

- Combustion Chamber Pressure P_c

- Specific Impulse I_{sp}

- Characteristic Velocity C^*

- Thrust T

- Nozzle throat and exit area A_t, A_e

- Rocket Length and Diameter l, d

The combustion chamber pressure is the first parameter to fix. It has a very important role in a solid rocket motor design: first of all it provides effects into chemical reactions inside the combustion chamber, but most importantly it drives the burning rate by means of the Vieille law [8].

More considerations are needed in terms of grain geometry and burning rate; for simplicity the combustion chamber pressure is taken as 50 bar as a reference value coming from typical operational solid rocket motors [8].

After the pressure another crucial parameter is the specific impulse. There are two different ways to estimate it that have been followed in this work:

- Look at already existing SRMs, and estimate the specific impulses based on those motors.

- Estimate the ideal values using a thermochemical code. Then that value is adjusted to account for all the different losses.

Starting from the first approach: table 3.2 reports every motors currently being developed and built by AVIO with its corresponding performances like specific impulse and altitude of ignition.

| Parameters | Thrust | $I_{sp} - vac$ | t_b | h_{ign} |
Units	kN	s	s	Km
P120 C	4500	278.5	132.8	0
P80	3015	280	110	0
Zefiro 23	1120	287.7	77.1	52
Zefiro 40	1304	293.5	92.9	52
Zefiro 9	317	295.9	119.6	127

Table 3.2: AVIO Solid Rocket Motors [9] [10]

So a good estimate of specific impulses based on that values can be the following:

$$
\begin{cases}
I_{sp1}^{avio} = 280s \\
I_{sp2}^{avio} = 293s \\
I_{sp3}^{avio} = 295s
\end{cases}
\tag{3.2}
$$

The second approach exploits the Chemical Equilibrium and Application (CEA) software developed by NASA [27]. Given a propellant composition, the combustion chamber pressure and the expansion ratio of the nozzle, the tool provides all thermochemical values and performances of the engine in the ideal case. The propellant composition and the chamber pressure are defined above, while the expansion ratios are hereinafter introduced. A shifting equilibrium is preferred with respect to a frozen model because the aim is to get the perfect ideal value. The results can be seen in (3.3)

$$
\begin{cases}
I_{sp1}^{id} = 301.2s \\
I_{sp2}^{id} = 313.3s \\
I_{sp3}^{id} = 317.4s
\end{cases}
\tag{3.3}
$$

As expected, those impulses are way greater than the estimated ones. In order to account for all the losses (two phase flow, divergence flow, chemical recombination, boundary layer, throat erosion etc...) two possibilities are present.

The first solution is to model of all the different losses, but at this stage of the development is not meaningful and too much complex to go through.

The other possibility is to take the efficiency of classical solid rocket motors from literature; and in this case the work of Landsbaum, Salinas and Leary comes in handy [28]. They compared experimental with ideal values of specific impulses from different solid rocket motors in order to check the validity of a losses model. The total efficiency resulting from their analysis ranges between 0.92 and 0.93: so the specific impulses of the motors simulated before with CEA can be adjusted, to get the values shown in equation (3.4).

$$
\begin{cases}
I_{sp1}^{cea} = 279s \\
I_{sp2}^{cea} = 290s \\
I_{sp3}^{cea} = 293s
\end{cases}
\tag{3.4}
$$

As can be noticed, the estimate is very precise with around 1% of error compared to the AVIO values (3.2).

The selection of the Thrust is another very important variable to define in a propulsion design: an high trust-to weight (T/W) ratio reduces gravity and drag losses but provokes the increase of the dynamic loads which is detrimental for the structure and the payload. Usual manned launchers have T/W around 1.2, but an air launched rocket can afford higher values [5]: taking as a reference the Pegasus XL, the thrust value for each stage is set as follows [7]:

$$
\begin{cases}
T_1^I = 2g_0 M_0^I \\
T_1^{II} = 2g_0 M_0^{II} \\
T_2 = 3g_0 \frac{M_{0_2}^I + M_{0_2}^{II}}{2} \\
T_3 = 3g_0 \frac{M_{0_3}^I + M_{0_3}^{II}}{2}
\end{cases}
\tag{3.5}
$$

The T/W ratio is imposed equal to 2 for the first stage, and 3 for the other stages. Since the second and third stages have different initial masses across the two rocket configurations, as explained in section 2.3, a mean has been considered.

Then, some brief considerations on the nozzle must be done to complete the propulsion analysis. First of all the throat area A_t is computed using the data previously assumed, in equation (3.6) C^* represents the characteristic velocity which is a parameter of merit of the combustion chamber performance; this has been computed along with the specific impulse using the CEA tool and it results 1578 m/s.

$$
A_t = \frac{C^* T}{P_c I_{sp} g_0}
\tag{3.6}
$$

It is worth pointing out that the throat area, in particular in SRMs, changes in time. Regenerative or film cooling cannot be applied like in LREs, so the only solution available not to melt the nozzle is to cover the throat with ablative materials like graphite; those however increase the throat area and change the motor performances during flight. For simplicity those effects are not considered in this work and the throat area is assumed constant throughout the whole burn.

Once defined the throat area, the next step is to select the expansion ratio of the nozzle. Usually it is optimized at the altitude of ignition, but that is true only in case of atmospheric flight; for vacuum stages it is usually fixed based on literature studies [8].

The first stage ignites at 11 Km altitude as explained in section 1.4, so from the external pressure and the specific heat ratio k coming again from CEA code, it is possible to compute the nozzle expansion ratio by means of the following isoentropic relation.

$$\frac{A_t}{A_e} = \frac{1}{\epsilon} = \left(\frac{k+1}{2}\right)^{\frac{1}{k-1}} \sqrt{\frac{k+1}{k-1}} \left(\frac{P_e}{P_c}\right)^{\frac{1}{k}} \sqrt{1 - \left(\frac{P_e}{P_c}\right)^{\frac{k-1}{k}}} \tag{3.7}$$

The other two expansion ratios are instead selected from literature because a nozzle is never optimized in vacuum. All the 3 expansion ratios are reported in the following equation.

$$\begin{cases} \epsilon_1 = 44 \\ \epsilon_2 = 80 \\ \epsilon_3 = 100 \end{cases} \tag{3.8}$$

The last part of the nozzle regards its shape: by assuming a double truncated cone shape which is by far the simplest choice, it is possible to compute the length of the divergent part. The convergent is considered to be inside the rocket case and in any case it does not give an high contribution to the overall length. Assuming a typical divergent angle θ_{dv} of about 20 degrees, the length is found as follows.

$$l_{nozz} = \frac{r_e - r_t}{\tan \theta_{dv}} \tag{3.9}$$

The shapes and dimensions of the nozzles are shown in figure 3.1 and compared to the rocket body.

Now the next step is to compute the rocket dimensions, given the overall propellant mass from the staging section, the volume of this latter is immediately found with its density imposed at $\rho_P = 1600\ Kg/m^3$.
η_v is the ratio between the propellant volume and the case volume, a typical value from literature is 0.9 [29].
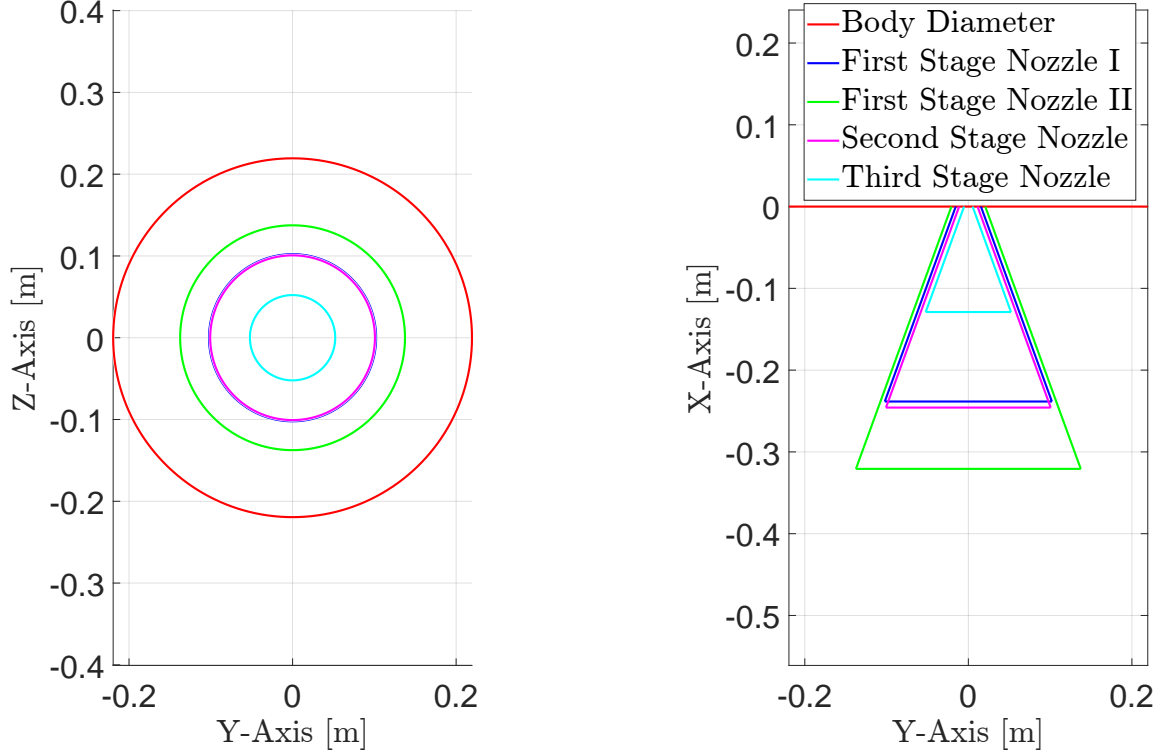
Figure 3.1: Nozzle Dimensions

$$\eta_v = \frac{v_P}{v_{case}} \tag{3.10}$$

$$fineness = \frac{4v_{tot}}{\pi d^3} + \frac{l_N}{d} + \frac{l_{nozz}}{d} \tag{3.11}$$

Standard fineness ratios for space launcher vary from 5 to 25, having the overall rocket volume and imposing a fineness ratio allows to solve equation (3.2) and compute the diameter D [3]. Constraints on the diameter and length are introduced by the carrier aircraft capability and the adapter dimensions.

The maximum length acceptable by the Eurofighter Typhoon is around 6 meters, so no problem from this point of view, while the payload deployer has dimensions a little bit greater than the CubeSat inside (assumed as 20% more), for instance a 6U CubeSat has a deployer of around 12x24x36 cm. Also the dynamic envelope of the fairing must be considered, so a rough estimation of the minimum diameter is 30 cm [21] [4].

Table 3.3 reports the propulsion performances of each stage as well as the whole rocket in both configurations.

Parameters	L	D	ϵ	T	I_{sp}	A_e
Units	m	m	$-$	kN	s	cm^2
1st Stage I	1.61	0.44	44	11.6	279	328
1st Stage II	3.40	0.44	44	21.1	279	594
2nd Stage	0.86	0.44	80	6.5	290	319
3rd Stage	0.24	0.44	100	1.4	293	85

Table 3.3: Propulsion Performances Overview

3.3   Masses Breakdown

As shown in the chapter 2, mass indexes are set as an initial guess for each stage.
A simple analytical procedure to compute the structural mass given the propellant mass, and to check the validity of those guesses is here introduced.

This procedure is very important especially for the 3rd stage, because it has a propellant mass too low to make comparison with existing solid rocket motors as can be noticed in table 2.3.
So estimating a structural mass index is very difficult and could result in outcomes very far from classical values.
The reference for the following models is the Humble book [29].

The inert mass of each stage can be divided into 6 main contributions:

$$M_s = M_{ign} + M_{ins} + M_{case} + M_{noz} + M_{tvc} + M_{misc} \tag{3.12}$$

Where, M_{ign} is the mass of the igniter, M_{ins} is the contribution of the thermal insulator, M_{case} is simply the propellant case, M_{noz} is the nozzle mass and finally M_{tvc} is due to the presence of a thrust vector control system. M_{misc} is made by every other element not considered in that list.

The first important contribution is the case. The structure must withstand inertia loads as well as the high pressure inside the vessel. Existing SRMs take advantage of the filament winding technology with pre-impregnated carbon fiber to build up SRM cases: a lighter solution with respect to metal vessels can then be realized. Taking advantage of this technique to make more efficient structures is crucial in the propulsion design, it provides mass indexes ξ lower than classical metal casings. Those facts give meaning to the choice of carbon composite casing in this work.

The case thickness is given by the thin walled formula where the main load is introduced by the combustion chamber pressure P_c.

$$t_{case} = f_s \frac{P_c R_{case}}{F_{tu}} \tag{3.13}$$

Where f_s is the safety factor imposed at 1.25 and F_{tu} is the ultimate tensile strength of carbon fiber, 600 MPa. Imposing a cylindrical shell with a planar bulkhead in front, the mass of the case can be immediately found.

The igniter is a device that starts the combustion process throughout the grain, solid rocket motors usually use a pyrogenic igniter, which is basically a small SRM that provides hot gases and pressure if triggered by an electrical current. A correlation to compute its mass is the following:

$$M_{ign} = 0.0138 v_{port}^{0.571} \tag{3.14}$$

Where v_{port} is the volume of the central port computed again my means of a correlation.

$$v_{port} = v_p \left(\frac{1}{\eta_v} - 1 \right) \tag{3.15}$$

Thermal insulation is critical in a solid rocket propulsion system, temperature inside the combustion chamber reaches around 3500 K that is too high to withstand for any casing, in particular if made by composite material. Standard insulation materials are rubber-based with low thermal conductivity and are around 1cm thick.
A correlation still taken from Humble suggests half of the case mass.

The nozzle is very difficult piece of hardware to model, it is made by many different parts with different materials. A very rough correlation can be set up but further analysis are required to get more precise values.

$$M_{noz} = 2.56 \times 10^{-5} \left[\frac{(M_p C^*)^{1.2} \epsilon^{0.3}}{P_c^{0.8} t_b^{0.6} \tan(\theta_{cn})^{0.4}} \right]^{0.917} \tag{3.16}$$

Where θ_{cn} is the angle of the converging nozzle, and t_b is the burning time.

Like the nozzle, the thrust vector control is hard to model, as a first approximation it can be thought to scale like the nozzle itself. So as Humble's book suggest, half of the nozzle mass can be a good first estimation.

$$M_{tvc} = \frac{1}{2} M_{noz} \tag{3.17}$$

At last there are all the elements which are not included in the just mentioned contributions, like the interstages for instance, to take those into account this miscellaneous mass is considered to be 10% of the total mass computed so far.

$$M_{misc} = 0.1(M_{ign} + M_{ins} + M_{case} + M_{noz} + M_{tvc}) \tag{3.18}$$

Table 3.4 shows all the masses breakdown of each stage and the entire launcher in both configurations.

Parameters	M_p	M_{case}	M_{ins}	M_{ign}	M_{noz}	M_{tvc}	M_{misc}	M_s
Units	Kg	Kg	Kg	Kg	Kg	Kg	Kg	Kg
1st Stage I	346.8	13.46	7.81	4.27	2.65	1.32	3.17	34.8
1st Stage II	778.9	28.95	15.93	6.78	5.73	2.86	6.32	69.5
2nd Stage	156.4	6.64	4.43	2.71	1.43	0.71	1.82	20
3rd Stage	27.8	2.03	1.60	1.01	0.25	0.13	0.62	6.8
Full Rocket I	531	22.13	13.84	7.99	4.33	2.16	5.60	61.6
Full Rocket II	963	37.62	21.96	10.50	7.40	3.70	8.75	96.3

Table 3.4: Mass Breakdown Budget

In table 3.5, the mass indexes assumed in the staging design are compared with the ones just computed. First and second stage have a low error, meaning that the assumption was good enough.

Parameters	Assumed ξ	Computed ξ
Units	-	-
1st Stage I	0.09	0.0902
1st Stage II	0.09	0.0830
2nd Stage	0.1	0.1042
3rd Stage	0.16	0.1755

Table 3.5: Mass Indexes Comparison

What it turns out is that the structural mass index of the third stage after many iterations approaches the value of 0.21, which is even higher than that for tactical missiles [3]. The meaning could be that the models used so far are based on existing rocket motors far bigger than the third stage, therefore those correlations are not perfectly suitable for that motor. A good compromise is to fix it at 0.16, between the space launchers world ($\xi \sim 0.1$) and the tactical missile value ($\xi \sim 0.2$).

3.3.1 Review of Results

To assess the validity of the obtained masses breakdown, results are compared to values of existing motors. The motors considered are: RSRM (Reusable Solid Rocket Motor), ASRM (Advanced Solid Rocket Motor) from the Space Shuttle, Titan IV, SRMU, Castor IVA, GEM, ORBUS 21, ORBUS 6E, Star 48B, Star 37XFP, Star 63D, Orion50SAL, Orion 50, Orion 38 [29].
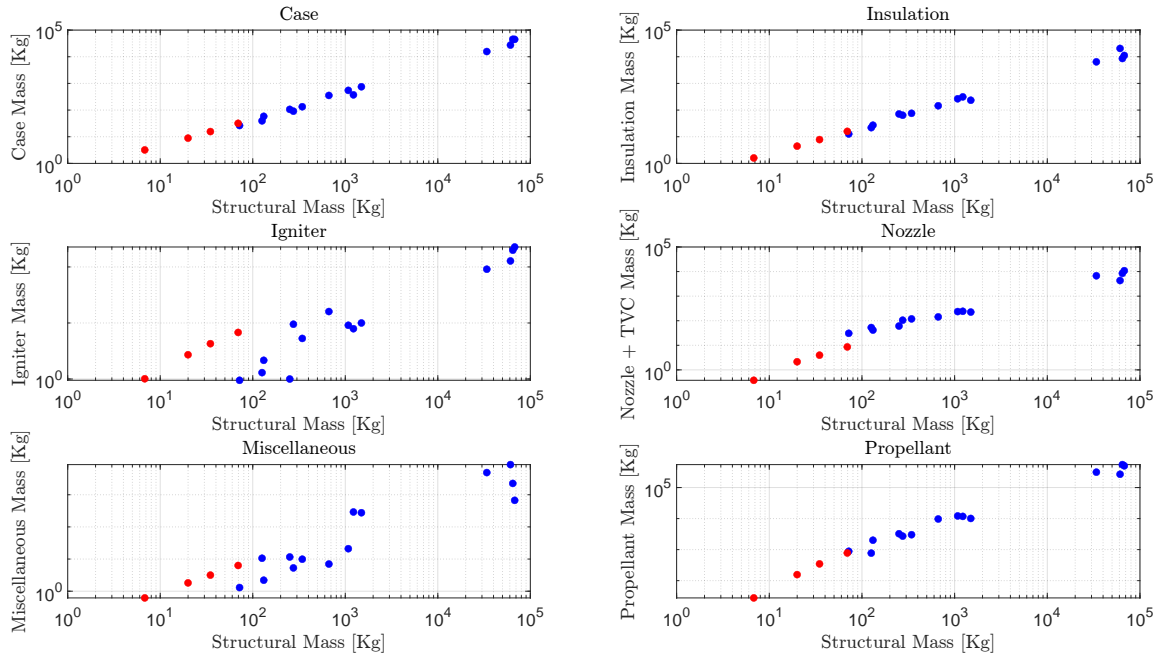

Figure 3.2: Breakdown Masses Validation

In figure 3.2, the blue dots represent the reference motors while the red ones show the 4 motors preliminary sized in this chapter. As can be noticed, case, insulation, nozzle and overall ratio between propellant and structures are well in line with the references. Igniter and miscellaneous instead varies a little bit, but it must be noticed that even the reference motors are more sparse than the other contributions. Therefore it is a fully acceptable result.

3.4 Hybrid Rocket Engine Alternative

Performing the orbit insertion with a solid upper stage can lead to a rough altitude precision, liquid rocket engines instead have the possibility of throttling the engine, and in case, shut it down when the velocity reaches the desired level with no particular issue. Looking at the two air launched rockets mentioned in section 1.1, the Pegasus XL with its solid third stage has an accuracy of $\pm 45\,km$ altitude and $\pm 15\,km$ with the addition of its hydrazine fourth stage, while LauncherOne

has a liquid second stage and its altitude accuracy is $\pm 15\, km$ [7] [6].

As a further reference, it is here reported that the VEGA launcher which is made of 3 solid rocket motors, works with a 4th stage that uses a liquid engine powered by hydrazine-based storable propellant; this allows VEGA to get, an altitude accuracy of $\pm 15\, km$ [10].

This work does not want to deal with toxic propellant, so the choice of a liquid upper stage powered by hydrazine has been discarded; classic liquid rocket engines using liquid oxygen as oxidizer are way too complex and can lead by many issues already discussed. Liquid green monopropellant based on Ammonium DiNitramide (ADN) may be an alternative, however no benefit exists from both the specific impulse point of view and the complexity that would derive from.

One very interesting solution is represented by the hybrid rocket engine (HRE). This engine can throttle up and down allowing a better orbit insertion than a solid, it has higher specific impulse and it does not introduce too much complexity in the design. Numerous works regarding the application of an HRE to air launched vehicles has already been done, this stresses the feasibility of such a concept [30] [31] [32] [33]. Moreover, the only hybrid rocket engine nowadays operational, is being used by the Virgin Galactic SpaceShipTwo vehicle, which, by the way, is aero-deployed.

The choice on the propellant couple falls over a classic HTPB as fuel and hydrogen peroxide as oxidizer. HTPB is a very common choice in hybrid rocket propulsion, it is very reliable, well known, and can lead to high specific impulses even in the absence of metallic additives. Most of the studies uses liquid or gaseous oxygen as oxidizer, but this choice leads to the storability and boil-off problems addressed before. Hydrogen peroxide instead is storable, can gives specific impulses comparable to gaseous oxygen if used in high concentration, and moreover it can be used as monopropellant for attitude control thruster as many studies proved it [34].

Standard architectures of HREs are mainly composed by a cylindrical shaped fuel grain with one or many ports where the oxidizer is injected in. This is done because one of the biggest issue of HREs is the low regression rate and therefore thrust. One interesting alternative could be a so-called Vortex Flow Pancake (VFP) configuration, where two fuel disks are placed on the top and bottom of the combustion chamber, and the oxidizer is injected in between forming a vortex flow. Another important feature of this exotic configuration, is the geometric ration between length and diameter which is below 1. Looking at the dimensions of the third stage reported in table 3.3, it can be noticed a length over diameter ratio of about 0.5. This gives further meaning of such a choice.

As already explained, this work is limited to near term feasible concept, therefore since the HRE propulsion has a Technology Readiness Level (TRL) below 6/7 this section has only the aim to show what could be achieved with such a technology and propose a future upgrade of the launcher. Therefore the following chapters use the third stage solid rocket motor designed in section 3.2.

First of all, a propulsion analysis is performed using again the CEA code. It turns out that at O/F of 6.5 (stoichiometric ratio) the specific impulse is around 330 s, literature suggests that using gaseous oxygen instead of hydrogen peroxide the specific impulse can get up to 350 seconds [35]. However, if the concentration of the hydrogen peroxide is high enough ($>95\%$), it can be compared as a first approximation to the results of gaseous/liquid oxygen [36].

Together with this value, a structural mass index is assumed from literature studies (despite being applied to classic hybrid configurations); further analysis are required to better estimate that value for VFP configurations. This, in general, is higher than the solid equivalent. Hybrid rocket engines require, case, insulation and nozzle that can be considered at a first approximation the same as SRMs; the usage of hydrogen peroxide allows saving the mass of the igniter since the propellant couple are hypergolic [36]. However HREs require the oxidizer tank as well as all the pressurizing gas and pipe lines that increase the overall inert mass. Preliminary analysis of HREs used in air to orbit applications, suggest a structural mass index ξ ranging between 0.22 and 0.28, therefore, the value selected for this preliminary work is 0.25 [31] [33].

Using this index together with the computed specific impulse it is possible to re-calculate the staging design with the multiconfiguration strategy explained in chapter 2. Table 3.6 reports the obtained results; the initial masses of the launchers in the two configurations are slightly lower than the standard rockets with solid upper stages.

Parameters	M_p	M_s	M_{tot}
Units	Kg	Kg	Kg
1st Stage I	353.7	31.8	385.5
1st Stage II	781.5	70.3	851.8
2nd Stage	149	14.9	164.3
3rd Stage	22.5	5.6	28.1
Full Rocket I	525.5	52.4	588.6
Full Rocket II	953.3	90.9	1064

Table 3.6: Staging Results with Hybrid Third Stage

One of the major aspect of an HRE that must be taken into account is the O/F shift during the burn, and, if the oxidizer mass flow rate is kept constant, also a thrust shift. A simple procedure can be settled to estimate that shift get more insights about this particular solution.

The first, very important equation is the fuel regression rate as a function of the total mass flux. The coefficients and the definition of mass flux in a VFP engine are taken from [37]. Those are referred to gaseous oxygen, but assuming an hydrogen peroxide concentration over 95% it is possible to consider true those relations as a first approximation.

$$r_b = 1.08 \times 10^{-4} G_{tot}^{0.595} \tag{3.19}$$

Where G_{tot} is the total mass flux composed by the fuel and the oxidizer. The cross section area is defined by the radius of the combustion chamber (assumed as 80% as the rocket radius) times the height which varies with time. The engine scheme can be seen in figure 3.3 to better understand this procedure.

$$G_{tot} = G_{ox} + G_f = \frac{\dot{m}_{ox}}{R_c H_c} + \frac{\dot{m}_f}{R_c H_c} \tag{3.20}$$

The fuel mass flow rate is a function of the regression rate and the burning area, assumed as the surface of the two disks decreased by 10% to account for the nozzle aperture.

$$\dot{m}_f = \rho_f A_b r_b \tag{3.21}$$

Imposing an initial oxidizer mass flow rate and combustion chamber height, it is possible to simulate the burning process of the fuel disks and get out propulsion performances as well as undesired effects such as the O/F shift.

Assuming a specific impulse of 330 s, a thrust equal to the nominal value of the third stage SRM, it is possible to compute the mass flow rate and, imposing an O/F of 6.5, the mass flow rates of oxidizer and fuel.
An initial combustion chamber height is assumed, H_0 then the fuel mass flow rate can be computed solving numerically equation (3.22) and get $\dot{m}_f$.

$$\dot{m}_f = \rho_f A_b 1.08 \times 10^{-4} \left(\frac{\dot{m}_{ox}}{R_c H_k} + \frac{\dot{m}_f}{R_c H_k} \right)^{0.595} \tag{3.22}$$

Then, the regression rate can be computed and used to update the combustion chamber height with a discretized time step Δt.

$$H_{k+1} = H_k + 2 r_b \Delta t \tag{3.23}$$

Finally the performances can be found.

$$\begin{cases} T = I_{sp} g_0 \left(\dot{m}_f + \dot{m}_{ox} \right) \\ O/F = \dot{m}_{ox}/\dot{m}_f \end{cases} \tag{3.24}$$

The specific impulse is a function of the O/F ratio, the values are taken from CEA simulation.
If the initial height is chosen wisely, at the end of the simulation both the oxidizer and the fuel web thickness t_{web} are over at the same time. Therefore the initial height H_0 is changed until that condition is completely satisfied.

The resulting performances are shown in figure 3.4. It can be seen that the O/F ratio changes a little during the burn, with a mean very close to the stoichiometric relation, therefore an high efficiency is expected throughout the whole burn. The thrust instead has not the mean close to the nominal value, however the variation is always below 2% of the nominal this means a good result overall.
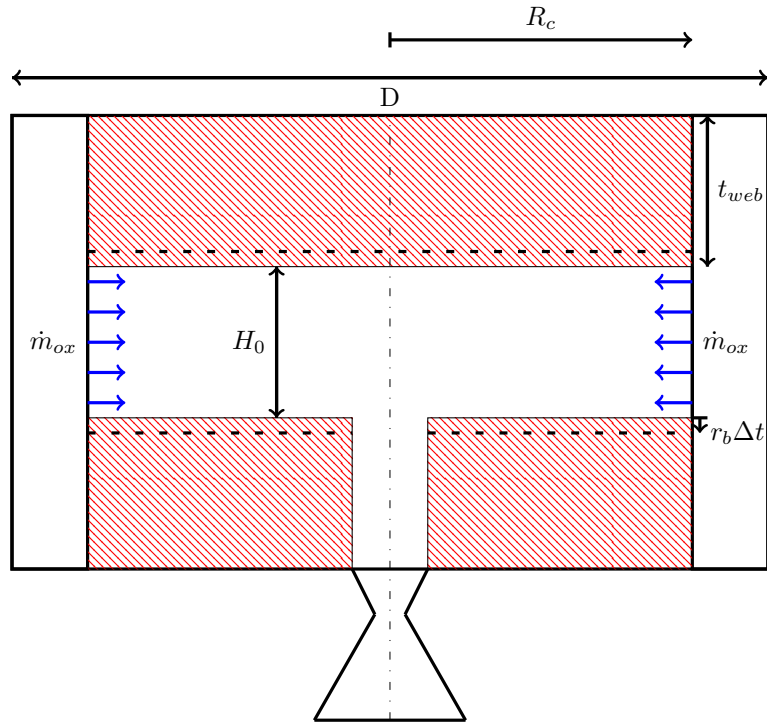
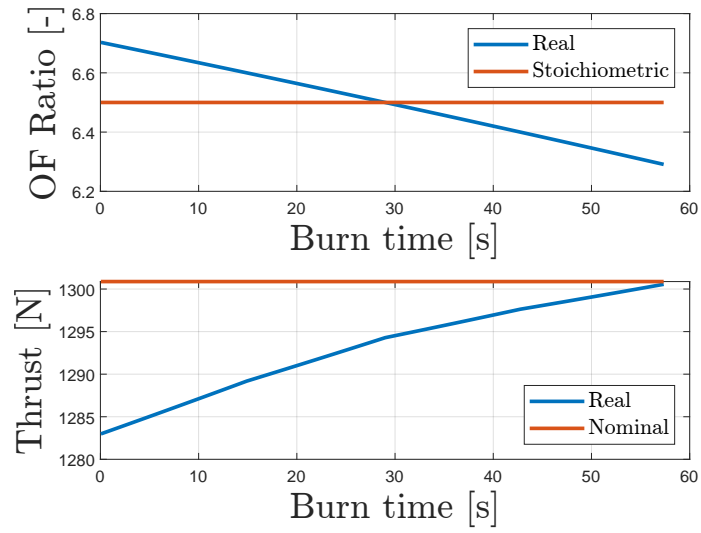Figure 3.3: VFP Hybrid Rocket Engine Scheme

Figure 3.4: Hybrid Performances

Finally, the resulting L/D of the combustion chamber results of around 0.8-0.9. Standard VFP Hybrid rocket engines usually have those value even smaller than that. It can be proved that if the thrust is increased the L/D ratio can decrease down to 0.5 or even below.
To sum up, in the following list are reported the pros and cons of such a solution:

PROS

➤ Higher I_{sp} (up to 350 s)

➤ Possibility of using H_2O_2 as monopropellant for RCS thrusters

➤ Throttlability $\implies$ Precision Orbit Insertion

➤ Possibility of 3rd stage controlled de-orbit

➤ Cracks Resistance

➤ Innovative Solution

CONS

➤ Higher Complexity

➤ Higher ξ

➤ Low TRL

➤ O/F Shift

Chapter 4

Trajectory and Launch Location

Once the staging and propulsion parameters are computed, the next step is to find out if those values allow reaching the desired orbit with a good trajectory. First of all a simple 3DOF model is implemented to simulate the rocket ascent trajectory, this could lead results such as a reference trajectory useful in the following 6DOF model, and considerations regarding the launch location and the possible threat given by the stages fall down. Furthermore, as explained in section 1.3, an iteration can be done to select the best propulsion parameters that achieve the best trajectory possible.

The trajectory selected for this launcher makes use of a free coasting phase between the second stage burnout and the third stage ignition, that exploits the gravity turn to decrease the flight path angle and to eliminate the vertical component of the velocity which is not desirable once in orbit. Pegasus XL does the same between its second and third stage burn, while LauncherOne does a small ballistic part between its two second stage ignitions.

4.1 3DOF Model

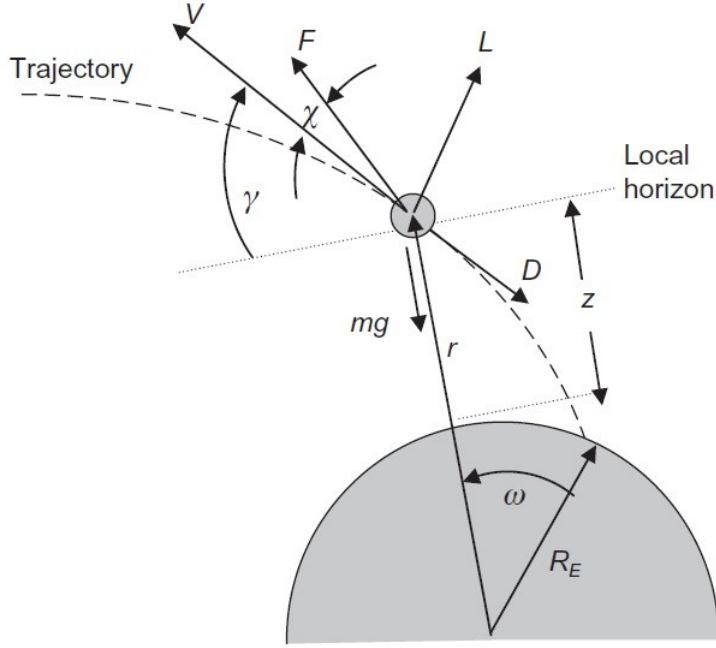For the purposes just explained a very simple point mass 3 degrees of freedom model can be implemented [5].

Figure 4.1: 3DOF Model Scheme [5]

The reference system is a round Earth centered non rotating model, the 3 degrees of freedom are: V velocity, γ flight path angle and r distance from the center of the planet with the addition of the mass m.

The set of Ordinary Differential Equations (ODE) to be integrated is the following:

$$\begin{cases} \dot{V} = T/m \cos\chi - D/m - g\sin\gamma \\ V\dot{\gamma} = T/m \sin\chi - g\cos\gamma + \frac{V^2}{r}\cos\gamma \\ \dot{r} = V\sin\gamma \\ \dot{x} = \frac{V}{r}R_E\cos\gamma \\ \dot{m} = -\frac{T}{g_0 I_{sp}} \end{cases} \tag{4.1}$$

Where R_E is the radius of the Earth and g the gravitational acceleration computed as:

$$g = \mu/r^2 \tag{4.2}$$

While D represents the drag computed in the following way.

$$D = \frac{1}{2}\rho V^2 S C_D \tag{4.3}$$

S is the cross section area of the rocket, ρ is the atmosphere density which is function of the altitude

and finally C_D is the drag coefficient. As a first estimate this can be considered to be constant, however a more refined model is explained in chapter 5.

The integration algorithm is a variable-step, variable-order (VSVO) Adams-Bashforth-Moulton PECE solver, with both relative and absolute tolerances set as 10^{-9}.
Since the burning time of each stage can be easily computed:

$$t_{b_i} = \frac{M_{p_i} I_{sp_i} g_0}{T_i} \qquad i = 1...3 \tag{4.4}$$

The only variables to be defined are:

- $\chi_i(t)$ thrust deflection angle as a function of time
  for $i = 1..3$

- $t_{coasting}$ time between second stage burnout and third stage ignition

It is important to point out that χ angle is considered from the velocity vector, therefore is not the real angle at which the nozzle is tilted as can be seen in figure 4.1. For simplicity the χ angle of each stage is considered linear with the burning time: so 2 variables are required for each one.

$$\chi_i = \chi_i^c + \chi_i^l (t - t_{0i}) \tag{4.5}$$

Where the superscripts c and l represent respectively the constant contribution and the linear one. One possible way to compute those 7 elements such that the rocket is able to reach orbit, is by means of an optimization. In this case the final orbit constraints are transformed into a scalar cost function to be optimized. This cost function is made up by a sum of many contributions that imply a good orbit insertion.
The result trajectory must arrive at 500 km altitude at the end of the simulation having flight path angle equal to 0 and moreover the maximum altitude shall not exceed the orbit one to avoid overshoot problems.
Therefore the cost function to be minimized is the following:

$$J_{3DOF} = \mid r_{end} - r_{orbit} \mid /r_{orbit} + \mid \gamma_{end} \mid /\pi + \mid r_{max} - r_{orbit} \mid /r_{orbit} \tag{4.6}$$

The final velocity is not part of the cost function since it depends on the staging process explained in chapter 2. The aim of the trajectory optimization is to arrive at the desired orbit with the highest velocity possible. The velocity constraint is therefore treated in a separate manner.
In chapter 5 the final trajectory velocity is computed with an higher accuracy. If then it is higher than the orbital one, the ΔV margin assumed in chapter 2 would be decreased accordingly. The opposite is done in case of lower velocity. This constraint is therefore solved through an iterative procedure.
The vector of independent variables is the following:

$$\underline{X}_{3DOF} = \begin{bmatrix} \chi_1^c & \chi_1^l & \chi_2^c & \chi_2^l & \chi_3^c & \chi_3^l & t_{coasting} \end{bmatrix} \tag{4.7}$$

61

This optimization makes use of a particle swarm method, similar to the one used for the multiconfiguration staging design in section 2.3. Since it is a global optimization, lower and upper bounds must be set up for each variable. Those can be seen in table 4.1.

Variable	Upper Bound	Lower Bound
χ_i^c	10 deg	-10 deg
χ_l^c	0.115 deg/s	-0.115 deg/s
$t_{coasting}$	450 s	250 s

Table 4.1: Trajectory Optimization, Lower and Upper bound of Independent Variables

An hard constraint is also introduced in the optimization to avoid the χ angle to overcome the upper and lower bounds. It can be proved that decreasing the initial flight path angle, leads to an increase in the χ angle required. This angle is then linked to the TVC deflection angle in chapter 5 which has a well defined technological limit at 8-10 degrees [8]. This underlines the hypothesis of an high initial pitch angle done in section 1.4.

The resulting trajectory can be seen in figure 4.2, while figure 4.3 shows velocity, flight path angle and χ as a function of time. As can be noticed the flight path reaches 0 at the end, and the altitude reaches the orbit one as well without any overshoot. This can be seen in more details in table 4.2, where the 3 components of the J cost function (4.6) are shown. This underlines the precision level obtained in the optimization process.

Configuration	J_1	J_2	J_3
I Configuration	-1.1×10^{-10}	-1.4×10^{-9}	-1.1×10^{-10}
II Configuration	6.3×10^{-9}	3.7×10^{-7}	6.3×10^{-9}

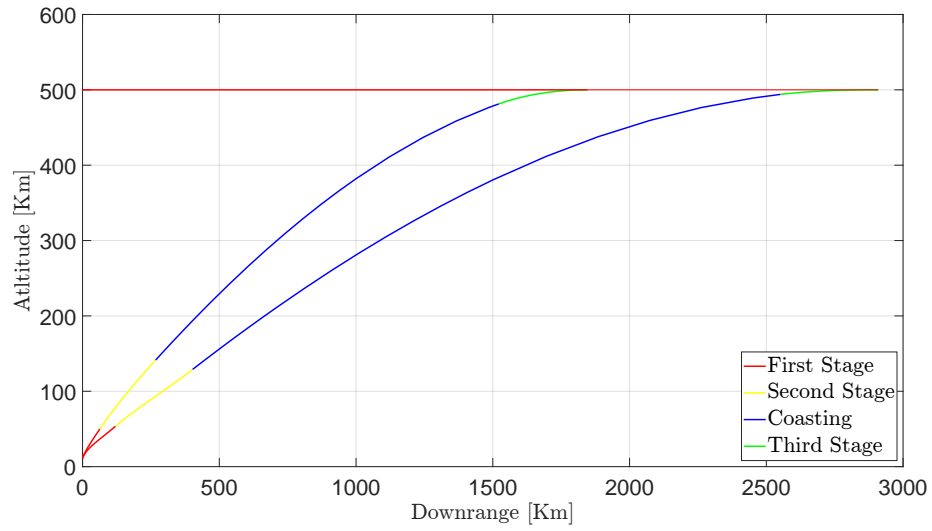Table 4.2: Trajectory Optimization, Cost Function Value
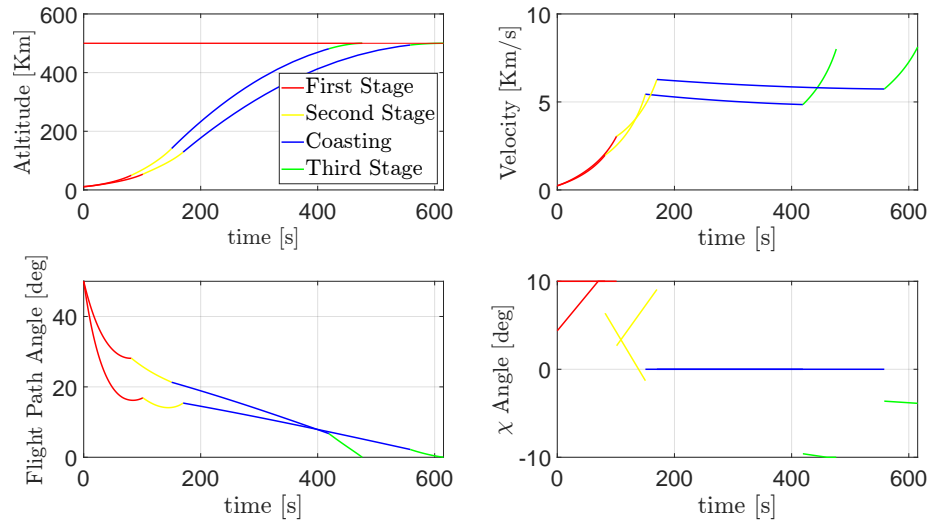
Figure 4.2: Rocket Ascent Trajectory

Figure 4.3: Altitude, Velocity, Pitch and χ During Ascent

4.2 Re-entry Considerations

The paragraph discusses the so far obtained launcher design compatibility with safe re-entry of exhausted stages. Usual rocket stages re-entry is done over the sea (like ESA or American does) or over inhabited land like Kazakhstan for RosCosmos to avoid any potential threat to people or buildings [38]. Atmospheric re-entry of stages is a very complex subject that is not the topic of this work, however a very brief analysis can be done to identify what happens to dead rocket bodies once detached in flight and to ensure a safe re-entry of all the stages.

A nice and simple way of introducing the topic of aerothermodynamic is given in [39]. An orbital or sub-orbital body has a very high kinetic energy during flight, across the re-entry phase only a small fraction (1% - 5%) of that energy is transferred to the body in terms of heat while the rest is dispersed in the atmosphere. This fraction depends on many factors like the ballistic coefficient, re-entry corridor and many others effects too difficult to estimate correctly.

The energy per unit mass of a body can be easily computed as:
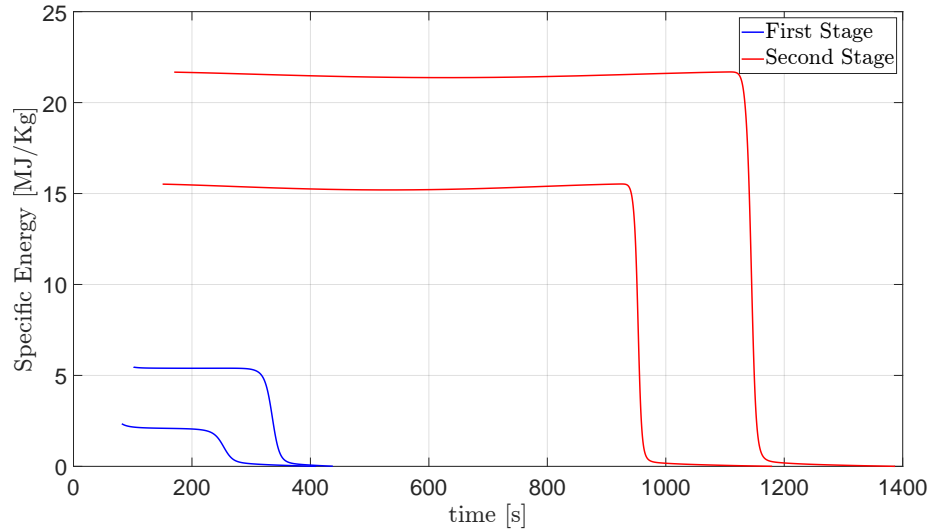
$$\frac{E}{m} = \frac{1}{2}V^2 + gh \tag{4.8}$$

Figure 4.4: Energy per unit mass of falling dead stages

Figure 4.4 shows the specific energy of first and second stage in both configurations from the detachment to the expected fall. The energies involved are in the order of tens of MJ per Kg, and it can be noticed that the second stage is affected by, roughly one order of magnitude more energy than the first. To give a sense of scale, water boils at 2.3 MJ/Kg, iron vaporizes at 6 MJ/Kg and

carbon at 60 MJ/Kg.

Due to its higher mass and lower absorbed energy, it is reasonable that the first stage body must fall into the sea not to create any potential threat.

The second stage dead motor instead has low mass and high surface area, which means that the ballistic coefficient, expressed by equation (4.9), is considerably smaller than the one of a thrusting rocket. Therefore the expected absorbed energy is higher.

$$BC = \frac{M}{C_d S} \tag{4.9}$$

Assuming a heat capacity of around 1000 J/Kg/K taken from carbon fiber composite [40], the temperature increment is roughly of 200-800 K depending of the percentage of that heat absorbed. This is clearly not enough to vaporize the carbon fiber composite which is the main component of the structure, neither any other metallic material. However it is enough to compromise its structural integrity given by the epoxy resin, this together with the high mechanical stresses introduced by aerodynamic forces, leads to the conclusion that the chances to become a threat are significantly lower than the first stage. However there is the possibility that chunks of metallic material could arrive at ground, to ensure it a detailed aerothermodynamic analysis must be performed in future works.

The third stage releases the payload at orbital velocity so basically is injected in the same orbit as the CubeSat. Since the target orbit is a LEO, the dead rocket body re-enters into the atmosphere and get destroyed in a few years [41], however using an liquid/hybrid upper stage a controlled de-orbit can be done like the VEGA rocket does with its fourth stage AVUM [10]. Controlled and fast de-orbit is always desirable; space debris is a big issue and the possibility of not introducing dead rocket bodies, even if for few years, is always nice to have.

To sum up what just explained, the first stage rocket body can be a threat if it falls over living areas, the second stage has a significant lower possibility but further analysis are required to ensure it, and the third stage is unlikely to be dangerous especially if a controlled de-orbit strategy is adopted.

4.3   Launch Location

A very nice solution is to find out a launch location that allows the rocket to fly above the sea for the entirety of the launch, but this could lead to candidates very far from the coast therefore creating issues for the carrier aircraft. As expressed in section 4.2, the first booster must absolutely fall into the ocean, while this requirement is not strictly true for the second stage (but of course, desirable), another important safety requirement is that the entirety of the first stage burn is performed above the sea. Therefore in case of a sudden engine shut-down, the flight termination system surely destroys the rocket but the falling debris do not create any threat to living areas. A good way to propose many different solutions is by means of some *Safety Levels*. A safety level is a number that goes from 1 to 5 that defines a certain requirement that the launch zone must fulfill in order to be taken into consideration. The expected result of this analysis is a set of launch zones where each one satisfies one or more those requirements.

Safety Level:

1. 1st booster falls into ocean

2. 1st booster falls into ocean and 1 stage flies above the sea

3. Both boosters fall into ocean

4. Both boosters fall into ocean and 1 stage flies above the sea

5. The whole launch happens above the sea

In order to identity the zones, an algorithm takes the falling distances from the previous section and computes the location of the expected rocket touchdown in terms of latitude and longitude by means of spherical triangles rules.

The procedure is expressed in the following way:

1. The algorithm discretizes both the longitude and the latitude creating a matrix of possible launch locations.

2. A check is performed if those points belong to land or sea. If are part of the land those launch locations are discarded.

3. From each feasible point the expected groundtrack of the launch is computed in terms of longitude and latitude. This has been done using spherical triangles theorems.

4. The groundtrack is then discretized and the same land/sea check is done on each point.

5. Based on which points the code identifies the sea check, a safety level is derived. For instance, is every points belong to the sea, safety level 5 is the outcome. If, instead, only the falling points of the first stage are above the sea, safety level 1 is considered. If no safety level is satisfied, that particular launch location is not considered as feasible.

It is important to point out that for simplicity and computational time reasons, small island and the north pole are not considered as proper "land" over which the code triggers the falling effects.

Since the modeling of the re-entry is a very complicated subject, and since it is absolutely not the aim of this thesis, a MonteCarlo analysis has been performed in order to estimate the range in which is more likely to land the stages. The analysis uses the same 3DOF model discussed so far to compute the falling trajectory of the dead body, the initial conditions are taken from the final ones of that particular stage, where the velocity is reduced due to the retro-rockets that help the stage separation.
The variables considered are the following:

- Position in terms of radius r and downrange x
  The uncertainties can be introduced by trajectory errors or environmental conditions such as wind.

- Flight path angle γ
  This uncertainty is again related with trajectory errors.

- Velocity V
  This value can change mainly due to propulsion errors, or a not predictable effect of the retrorockets.

- Mass m
  The uncertainty of the mass is due to propulsion effects: such as un-burned propellant, throat erosion and insulation pyrolisis.

Since the modeling of those effects is very difficult, the standard deviation has been imposed equal to 1% of the initial condition just explained. The mean instead has been considered equal to those initial conditions except for the velocity which is reduced by the retrorockets.
The results of the MonteCarlo analysis can be seen in figures 4.5 and 4.6 for the first and second configuration respectively.
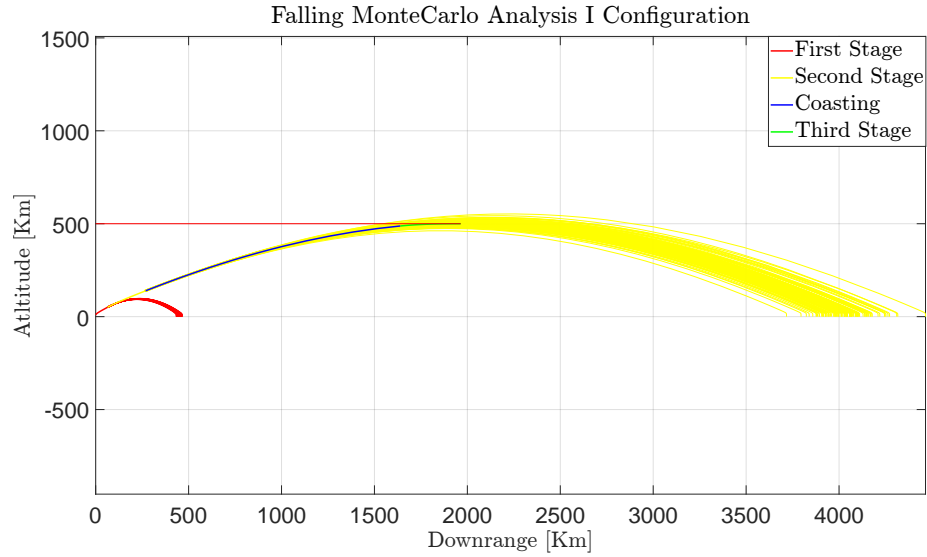

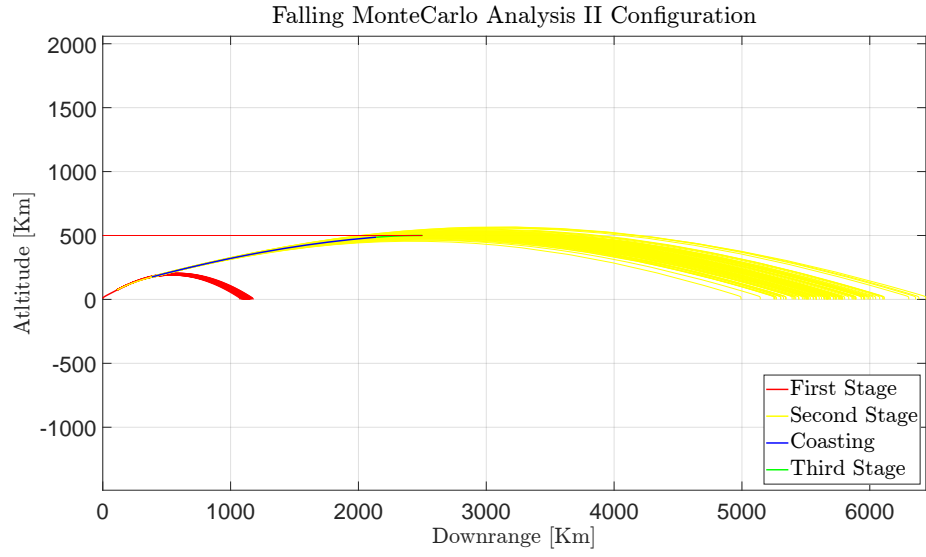Figure 4.5: MonteCarlo Analysis of Stages Re-entry I Configuration

Figure 4.6: MonteCarlo Analysis of Stages Re-entry II Configuration

In figures 4.7, 4.8, 4.9, 4.10, 4.11 the possible launch locations for each safety level can be seen. The blue line represents the groundtrack of the falling first stage, the green line the second stage instead, and finally the red line represents the probable falling areas given by the MonteCarlo analysis.
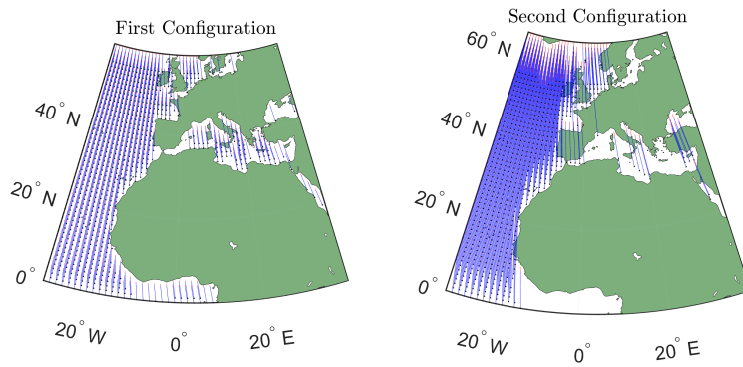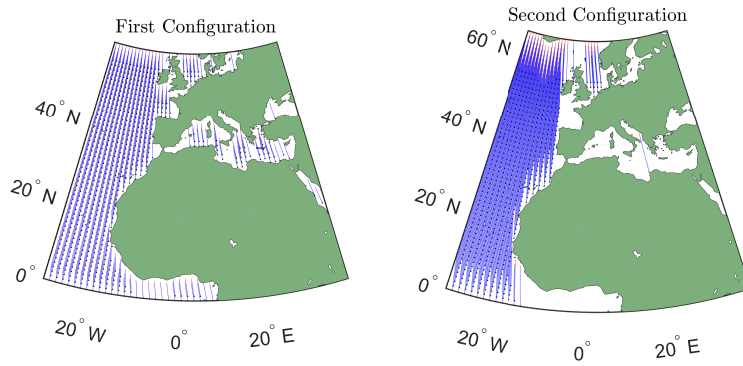

Figure 4.7: Safety Level 1 Zones

68

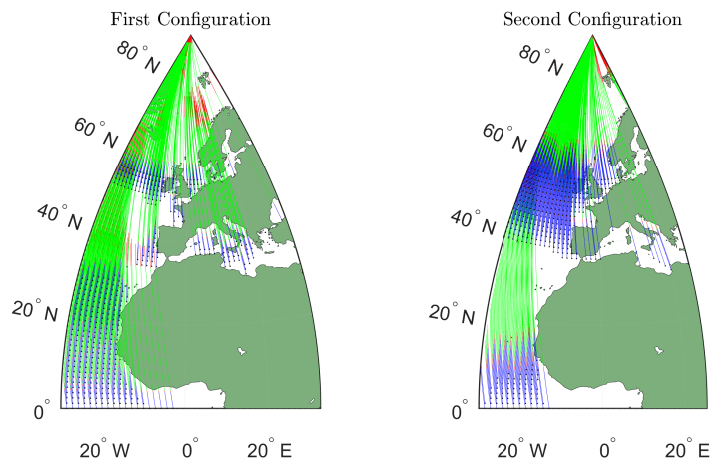Figure 4.8: Safety Level 2 Zones
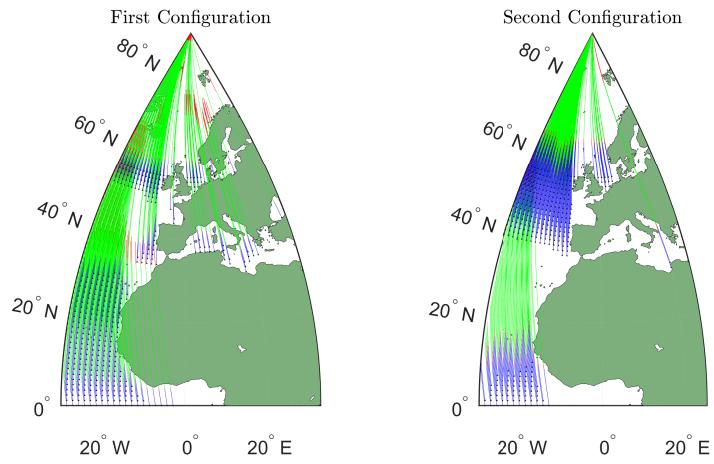

Figure 4.9: Safety Level 3 Zones
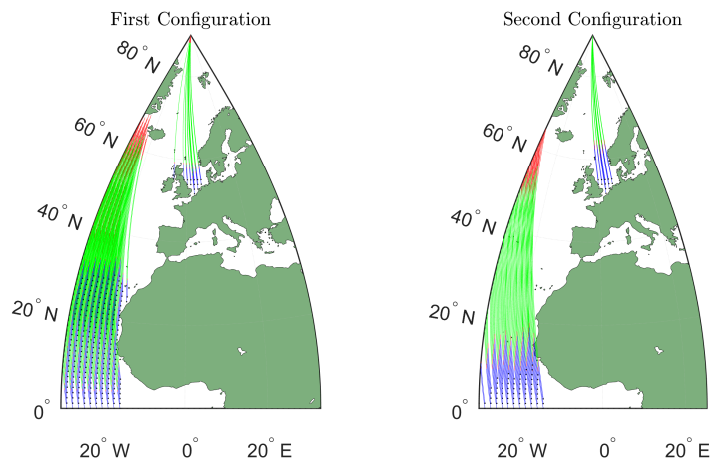
Figure 4.10: Safety Level 4 Zones

Figure 4.11: Safety Level 5 Zones

5 different zones can be identified by this analysis.

Launch Locations:

- **ESS** East Sardegna Sea

- **SIS** South Ionio Sea

- **WSA** West Spain Atlantic

- **WAA** West Africa Atlantic

- **NES** North European Sea
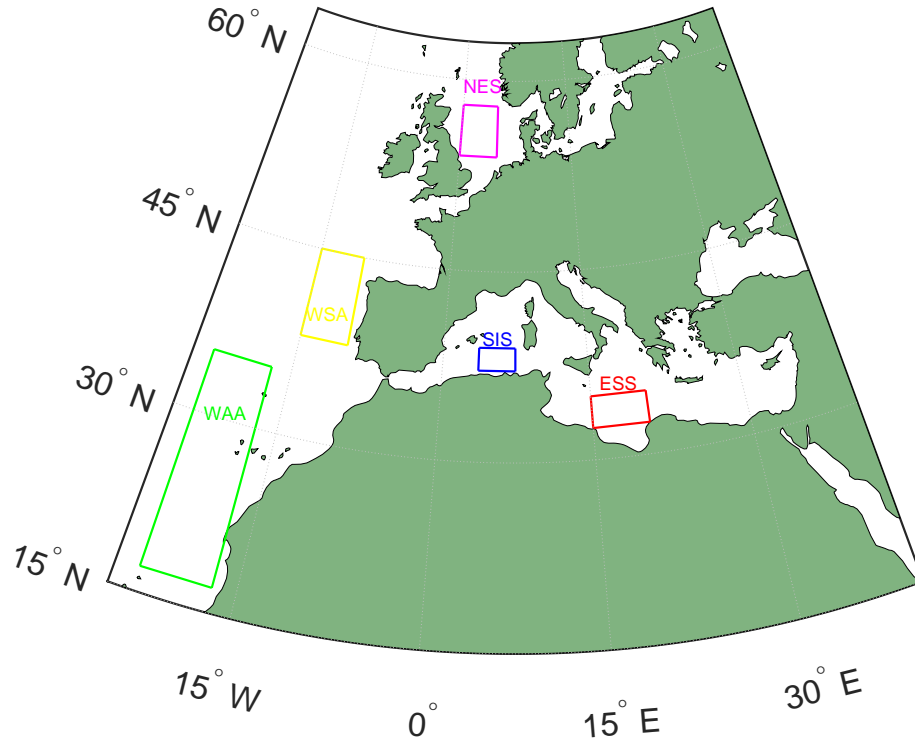
Figure 4.12: Launch Zones

Of course **ESS** and **SIS** are the most desirable ones, in those zones the aircraft can lift off from italian territory but not every safety level is guaranteed. **NES** instead is far from Italy, thus the aircraft must lift off from north Europe, but in this zone the maximum safety is guaranteed. **WSA** and **WAA** provides good results from the first configuration point of view, and average from the second. Even the choice of those zones requires a foreign airport.

Table 4.3 shows what safety levels are respected by each zone in both configurations [1]
.

---

[1] Green means feasible, red not feasible, yellow partially feasible

Safety Level	ESS	SIS	WSA	WAA	NES
Configuration I					
Safety Level 1	green	green	green	green	green
Safety Level 2	green	green	green	green	green
Safety Level 3	green	green	green	green	green
Safety Level 4	green	green	green	green	green
Safety Level 5	red	red	red	green	green
Configuration II					
Safety Level 1	red	green	green	green	green
Safety Level 2	red	red	green	green	green
Safety Level 3	red	yellow	green	yellow	green
Safety Level 4	red	red	green	yellow	green
Safety Level 5	red	red	red	yellow	green

Table 4.3: Launch Zones Feasibility

What turns out from this analysis is not a single feasible launch zone, but 5 different possibilities with pros and cons each. At this level a decision is impossible, further work is required to get better trajectory results and most importantly, political agreements between countries regarding rocket flights over foreign territory or usage of military airports for payload integration and aircraft lift off.

Chapter 5

6DOF Rocket Model

The chapter discusses the system modeling enhancement to take into account the attitude dynamics and extend the forces acting on the launcher. In particular, being aerodynamic actions further considered, the further degree of freedom of introducing aerodynamics fins is presented as well.
This model is not a point mass but a 3D body with a well-defined attitude, also the aerodynamic forces are augmented and some consideration are done about the presence or not of aerodynamic surfaces on the body.

Two reference systems are exploited:

- An inertial reference system where the equations of motion are integrated.
  This system is placed at the launch location, the Z axis is in the direction of the local zenith, while X and Y axes represent the downrange and cross-range directions respectively, the scheme is shown in figure 5.2. A round, non rotating Earth is considered; to cope with that assumption, a ΔV component is included, as explained in section 1.4.1.

- A body reference system where are defined aerodynamic and thrust forces. This system has the origin in the center of mass, the X axis is simply the longitudinal axis of the body, while Y and Z can be placed everywhere since up to this level of detail the rocket is assumed to have cylindrical symmetry, the scheme is represented in figure 5.1. Even if the launcher is modeled as a rigid body, some considerations on its vibrations are briefly discussed as well.
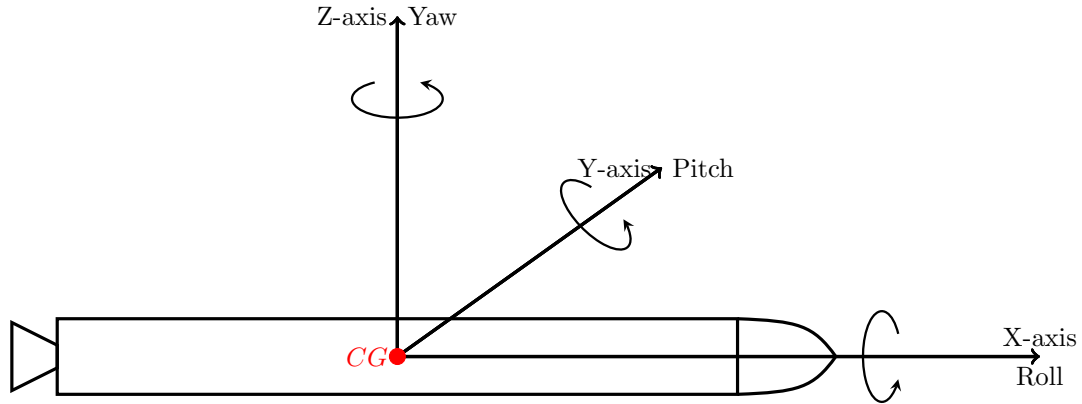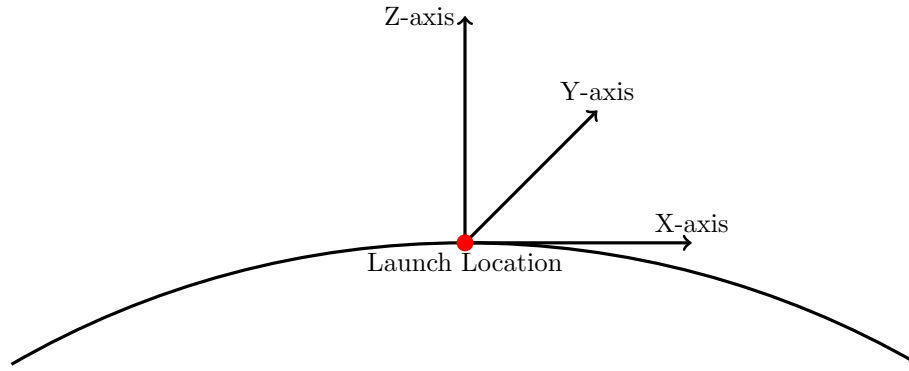
Figure 5.1: Rocket Body Reference System

Figure 5.2: Inertia Reference System

5.1 Atmosphere Model

The *1976 U.S. Standard Atmoshpere Model* is here adopted, according to [5]; this model is based on different layers each of which has a linear variation of the temperature with respect to the altitude. Once the temperature profile is known $Temp = Temp(h)$ the pressure can be computed using the hydrostatic relation $P = P(h)$ and finally the density which if found thanks to the perfect gas assumption $\rho = \rho(h)$. The temperature at sea level is fixed to $15°C = 288.5K$. This model is quite simple because it does not account for any diurnal/nocturnal variation, as well as, solar cycles; the atmosphere composition is considered constant which is not too strong as an hypothesis below 100

Km. As expressed in chapter 1, air launched rocket are affected by lower aerodynamic forces than classical launchers, so this simple model is more than enough to estimate the effects on the launch dynamics.

The temperature rates and the atmosphere layers up to 100 Km are set in table 5.1.

Layer	Altitude [Km]	Temperature rate [K/Km]
1	0	-6.5
2	11.02	0
3	20.06	1
4	32.16	2.8
5	47.35	0
6	51.41	-2.8
7	71.80	-2
8	86	0
9	92	1.03

Table 5.1: Atmosphere Layers

The procedure to compute pressure and density is straightforward and it is reported in [5].
Above 100 Km the temperature can be modeled as an exponential that tends to 1000 K just for Mach number purposes as can be seen in figure 5.3, pressure and density instead are too low to give significant contributions to the problem, for this reason over 100 Km are set to 0.
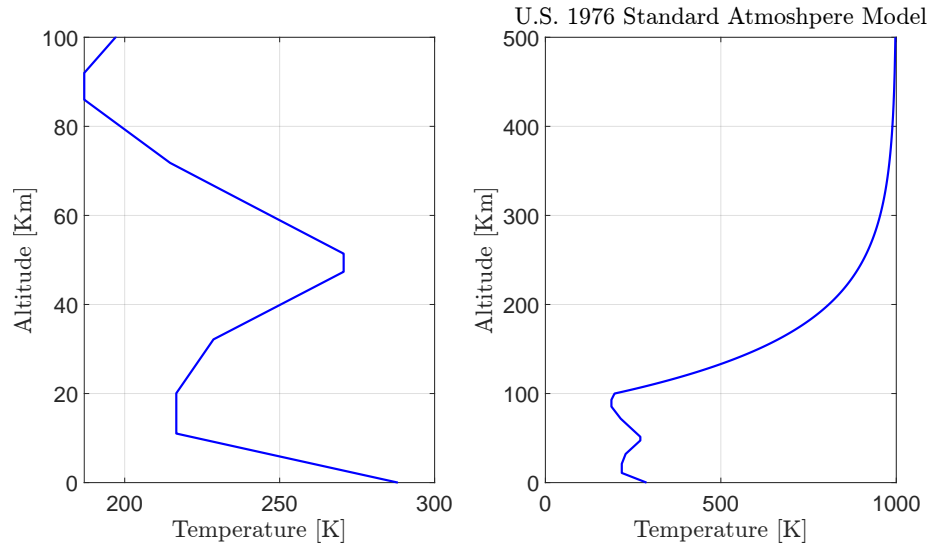
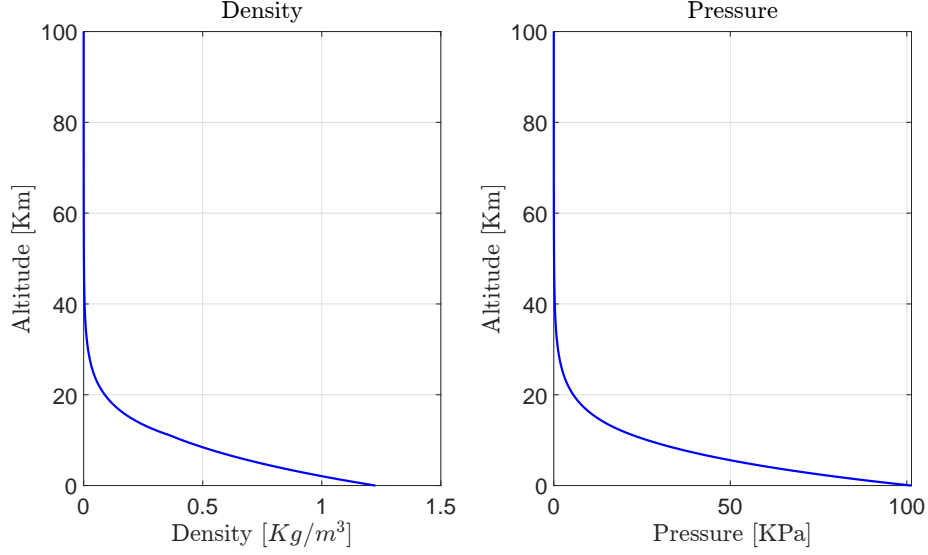

Figure 5.3: Atmospheric Temperature

Figure 5.4: Atmospheric Pressure and Density

5.2 Aerodynamic Model

In this section the passages and models to compute the aerodynamic forces acting on the launcher are shown. The models are taken from [3], the validity hypotheses are discussed at each contribution, however it is important to point out that those models have been chosen for their simplicity. For a complete rocket design, tools such as CFD (Computational Fluid Dynamics) must be used, but for a preliminary analysis analytical expression and correlations are a good compromise.

Aerodynamic forces have a major contribution in the first phases of a rocket launch, drag is responsible for ΔV losses, while lift provides an instability effect on the vehicle to be fixed using control actions. Despite an air launched rocket has a significantly lower contribution of those latter than a standard launcher, they can't be discarded.

Starting from the aerodynamic drag, the zero-lift drag coefficient can be seen as a sum of three different contributions.

$$C_{D0} = C_{D0_{Base}} + C_{D0_{Wave}} + C_{D0_{Friction}} \tag{5.1}$$

76

$C_{D0_{Base}}$ is due to the pressure difference between the nose and the engine section that feels a lower pressure given by the flow separation at the base. This contribution can be correlated with the following expressions.

$$\begin{cases} C_{D0_{Base}} = \left(1 - \frac{A_e}{S_{ref}}\right)\frac{0.25}{Ma} & if \ Ma < 1 \\ C_{D0_{Base}} = \left(1 - \frac{A_e}{S_{ref}}\right)(0.12 + 0.13 Ma^2) & if \ Ma > 1 \end{cases} \tag{5.2}$$

Where S_{ref} is the reference surface, computed as the cross section of the rocket body. This contribution increase significantly during un-powered coast (so when A_e goes to zero).

Skin friction can be a primary contribution in subsonic flights: the following relation is based on empiric correlations with the Reynolds number and it's valid within the hypothesis of turbulent boundary layer which can be an issue for low Mach numbers ($Ma < 0.2$) [1].

$$C_{D0_{friction}} = 0.031(l/d)\left(\frac{Ma}{qL}\right)^{0.2} \tag{5.3}$$

The last contribution is the wave drag: this is created by the effects of a shock wave at the nose.

$$C_{D0_{Wave,Sharp}} = \left(1.586 + \frac{1.834}{Ma^2}\right)\left[\arctan\left(\frac{0.5}{l_N/d}\right)\right]^{1.69} \qquad if \ Ma > 1 \tag{5.4}$$

Where L_N is the length of the nose, which for a launcher is identified as the fairing.
The above equation is valid only on sharp noses; the bluntness of a launcher fairing is here taken into account, by fixing l_N/D equal to 0,5 in equation (5.4) to get to the $C_{D0_{Wave,Hemi}}$. Finally scaling those two contributions is enough to get an accurate compromise for a blunt nose as reported by (5.5).

$$C_{D0_{Wave,Blunt}} = \frac{S_{ref} - S_{nose}}{S_{ref}} C_{D0_{Wave,Sharp}} + \frac{S_{nose}}{S_{ref}} C_{D0_{Wave,Hemi}} \tag{5.5}$$

Where S_{nose} is the area of the circle describing the bluntness.
All the above relations are only valid for supersonic flow, however shock waves can form also before the supersonic regime; in particular this coefficient starts increasing at a certain Mach called "critical Mach number", this is usually found between Mach 0.6 and 0.8. The drag contribution in the transonic regime is very hard to compute and it's very shape-dependent: a simple way not to create any discontinuity is to increase this value from 0 (at critical Mach) to the maximum (at Mach 1) by means of a polynomial function of the second order.

The normal coefficient expressed by equation (5.6) is by far easier than the drag one. This relation is based on the hypothesis of slender body theory (fineness ratio > 5) and cross flow theory.

$$C_N = \sin(2\alpha)\cos(\alpha/2) + 2l/d\sin(\alpha)^2 \tag{5.6}$$

---

[1] All the variables are in S.I units

Finally the drag and lift coefficient can be computed.

$$C_L = C_N \cos(\alpha) - C_{D0} \sin(\alpha) \tag{5.7}$$

$$C_D = C_N \sin(\alpha) + C_{D0} \cos(\alpha) \tag{5.8}$$

The lift and drag forces are immediately found.

$$L = \frac{1}{2}\rho V^2 S_{ref} C_L \tag{5.9}$$

$$D = \frac{1}{2}\rho V^2 S_{ref} C_D \tag{5.10}$$

If the cross flow and the slender body theories still hold, the analytical relationship in (**??**) outputs the aerodynamics action application point location.

$$(\mathbf{??}) X_{AC} = 0.63 l_N (1 - \sin(\alpha)^2) + 0.5 l \sin(\alpha)^2 \tag{5.11}$$

X_{AC} is considered from the tip of the nose.

Despite a normal launcher does not feel high angular velocities during launch, a rotation in the atmosphere generates an opposite torque on the body. Since this factor has a very minor contribution with respect to torques induced by either the thrust or aerodynamic forces, the model is quite simple. Considering the rocket body modeled as a rigid cylinder, the rotation around the roll axis does not generate dynamic pressure on the body, but just skin friction which is in general smaller compared to the normal skin friction: for those reasons a rotation around the roll axis does not generate an aerodynamic torque. For what concerns pitch and yaw rotations, if the static pressure is assumed to be always constant, a rotation would create a distribution of dynamic pressure on the body that can be seen as an opposed force couple on the rocket body.

$$M_{y,z} = -\frac{3}{4}\frac{l^4 \rho d \omega_{y,z}^2}{48} sign(\omega_{y,z}) \tag{5.12}$$

5.3 Aerodynamic Surfaces

The addition of aerodynamic surfaces can provide benefits in aerodynamic lift maneuverability and can also reduce the instability induced by the body normal force. However there are also disadvantages like the inevitable inert mass increment as well as the increase in drag. The choice of using fins or not is influenced by many factors, first among all the carrier aircraft interface that can limit

the number and the dimensions of them. It is here remarked that the current thesis focuses on the air launched rocket feasibility and operability together with main budgets assessment; detailed design is out of scope. Therefore the paragraph gives an overview on wings, show how are modeled and provides elements to support the tradeoff finalization.

Looking at existing launchers, both Pegasus and LauncherOne have tail wings as can be seen in figure 5.5; furthermore Pegasus also has a bigger Delta wing on top of the first stage since the trajectory control of this latter is done controlling those aerodynamic surfaces and not by TVC.
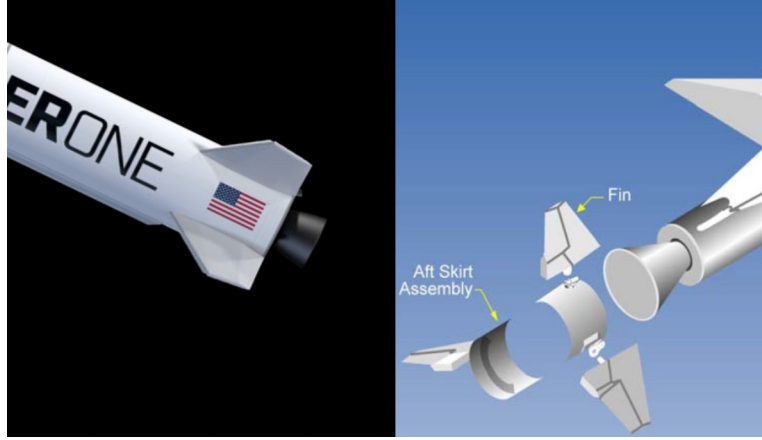

Figure 5.5: LauncherOne and PegasusXL Tail Fins [6] [7]

The work in [23] comes in handy, since its study discussess the benefits of aerodynamics fins on rocket bodies. The result is a small increase of ΔV with wings if the initial flight path angle is quite small, however the final choice is again more complex and further analyses are required to get a definitive answer.

All the models in the following section come from [3].

First of all the aspect ratio of the wing must be defined.

$$A_r = \frac{b_e^2}{S_e} \tag{5.13}$$

It is important to point out that the base of the wing b_e is not the distance from the tip of the wing to the body, but twice as figure 5.6 shows.
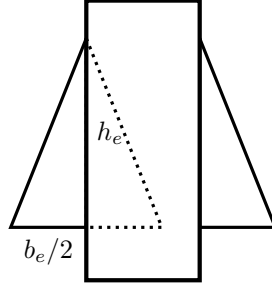
Figure 5.6: Triangular Wing Scheme

The normal coefficient of the wing is computed by means of equations (5.14). Those relations are based on the Newtonian impact theory, then if the Mach number is lower than a certain critical value that theory is augmented using the slender wing theory, if higher the linear wing theory is used.

$$
\begin{cases}
C_{n_{wing}} = \left(\frac{\pi A_r}{2} |\sin\alpha_w \cos\alpha_w| + 2\sin^2\alpha_w \right) \frac{S_{surf}}{S_{ref}} & if \ Ma < Ma_{cr,wing} \\
C_{n_{wing}} = \left(\frac{4|\sin\alpha_w \cos\alpha_w|}{(Ma^2-1)^{1/2}} + 2\sin^2\alpha_w \right) \frac{S_{surf}}{S_{ref}} & if \ Ma > Ma_{cr,wing}
\end{cases}
\tag{5.14}
$$

Where the critical mach number for the wing is found as follows:

$$
Ma_{cr,wing} = \sqrt{1 + \left(\frac{8}{\pi A_r} \right)^2}
\tag{5.15}
$$

In this case the angle α_w differs the angle of attack of the body, angular velocities may cause different flow velocities even between wings themselves.

The drag coefficient, similarly as equation (5.1) is made of some contributions, but in this case since wings are usually very thin, the base drag coefficient is negligible.

The friction drag and the wave drag coefficients are computed according to the following equations.

$$
C_{D0_{wing,friction}} = 0.0078 \left(\frac{Ma}{qc_{mac}} \right)^{0.2} \frac{2S_{surf}}{S_{ref}}
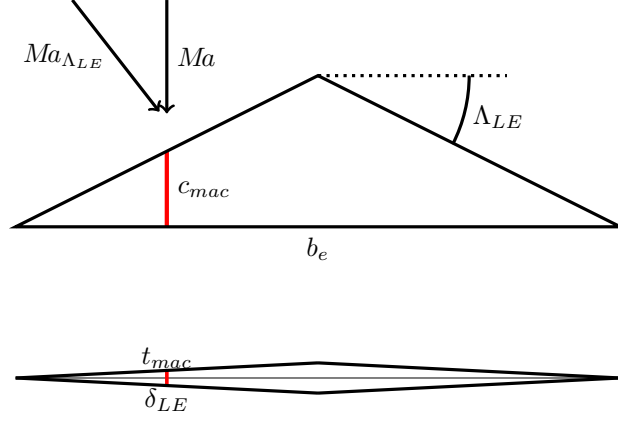\tag{5.16}
$$

Figure 5.7: Delta Wing Scheme

$$C_{D0_{wing,wave}} = \frac{1.429}{Ma_{\Lambda LE}^2}\left((1.2Ma_{\Lambda LE}^2)^{3.5}\left(\frac{2.4}{2.8Ma_{\Lambda LE}^2 - 0.4}\right)^{2.5} - 1\right)\frac{(\sin^2 \delta_{LE}\cos\Lambda_{LE}t_{mac}b_e)}{S_{ref}} \quad (5.17)$$

Where, t_{mac} is the thickness of the wing in the mean chord position, δ_{LE} is the leading edge angle in the same position, and $Ma_{\Lambda LE}$ is the Mach number component perpendicular to the leading edge; those contributions can be seen in figure 5.7.
This contribution has the same discontinuity issue discussed for equation (5.4), and it's solved again using a polynomial function.
So the normal force and the zero-lift drag can be computed.

$$\begin{cases} N_{wing} = qS_{ref}C_{n_{wing}} \\ D_{0wing} = qS_{ref}C_{D0_{wing}} \end{cases} \quad (5.18)$$

Regarding the position of the center of pressure, the following procedure can derive it.

$$\begin{cases} \frac{X_{AC_{wing}}}{c_{mac}} = 0.25 & Ma < 0.7 \\ \frac{X_{AC_{wing}}}{c_{mac}} = \frac{A_r\sqrt{Ma^2-1}-0.67}{2A_r\sqrt{Ma^2-1}-1} & Ma > 2 \end{cases} \quad (5.19)$$

In this case $X_{AC_{wing}}$ is considered from the leading edge of the wing in the mean chord position. For values of Mach number between 0.7 and 2 a linear interpolation has been used.

Classical wing shapes are triangular or trapezoidal, however other shapes can be used with their respective advantages and disadvantages. A list of possible shapes and performances can be seen in figure 5.8.
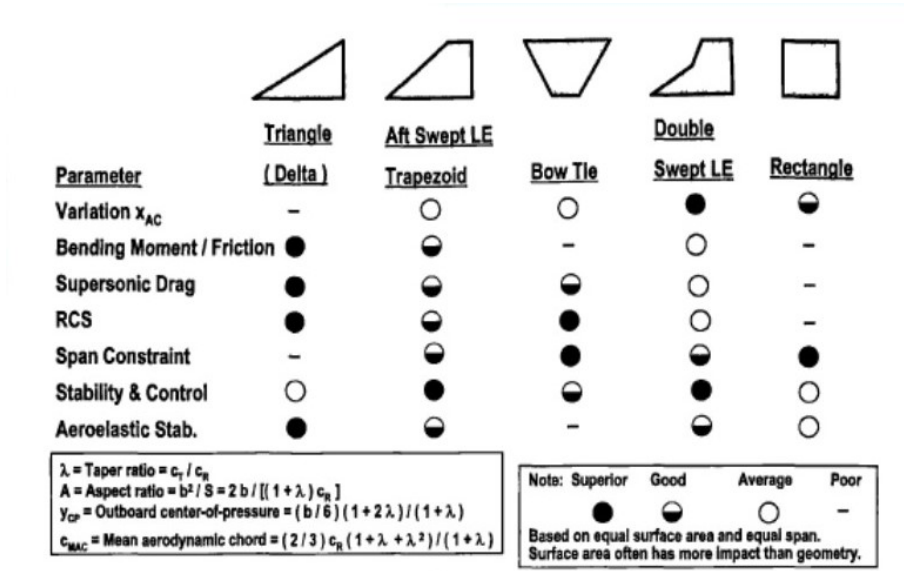
Parameter	Triangle (Delta)	Aft Swept LE Trapezoid	Bow Tie	Double Swept LE	Rectangle
Variation x_{AC}	–	O	O	●	◗
Bending Moment / Friction	●	◗	–	O	–
Supersonic Drag	●	◗	◗	O	–
RCS	●	◗	●	O	–
Span Constraint	–	◗	●	◗	●
Stability & Control	O	●	◗	●	O
Aeroelastic Stab.	●	◗	–	◗	O

λ = Taper ratio = c_t / c_R
A = Aspect ratio = $b^2 / S = 2b / [(1+\lambda)c_R]$
y_{CP} = Outboard center-of-pressure = $(b/6)(1+2\lambda)/(1+\lambda)$
c_{MAC} = Mean aerodynamic chord = $(2/3)c_R(1+\lambda+\lambda^2)/(1+\lambda)$

Note: Superior ● Good ◗ Average O Poor –
Based on equal surface area and equal span. Surface area often has more impact than geometry.

Figure 5.8: Fins Shape Parameters [3]

The effects of the aerodynamic surfaces on the body is shown in figure A.1 in Appendix A.

5.4 Thrust

Thrust is the main contribution among the forces acting on a rocket, the way to model it comes from the momentum balance across the vehicle and the result is quite simple.

$$T = \dot{m}V_e + (P_e - P_a)A_e \tag{5.20}$$

V_e and P_e are engines parameters and do not change during flight, $\dot{m}$ instead is function of the grain properties for a solid rocket motor and the throttling for a liquid/hybrid rocket engines so in general can change during the mission; P_a is simply the ambient pressure and so it changes with the altitude becoming negligible from the second stage ignition on.
Since the static contribution does not play an important role during the flight, a constant thrust approach can be followed.

$$T = \dot{m}g_0 I_{sp-vac} \tag{5.21}$$

Thrust Vector Control (TVC) is a control method that orients the force direction without changing its magnitude; it can be used to steer the vehicle even without atmospheric action like Pegasus uses for its first stage. Several ways exist to orient the thrust vector so that the rocket follows the

reference trajectory.

Classical SRMs move only the nozzle since the combustion chamber in this case is basically the entire rocket, LREs instead orient the whole engine using gimbals.

Considering the two deflection angles δ and β respectively along Y and Z direction (fig:5.1), the force vector in the body reference frame becomes:

$$\underline{F}_{thrust} = \begin{bmatrix} T\cos\beta\cos\delta \\ T\sin\delta \\ T\sin\beta\cos\delta \end{bmatrix} \tag{5.22}$$

Boundaries have been imposed to those two angles in order not to overcome technological limits, the maximum and minimum are set as 10 degrees. It is here remarked that the tilting rate shall respect the technological constraints and avoid dangerous vibrations. Those requirements are not currently taken into account in this feasibility study.

5.5 Inertia

Inertia was not considered in the simplified model in chapter 4. The inertia matrix is required to compute the attitude of the launcher as well as the moments acting on the body introduced by thrust and lift.

A simple procedure is followed to compute that matrix. First of all, the rocket body is assumed to be a perfectly homogeneous cylinder. If the cylindrical symmetry is reasonable, the homogeneity of the body is usually not true, however it is used to simplify a lot the computations. Each stage is treated as a independent cylinder, where only the thrusting one is changing its moment of inertia due to propellant burning; the payload is modeled, again, as cylinder whose height is the fairing length. The inertia scheme of the rocket can be seen in figure 5.9.

The position of the center of mass is therefore computed as equation (5.23) shows.

$$X_{cg} = \frac{\sum_{i=1}^{n} M_i X_{cgi}}{\sum_{i=1}^{n} M_i} \tag{5.23}$$

After computed the position of the center of mass, the 3 principal moment of inertia can be computed recalling that two of them are equal by means of the cylindrical symmetry hypothesis.

$$I_y = I_z = \sum_{i=1}^{n} \frac{M_i L_i^2}{12} + (X_{cgi} - X_{cg})^2 \tag{5.24}$$

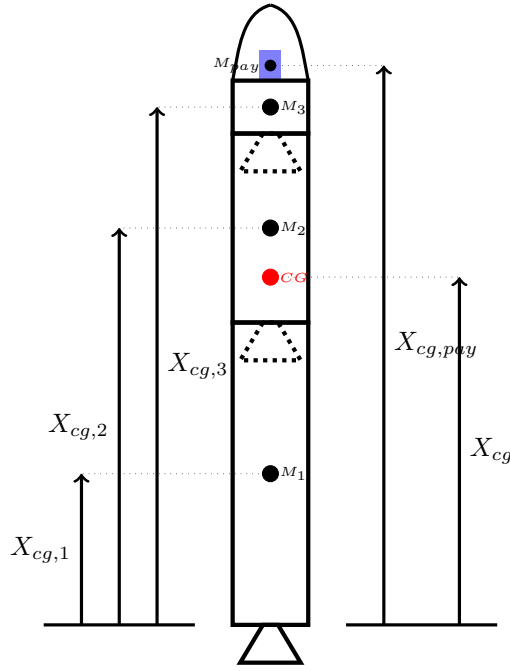$$I_x = \sum_{i=1}^{n} \frac{M_i D}{2} \tag{5.25}$$

Figure 5.9: Rocket Center of Mass scheme

5.6 Attitude

The attitude of the launcher plays a very critical role during the ascent phase, it determines the angle of attack which is the base of all aerodynamic force and torques and also the thrust direction. There are many different ways to represent the attitude of the body frame with respect to the inertial one:

- Direction Cosine Matrix (DCM)

- Quaternions

- Euler Angles (EA)

Euler angles are the fastest computationally speaking since they rely only on 3 variables, however there are singularities that may lead to several issues, it may be useful in some parts of the launch where the attitude is far from those singularities. Moreover, under the hypothesis of small angles the attitude can be linearized.

DCM is a very robust solution, it is both unique and global but has 9 variables to integrate at each step, and should also be orthonormalized not to loose accuracy.

The attitude matrix $\mathbf{A}$ is defined as follows:

$$\mathbf{A}_{B/N} = \begin{bmatrix} \hat{x} \\ \hat{y} \\ \hat{z} \end{bmatrix} \tag{5.26}$$

Its integration and orthonormalization are done in the following ways:

$$\dot{\mathbf{A}}_{B/N} = - \begin{bmatrix} 0 & -\omega_z & \omega_y \\ \omega_z & 0 & -\omega_x \\ -\omega_y & \omega_x & 0 \end{bmatrix} \mathbf{A}_{B/N} \tag{5.27}$$

$$\mathbf{A}_{k+1} = \frac{3}{2}\mathbf{A}_k - \frac{\mathbf{A}_k \mathbf{A}_k^T \mathbf{A}_k}{2} \tag{5.28}$$

Quaternions instead have 4 variables, are global but not unique and must be normalized as well at each step; despite their computational velocity, are still comparable with DCM because they require a further passage to get the attitude matrix.

$$\dot{q} = \begin{bmatrix} \dot{q}_1 \\ \dot{q}_2 \\ \dot{q}_3 \\ \dot{q}_4 \end{bmatrix} = \frac{1}{2} \begin{bmatrix} 0 & \omega_z & -\omega_y & \omega_x \\ -\omega_z & 0 & \omega_x & \omega_y \\ \omega_y & -\omega_x & 0 & \omega_z \\ -\omega_x & -\omega_y & -\omega_z & 0 \end{bmatrix} \begin{bmatrix} q_1 \\ q_2 \\ q_3 \\ q_4 \end{bmatrix} \tag{5.29}$$

$$\mathbf{A}_{B/N} = \begin{bmatrix} q_1^2 - q_2^2 - q_3^2 + q_4^2 & 2(q_1 q_2 + q_3 q_4) & 2(q_1 q_3 - q_2 q_4) \\ 2(q_1 q_2 - q_3 q_4) & -q_1^2 + q_2^2 - q_3^2 + q_4^2 & 2(q_2 q_3 + q_1 q_4) \\ 2(q_1 q_3 + q_2 q_4) & 2(q_2 q_3 - q_1 q_4) & -q_1^2 - q_2^2 + q_3^2 + q_4^2 \end{bmatrix} \tag{5.30}$$

To sum up, DCM is attitude representation method used for the attitude determination of the 6DOF model, however quaternions provides a good alternative in case of particularly heavy computational load therefore can be adopted for future simulations that would probably be computationally heavier. Euler Angles method is useful in the linear model [42].

5.7 Equation of Motion

In this paragraph the passages to compute and integrate the equation of motion are shown. This section also derives: altitude, downrange and cross-range from the inertia position vector $[x, y, z]$ shown in figure 5.2.
The first step is to define the launch location with respect to the center of the Earth:

$$\underline{X}_{launch} = \begin{bmatrix} 0 & 0 & R_E \end{bmatrix} \tag{5.31}$$

Then the position of the launcher can be computed with respect to the center of the Earth.

$$\underline{X}_{earth} = \underline{X}_{launch} + \begin{bmatrix} x & y & z \end{bmatrix} \tag{5.32}$$

The altitude, shown in equation (5.33), can be derived which is used to compute the atmospheric properties.

$$h = \|X_{earth}\| - R_E \tag{5.33}$$

Finally downrange and crossrange can be derived as follows:

$$\begin{cases} s = R_E \angle \left(\underline{X}_{launch}, \underline{X}_{earth}^{\searrow} \right) \\ c = R_E \angle \left(\underline{X}_{launch}, \underline{X}_{earth}^{\searrow} \right) \end{cases} \tag{5.34}$$

Where $\underline{X}_{earth}^{\searrow}$ means that the z component of that vector is zero. Those distances are crucial in the control formalization since the reference trajectory, computed in chapter 4, is expressed by downrange and altitude.

The representation and the meaning of those vectors can be seen in figure 5.10.
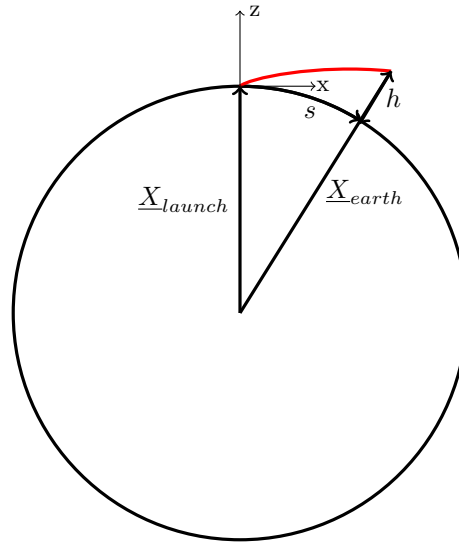

Figure 5.10: Equation of Motion Framework

The force vector in the inertial frame is made up by contributions coming from aerodynamic forces, thrust and gravity.

$$\begin{bmatrix} F_x \\ F_y \\ F_z \end{bmatrix} = \mathbf{A}_{B/N}\underline{F}_{aero} + \mathbf{A}_{B/N}\underline{F}_{thrust} - \mu\frac{\underline{X}_{earth}}{\|\underline{X}_{earth}\|^3} \tag{5.35}$$

The derivatives of mass and velocities are immediately found.

$$\begin{cases} \ddot{x} = F_x/m \\ \ddot{y} = F_y/m \\ \ddot{z} = F_z/m \\ \dot{m} = \frac{T}{I_{sp}g_0} \end{cases} \tag{5.36}$$

While the angular velocities are integrated using the common Euler equations:

$$\begin{cases} \dot{\omega}_x = \frac{I_y - I_z}{I_x}\omega_y\omega_z + \frac{M_x}{I_x} \\ \dot{\omega}_y = \frac{I_z - I_x}{I_x}\omega_x\omega_z + \frac{M_y}{I_y} \\ \dot{\omega}_z = \frac{I_x - I_y}{I_x}\omega_x\omega_y + \frac{M_z}{I_z} \end{cases} \tag{5.37}$$

Both the integration algorithm and the tolerances are the same of the 3DOF model used in chapter 4.

5.8 Linearization

In case the control law is not based on the non linear equation of the dynamics, integrated in section 5.7, yet it moves towards potentially adaptive forms of control on board, it is necessary to go through the linearization of the dynamics. For those reasons the section is dedicated to the linearization process and the obtainable accuracy that would derive from.

The vast majority of MPC controllers makes use of a linear model in the form of a state space model. Moreover, the literature followed to design that kind of control is based on a discrete state space model, therefore the aim of this section is to pass from the complete 6DOF rocket model just explained to a discrete linear model. Each linearization is discussed in details and at the end a validation phase across every model used so far is made.

First of all, there are many non-linear elements in the complete model. They are listed hereinafter:

1. Mass and inertia

2. Atmosphere properties

3. Aerodynamic Forces

4. Attitude

5. Euler Equations

6. TVC angles

5.8.1 Mass and Inertia

Mass, inertia appear at the denominator in the equations of motion, therefore a linearization is basically impossible. The only solution left is to update those values, together with the center of mass position, at each time step and keep them constant across the MPC optimization phase, this could probably introduce the highest error in the linearization process.

5.8.2 Euler Equations

The non-linear part in those equations are the cross-term between each angular velocity, in order to get rid of them a few considerations must be done. Since the rocket is assumed to have cylindrical symmetry, two of the three principal moment of inertia are equal $I_y = I_z$. This assumption makes the roll angular velocity independent from the yaw and pitch ones, and since in this model no torque is applied along that axis, the roll angular velocity ω_x is assumed to be equal to 0 for the whole launch. This consideration leads to the fact that all the cross-terms of angular velocity are equal to 0 and the Euler equations shown in equation 5.37 become linear.

$$
\begin{cases}
\dot{\omega}_x = \frac{M_x}{I_x} \\
\dot{\omega}_y = \frac{M_y}{I_y} \\
\dot{\omega}_z = \frac{M_z}{I_z}
\end{cases}
\tag{5.38}
$$

5.8.3 Attitude

The only way to linearize the rocket attitude system is by means of the Euler Angles and the hypothesis of small rotations, however the pitch angle varies far over the threshold of that hypothesis; for this reason the following procedure has been adopted.
A first rotation is performed using classical Euler angles that connect the inertia position to the so-called *"zero-angular position"*, which is the initial attitude of the launcher.
The rotation matrix is computed according to a $(X - Y - Z)$ rotation, and it's called *Eulerian Attitude Matrix* $\mathbf{A}_{eul}$.

$$
\mathbf{A}_{eul}(\phi, \theta, \psi) =
\begin{bmatrix}
\cos\psi\cos\theta & \cos\psi\sin\theta\sin\phi + \sin\psi\cos\phi & -\cos\psi\sin\theta\cos\phi + \sin\psi\sin\phi \\
-\sin\psi\cos\theta & -\sin\psi\sin\theta\sin\phi + \cos\psi\cos\phi & \sin\psi\sin\theta\cos\phi + \cos\psi\sin\phi \\
\sin\theta & -\cos\theta\sin\phi & \cos\theta\cos\phi
\end{bmatrix}
\tag{5.39}
$$

Then, a second rotation is performed, this one brings a vector from the previous Eulerian frame, to the true attitude of the launcher by means of small angles approach. This rotation matrix is again a $(X - Y - Z)$ type, and it's called *Linearized Attitude Matrix* $\mathbf{A}_{lin}$.

$$
\mathbf{A}_{lin}(\alpha_x, \alpha_y, \alpha_z) =
\begin{bmatrix}
1 & \alpha_z & -\alpha_y \\
-\alpha_z & 1 & \alpha_x \\
\alpha_y & -\alpha_x & 1
\end{bmatrix}
\tag{5.40}
$$

The product of those two matrices gives a good link between the inertial and the body frame of reference, the small angles $\alpha_x, \alpha_y, \alpha_z$ are part of the state vector of the system while the Euler angles ϕ, θ, ψ are updated at each time step using the final value of the small ones.

$$\underline{F}_n = \mathbf{A}_{eul}^T \mathbf{A}_{lin}^T \underline{F}_b \qquad (5.41)$$

5.8.4   Atmosphere properties

As well as the mass, Temperature, density and pressure are computed using the altitude and kept constant for the current time step.

$$[\rho, Temp, P] = Atmosphere(Z_k) \qquad (5.42)$$

5.8.5   Aerodynamic Forces

Aerodynamic forces are intrinsically non-linear.
The force vector in the body frame can be computed as follows:

$$F_{aero} = \begin{bmatrix} -D0 \\ N_y \\ N_x \end{bmatrix} \qquad (5.43)$$

Where $D0$ is the zero-lift drag force, and Ny, Nz are the normal forces acting respectively on the Y and Z axis.
$D0$ is computed using the pressure and velocity coming from the previous time step, and the drag coefficient is equal to the complete one explained in section 5.2 using dynamic pressure and mach number again from the previous time step.
Regarding the normal forces derivation, this is more complex because the angle of attack must be referred to the Euler angles of the attitude; to do so an important approximation must be done.
In 3D a generic angle of attack α generates a normal force N acting on the body which is function of that angle, this force can be simply decomposed into the Y and Z contributions N_y and N_z.
Under the hypothesis of small angles (a spherical triangle approximates a planar one) the angle of attack α could be seen as the result of two angular contributions α_y and α_z which give rise to the two normal forces N_y and N_z.

Taking into account the possibility that there could be an angle of attack even if the Euler angles are equal to 0, some initial angles α_{y0}, α_{z0} must be used and computed at each time step.
The force vector can be re-written in this way:

$$F_{aero} = \begin{bmatrix} -D0 \\ N_{y0} + N_{y/\alpha}\alpha_z \\ N_{z0} + N_{z/\alpha}\alpha_y \end{bmatrix} \qquad (5.44)$$

89

With:

$$
\begin{cases}
D0 = \frac{1}{2}\rho V^2 S C_{D0} \\
N_{y0} = \frac{1}{2}\rho V^2 S C_{N/\alpha}\alpha_{z0} \\
N_{z0} = \frac{1}{2}\rho V^2 S C_{N/\alpha}\alpha_{y0} \\
N_{y/\alpha} = N_{z/\alpha} = \frac{1}{2}\rho V^2 S C_{N/\alpha}
\end{cases}
\tag{5.45}
$$

And $C_{N/\alpha} = 2$ that comes from equation (5.6).

5.8.6 TVC

Since the TVC deflection angles are usually below $10°$, the small angle approximation can be used to get rid of the sinusoidal functions present in the complete case; so the body forces given by the thrust becomes:

$$
F_{thrust} = \begin{bmatrix} T \\ T\delta \\ T\beta \end{bmatrix}
\tag{5.46}
$$

5.8.7 Linear System

The state vector is made of three spatial coordinates, three velocities, the three Euler angles and the angular velocities. The control vector u represent the two TVC deflection angles, and the disturbance d is simply put equal to 1.

$$
X_c = \begin{bmatrix} x & y & z & \dot{x} & \dot{y} & \dot{z} & \alpha_x & \alpha_y & \alpha_z & \omega_x & \omega_y & \omega_z \end{bmatrix}^T
\tag{5.47}
$$

$$
u = \begin{bmatrix} \delta \\ \beta \end{bmatrix}
\tag{5.48}
$$

While the overall force vector expressed in the body frame is the following:

$$
\underline{F}_b = \begin{bmatrix} T - D0 \\ T\delta + N_{y0} + N_{y/\alpha}\alpha_z \\ T\beta + N_{z0} + N_{z/\alpha}\alpha_y \end{bmatrix}
\tag{5.49}
$$

Computing the inertial force vector from equation (5.41) and expressing it as a function of the state vector results in a state space system whose matrices are the following.

$$
\mathbf{A}_c =
\begin{bmatrix}
0 & 0 & 0 & 1 & 0 & 0 & 0 & 0 & 0 & 0 & 0 & 0 \\
0 & 0 & 0 & 0 & 1 & 0 & 0 & 0 & 0 & 0 & 0 & 0 \\
0 & 0 & 0 & 0 & 0 & 1 & 0 & 0 & 0 & 0 & 0 & 0 \\
0 & 0 & 0 & 0 & 0 & 0 & A_{\alpha x1}/m & A_{\alpha y1}/m & A_{\alpha z1}/m & 0 & 0 & 0 \\
0 & 0 & 0 & 0 & 0 & 0 & A_{\alpha x2}/m & A_{\alpha y2}/m & A_{\alpha z2}/m & 0 & 0 & 0 \\
0 & 0 & 0 & 0 & 0 & 0 & A_{\alpha x3}/m & A_{\alpha y3}/m & A_{\alpha z3}/m & 0 & 0 & 0 \\
0 & 0 & 0 & 0 & 0 & 0 & 0 & 0 & 0 & 1 & 0 & 0 \\
0 & 0 & 0 & 0 & 0 & 0 & 0 & 0 & 0 & 0 & 1 & 0 \\
0 & 0 & 0 & 0 & 0 & 0 & 0 & 0 & 0 & 0 & 0 & 1 \\
0 & 0 & 0 & 0 & 0 & 0 & 0 & 0 & 0 & 0 & 0 & 0 \\
0 & 0 & 0 & 0 & 0 & 0 & 0 & -N_{z/\alpha}l_{aero}/I_y & 0 & 0 & 0 & 0 \\
0 & 0 & 0 & 0 & 0 & 0 & 0 & 0 & N_{y/\alpha}l_{aero}/I_z & 0 & 0 & 0
\end{bmatrix}
\tag{5.50}
$$

$$
\mathbf{B}_c =
\begin{bmatrix}
0 & 0 \\
0 & 0 \\
0 & 0 \\
B_{\delta 1}/m & B_{\beta 1}/m \\
B_{\delta 2}/m & B_{\beta 2}/m \\
B_{\delta 3}/m & B_{\beta 3}/m \\
0 & 0 \\
0 & 0 \\
0 & 0 \\
0 & 0 \\
0 & Tl_{TVC}/I_y \\
-Tl_{TVC}/I_z & 0
\end{bmatrix}
\tag{5.51}
$$

$$
\mathbf{B}_{dist} =
\begin{bmatrix}
0 \\
0 \\
0 \\
B_{c1}/m \\
B_{c2}/m \\
B_{c3}/m \\
0 \\
0 \\
0 \\
0 \\
-N_{z0}l_{aero}/I_y \\
N_{y0}l_{aero}/I_z
\end{bmatrix}
\tag{5.52}
$$

Where l_{aero} is the distance between the center of gravity and the aerodynamic center of the vehicle. l_{TVC} is instead the distance from the center of gravity to the thrust application point, assumed to be at the nozzle section.

Each matrix contribution can be seen expanded in appendix A.

The resulting matrices are then placed in a continuous state space model.

$$\begin{cases} \dot{X}_c = \mathbf{A}_c X_c + \mathbf{B}_c u + \mathbf{B}_{dist} d \\ y_c = \mathbf{C}_c X_c \end{cases} \tag{5.53}$$

The subscript c means that the state vector and matrices are continuous. y instead represents the position output, so simply the 3 spatial coordinates.

The discretization is done using a zero order hold method, and a time step of 0.01 seconds taken from MPC studies on rockets [43] [44].
The results is the following.

$$\begin{cases} X_d(k+1) = \mathbf{A}_d X_d(k) + \mathbf{B}_d u(k) + \mathbf{B}_{dist} d(k) \\ y_d(k) = \mathbf{C}_d X_d(k) \end{cases} \tag{5.54}$$

Where the subscript d means the discreteness of the model.

5.9   Trajectory Validation

Across this work, 4 different dynamics models have been used. At first the simple 3 degrees of freedom point mass explained in section 4.1, secondly, the full and complex six degrees of freedom derived in chapter 5, and last but not least, the linearized model together with its discretized just shown for MPC. To check the validity of the trajectory that comes out from this work, is to compare them with appropriate benchmarks. Unfortunately the Pegasus launcher does not have any trajectory or precise mission profile available, just some rough numbers regarding the expected staging altitudes and velocities. Even the LauncherOne does not have any of those, maybe they can arrive later on when the launcher becomes fully operational.

One alternative to prove the validity of those trajectories, is to integrate those models with the same initial conditions and look how they compare to each other. 3 different tests have been performed, the first using no TVC deflection and normal aerodynamic forces not considered, the second with a TVC control law applied and still no lift force, and last with TVC and all the aerodynamic forces considered. Table 5.2 shows all the tests in more details.

Test	TVC Peak	TVC Period	Normal Aerodynamic Forces	Simulation Time
Units	deg	s	-	s
Test **1**	0	-	OFF	60
Test **2**	1	2	OFF	10.5
Test **3**	0.5	0.4	ON	1.4

Table 5.2: Trajectory Tests Scenario

As regards the control law just mentioned, a triangular function has been considered with 0 mean to avoid uncontrolled rotations. Figure 5.11 shows the control law with the TVC peak and period mentioned in table 5.2.
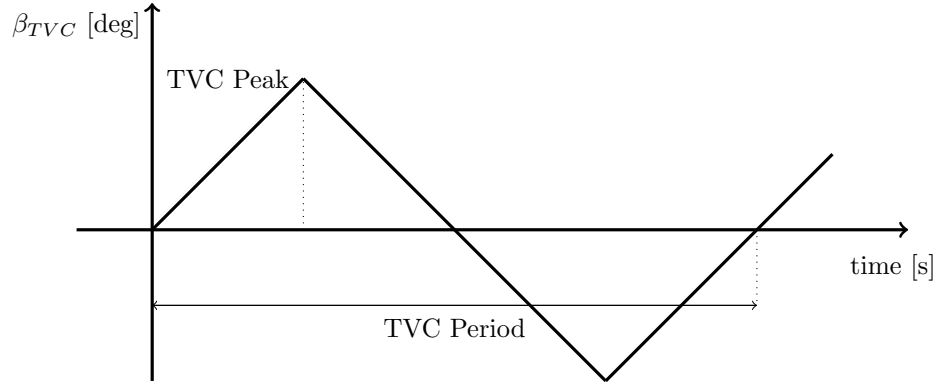

Figure 5.11: Trajectory Test, TVC Control Law

The first test is supposed to prove the accelerations due to thrust, drag and gravity acting on the rocket.
Figure 5.12 shows trajectory and velocity for all four models of the first test. Despite being simulated for a long time (60 sec), the results are very nice. The trajectories are very close between each others, and the velocities are almost indistinguishable.
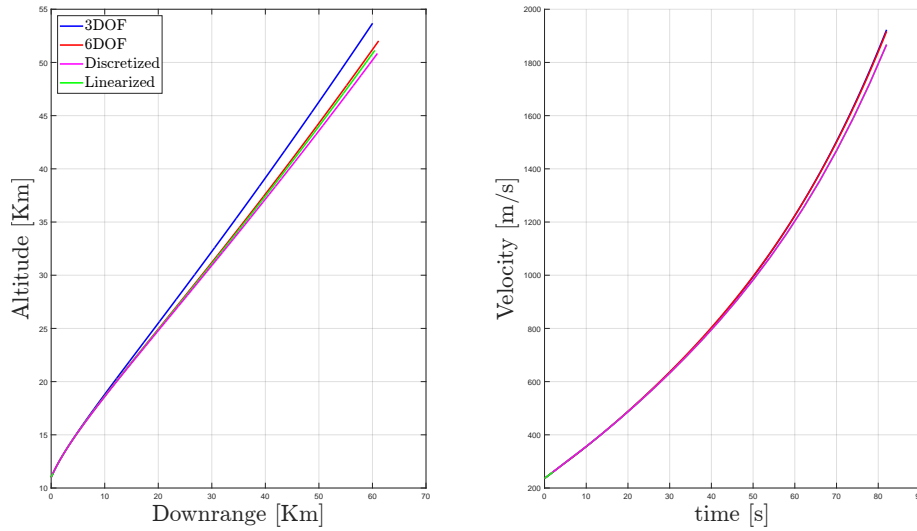

Figure 5.12: Static Trajectory Validation

The second test aims to validate the TVC action on the rocket dynamics. As just expressed, a triangular control law has been applied; otherwise a constant action would have induced an uncontrolled rotation.

In figure 5.13 what can be noticed is that the 6DOF, the linearized and the discrete models give almost the same results, the 3DOF instead differs a lot from them. The meaning of this deviation is due to the missing attitude of that model, therefore rotations have no effects on the trajectory. Moreover the χ angle is always considered from the velocity vector as figure 4.1 shows, while for the other models the β angle is defined in body coordinates. Therefore its inertial orientation depends on the attitude.
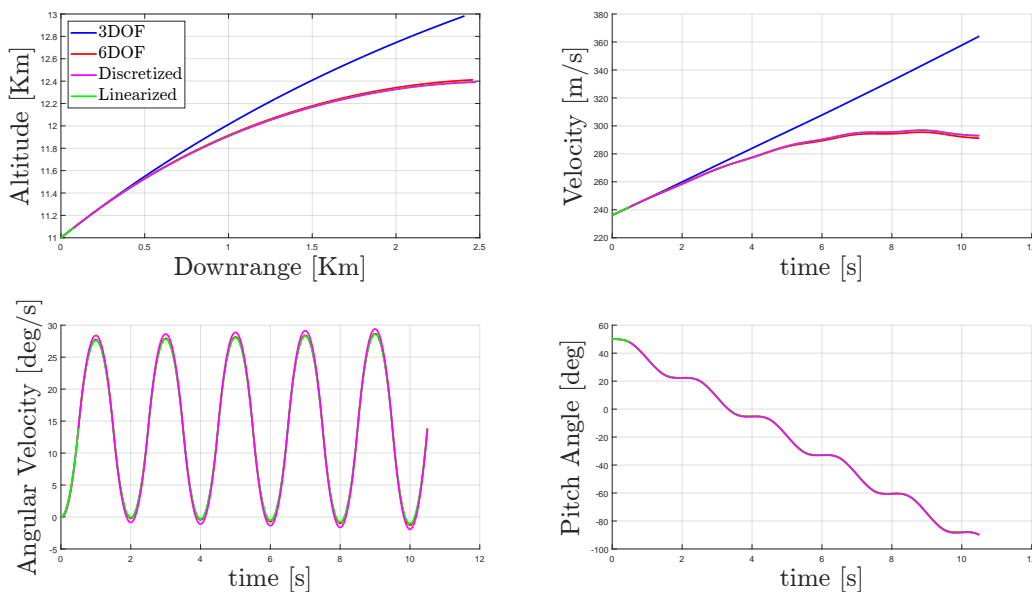

Figure 5.13: Dynamic Models comparison-tests results

Finally, the third test is thought to prove the validity of the aerodynamic model. In particular between the linearized model explained in section 5.8.5, and the complete 6DOF, since the 3DOF does not account for normal aerodynamic forces.

As figure 5.14 shows, the models are integrated switching on the normal aerodynamic forces. In this case the 3DOF model has not been used since it cannot account for normal aerodynamic forces, and its limits has already been exposed in the previous test.

The control law in this case is still a triangular function: peak and period are shown in table 5.2. The two results are quite close up to 1 second, then the two attitudes start diverging This is mainly due to all the simplifications done to include a linear aerodynamic model, and also the hypothesis of small angle of attack. Far from that situation the two models are very different from each other.
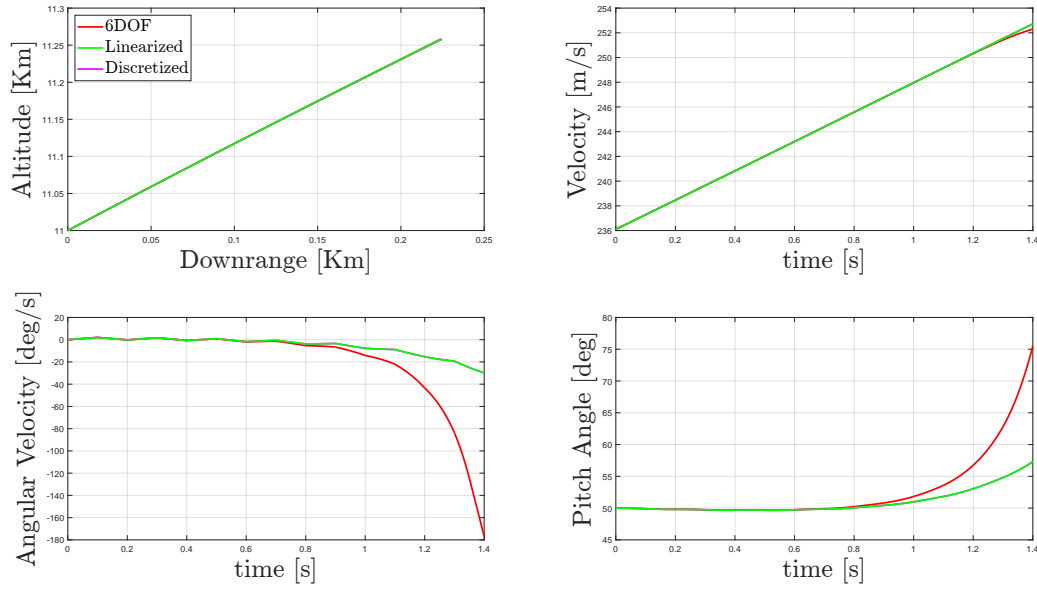
94

Figure 5.14: Dynamic Models comparison with Aerodynamics action active - test results

From this validations a few very important outcomes arise: The first is the validity of the models used so far, one of them has been taken from a book, while all the rest were being developed during this master thesis work. The other important result regards the precision of the linear system, if no normal aerodynamic force is applied (that is the case of second and third stage), this model should be updated every 10 seconds. Otherwise the instability effects of the lift constrains the update to be performed each second.

Chapter 6

Ascent Control Law

A rocket launcher is intrinsically unstable during the atmospheric flight, so it requires a very precise control law, this control is introduced in the form of the TVC already modeled in section 5.4. A first very simple control law here adopted is a Proportional-Derivative (PD), it gives quite good results despite the simplicity of the implementation so as a first guess is a good choice.

It is here highlighted that this control is in line with the preliminary multidisciplinary design here adopted to assess the air launched rocket feasibility. Moreover this might be the first guess for further refinements. Therefore the simplicity in this case is a good and wise choice.

In the last section of this chapter the Model Predictive Control approach is present. The MPC has been widely used in the oil and chemical industries since decades but is quite innovative in the space domain. The aim of this last part is to derive the control law of the MPC, and then test it using the linearized model derived in section 5.8.

6.1   PD Controller

One of the most easy control law, nevertheless widely used, is the PD. Multiplying an error and its derivative with two scalar values results in a very easy and reliable control law for the ascent trajectory. More often PID controllers are used than PD, in this work the integral action has been discarded mainly for simplicity and computational speed purposes. Nevertheless it is an enough good model to control the dynamics and follow the reference trajectory.

Given the fact that the reference trajectory has been computed using a 3DOF model with simplified atmospheric actions, the difference in velocity is expected to diverge with respect to a model with a more complex aerodynamic model. This means that the temporal evolution of the altitude and the downrange diverges with the reference. Therefore a geometric trajectory, in terms of altitude and downrange, is followed dropping all the time dependencies.

The control is given by the two TVC angles, where one affects the altitude and the other the cross-range. This means that two controllers would be required. For simplicity purposes, the same PD coefficients has been used for both angles

The error is therefore defined as the difference between the altitude with its reference for the β angle, and the cross-range with its reference for the δ angle. The reference altitude and cross-range are interpolated using the downrange value.

Since the lift contributes the most to the vehicle instability, a good choice is to add the TVC contribution that cancel out the moments introduced by the normal forces, those angles are defined β_0 and δ_0. In this way, if the launcher is on the right trajectory, it is placed in a control regime aimed at minimizing the angle of attack, that otherwise would induce instability effects. This is also done by the Pegasus rocket in one phase of its flight [7].

The control law is defined by equation (6.1).

$$\begin{cases} \beta = -K_p \left(\frac{h - h_{ref}}{h_{ref}} \right) - K_d \left(\frac{\dot{h} - \dot{h}_{ref}}{\dot{h}_{ref}} \right) + \beta_0 \\ \delta = -K_p \left(\frac{c - c_{ref}}{c_{ref}} \right) - K_d \left(\frac{\dot{c} - \dot{c}_{ref}}{\dot{c}_{ref}} \right) + \delta_0 \end{cases} \tag{6.1}$$

While the two 0-angles are shown in equation (6.2).

$$\begin{cases} \beta_0 = \arcsin \left(\frac{N_z l_{aero}}{T l_{TVC}} \right) \\ \delta_0 = \arcsin \left(\frac{N_y l_{aero}}{T l_{TVC}} \right) \end{cases} \tag{6.2}$$

The next question is how to compute the parameters K_p and K_d. First of all, it is worth mentioning that only one set of K_p and K_d is not enough to get a good tracking of the reference. For this reason the launch is divided into different temporal steps where each one has its own K_p and K_d. The number of steps per stage is arbitrary, a low number leads to a poor reference tracking, while an high number of steps provokes an issue similar to chattering. The number of steps adopted for each stage is shown in table 6.1.

One possible way to compute this set of K_p and K_d, is transforming the reference tracking constraint into a cost function, and optimize it. This procedure is very similar to what has been done in chapter 4 for the 3DOF rocket model. This time instead, a scalar cost function can not take into account a whole trajectory tracking. A cost function vector is then created considering the geometric error at the end of each time interval.
The error is considered the difference between the altitude and the reference at the same downrange plus the difference between cross-range and reference. The error definition can be seen in equation (6.3).

$$e_i = |h_{ref}(s_{end_i}) - h_{end_i}| + |c_{ref}(s_{end_i}) - c_{end_i}| \tag{6.3}$$

The cost function vector instead is shown in equation (6.4).

$$\underline{J}_{opt} = \begin{bmatrix} e_1 & e_2 & \dots & e_{nsteps} \end{bmatrix} \tag{6.4}$$

While the independent variable vector is shown in equation (6.5).

$$\underline{X}_{opt} = \begin{bmatrix} K_{p_1} & K_{d_1} & K_{p_2} & K_{d_2} & K_{p_3} & K_{d_3} & \dots & K_{p_n step} & K_{d_n step} \end{bmatrix} \tag{6.5}$$

This procedure is valid up to the second stage burnout, the third stage is discussed later on. The minimization is performed using a nonlinear least-square solver. The initial conditions vector has been placed as a zero vector due to the impossibility of inferring a good first guess. However in a few iterations the algorithm converges to a good result.

To account for the missing RCS of the third stage, the angular velocities has been forced to zero at the beginning of the burn, and the orientation of the rocket is imposed such that it is completely aligned with the velocity, therefore at 0 angle of attack. In a future work the RCS should be modeled and added to the control law.

After the second stage burnout there is a free coasting phase: during this part there is no control on the trajectory but only on the attitude. This means that a perfect tracking of this phase is possible only if the initial conditions on that phase are identically equal to the reference one. Since that condition is basically impossible, a full-tracking like the previous stages is not meaningful, therefore a new set of independent variables and errors is required.

As just explained, an altitude difference is unavoidable, but the only element that is worth following is the vertical velocity. Therefore only K_d has a particular meaning. The best way to achieve such a control, is to target the orbit insertion as precise as possible. Again, the final orbit constraints are switched to a cost function vector, shown in equation (6.6), and the same optimization algorithm has been used.

$$\underline{J}_{3rd} = \begin{bmatrix} (h_{end} - h_{orbit})/h_{orbit} & (\gamma_{end})/\pi & (V_{end} - V_{orbit})/V_{orbit} \end{bmatrix} \tag{6.6}$$

This time, the cost function vector is made by the final constraints in terms of altitude, flight path angle and velocity. A penalty is imposed also if the angular velocities overcome a certain threshold (5 deg/s). In the angular velocities are small, the RCS of the third stage or the CubeSat can simply get rid of it using thrusters or other RCS hardware, but it is desirable to be as low as possible. Table 6.1 shows the control strategy for each stage in each of the two launcher configuration, including the number of time interval considered.

Stage	Control Type	n of steps
1st I Configuration	PD	6
2nd I Configuration	PD	10
3rd I Configuration	D	10
1st II Configuration	PD	6
2nd II Configuration	PD	20
3rd II Configuration	D	10

Table 6.1: PD Control Strategy

6.2 MPC Controller

Model Predictive Control is an advanced method of process control that aims to compute a future control inputs to optimize the future behavior of the dynamic system. The optimization is performed over a finite time window called "horizon", furthermore its suitable for constrained systems since the optimization can be made thank to Quadratic Programming (QP) that can impose boundaries over inputs and outputs directly in the optimization process, this avoid finding nonphysical solutions [45].

Autonomy in a spacecraft or in a launch vehicle is always a big advantage. Nowadays, the vast majority of launches are carefully planned with large advance; the weather conditions, that are known only few hours before lift off, strongly constrain the launch window.
MPC is an online adaptive control strategy built onboard of the vehicle, this control law is able to react to any sudden change in weather conditions such as wind gusts. One of the challenges for having a real time adaptive control strategy onboard, is the computational time of the rocket model built inside the controller. This has to be precise and fast at the same time; this challenge has been addressed with the linearization procedure done in section 5.8 [44].
What MPC practically does, is computing the predicted output of a dynamic system as a function of the initial plant conditions, and the manipulated variables for each time step [46]. Then a cost function is defined that aims to the minimization of both the error between output and reference, and the control inputs themselves. If no constraints are imposed the optimal solution can be found analytically like a Linear Quadratic Regulator (LQR) process, otherwise using QP the constrained solution can be computed.
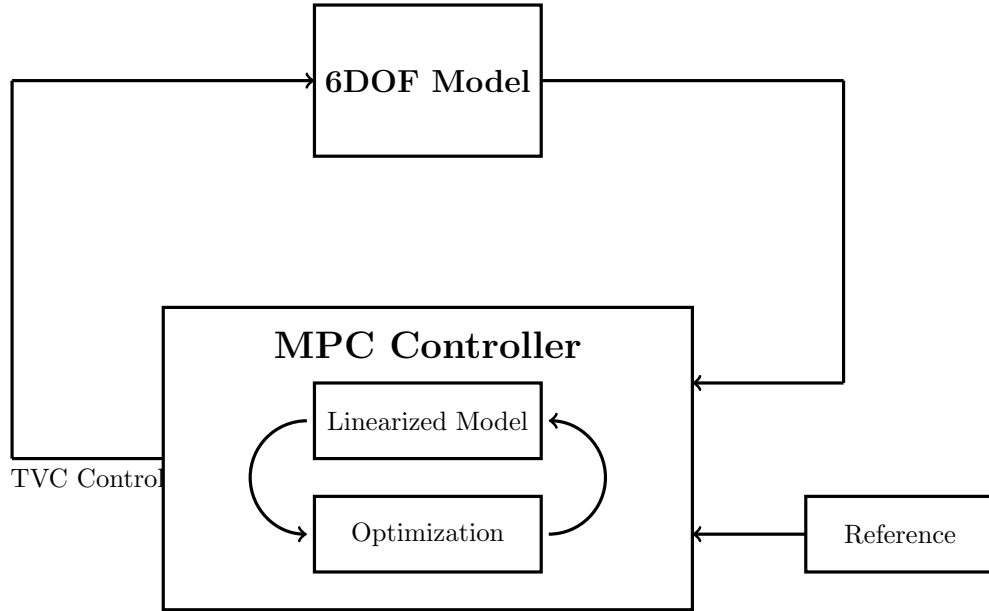
Figure 6.1: Model Predictive Control Scheme

Figure 6.1 shows the Model Predictive Control scheme. The rocket dynamic is integrated using the most complete model derived so far, the 6DOF.

The state coming out from that integration is used in two different ways: first it is needed to update the linear model inside the controller, and most importantly, it is necessary to compute the error between the current state and the reference. The reference is computed using the 3DOF model explained in chapter 4.

Inside the controller, the linear model provides the future predictions at each time step, those are needed by the optimization to compute the future control actions such that the error between predictions and reference is minimized.

Once the optimized control actions are computed, their contribution at the first time step is extracted and used as TVC control in the 6DOF dynamic. After that the entire procedure is iterated again.

The paragraph shows how the MPC controller is modeled and discuss about the results and possible future development [45].

The 6 degrees of freedom rocket dynamics has been linearized and discretized in section 5.8, this procedure starts with the discrete state space model shown in equation (5.54).

The first step is defining the difference between two intervals of the state and the input. Since the disturbance d is basically constant it cancels out from the model and it is useful only to update the current state.

$$\begin{cases} \Delta X_d(k) = X_d(k) - X_d(k-1) \\ \Delta u(k) = u(k) - u(k-1) \end{cases} \tag{6.7}$$

Then, it is possible to create an augmented system.

$$X(k) = \begin{bmatrix} \Delta X_d(k) \\ y(k) \end{bmatrix} \tag{6.8}$$

And therefore its corresponding state space model.

$$\begin{cases} X(k+1) = \mathbf{A}X(k) + \mathbf{B}u(k) \\ y(k) = \mathbf{C}X(k) \end{cases} \tag{6.9}$$

Where the Matrices are found in the following way:

$$\mathbf{A} = \begin{bmatrix} \mathbf{A}_d & \mathbf{0} \\ \mathbf{C}_d\mathbf{A}_d & \mathbf{I} \end{bmatrix} \tag{6.10}$$

$$\mathbf{B} = \begin{bmatrix} \mathbf{B}_d \\ \mathbf{C}_d\mathbf{B}_d \end{bmatrix} \tag{6.11}$$

$$\mathbf{C} = \begin{bmatrix} \mathbf{0} & \mathbf{I} \end{bmatrix} \tag{6.12}$$

Now, let's define a couple of further matrices.

$$\Delta U = \begin{bmatrix} \Delta u(k_1)^T & \Delta u(k_1+1)^T & \dots & \Delta u(k_1+N_c-1)^T \end{bmatrix}^T \tag{6.13}$$

$$\mathbf{Y} = \begin{bmatrix} y(k_1+1 \mid k_1)^T & y(k_1+2 \mid k_1)^T & \dots & y(k_1+N_p \mid k_1)^T \end{bmatrix}^T \tag{6.14}$$

Where N_c and N_p are respectively the controlled horizon and the prediction horizon, and the latter is always grater or equal than the former. The prediction horizon represent the number of time steps over which the dynamic is integrated and compared to the reference. The controlled horizon instead means the number of time steps where the control is applied.
The vertical bar in the second matrix means that the output is computed using the information at the sample k1.

Without reporting all the passages, it is possible to get a link between those two matrices and the initial sample of the state vector.

$$\mathbf{Y} = \mathbf{F}X(k_1) + \mathbf{\Phi}\Delta U \tag{6.15}$$

101

Where the $\mathbf{F}$ and $\boldsymbol{\Phi}$ are defined as follows:

$$\mathbf{F} = \begin{bmatrix} \mathbf{CA} \\ \mathbf{CA^2} \\ \mathbf{CA^3} \\ \vdots \\ \mathbf{CA^{N_p}} \end{bmatrix} \tag{6.16}$$

$$\boldsymbol{\Phi} = \begin{bmatrix} \mathbf{CB} & \mathbf{0} & \mathbf{0} & \ldots & \mathbf{0} \\ \mathbf{CAB} & \mathbf{CB} & \mathbf{0} & \ldots & \mathbf{0} \\ \mathbf{CA^2B} & \mathbf{CAB} & \mathbf{CB} & \ldots & \mathbf{0} \\ \vdots & \vdots & \vdots & \vdots & \vdots \\ \mathbf{CA}^{N_p-1}\mathbf{B} & \mathbf{CA}^{N_p-2}\mathbf{B} & \mathbf{CA}^{N_p-3}\mathbf{B} & \ldots & \mathbf{CA}^{N_p-N_c}\mathbf{B} \end{bmatrix} \tag{6.17}$$

The reference to be followed can be modeled as:

$$\mathbf{R}_s = \begin{bmatrix} 1 & 1 & 1 & \ldots & 1 \end{bmatrix} r(k_1) = \bar{\mathbf{R}}_s r(k_1) \tag{6.18}$$

Where $r(k_1)$ is the reference vector at the sample k_1.

Finally the cost function can be set.

$$J = (\bar{\mathbf{R}}_s - \mathbf{Y})^T (\bar{\mathbf{R}}_s - \mathbf{Y}) + \Delta U^T \mathbf{R}_u \Delta U \tag{6.19}$$

$\mathbf{R}_u$ is simply an identity matrix multiplied by a certain factor where the greater is the more important is getting a small control values for the optimization process.
If no constraints over the control inputs are applied, the optimal control can be computed in the following way.

$$\Delta U = \left(\boldsymbol{\Phi}^T \boldsymbol{\Phi} + \mathbf{R}_u\right)^{-1} \left(\boldsymbol{\Phi}^T \bar{\mathbf{R}}_s r(k_1) - \boldsymbol{\Phi}^T \mathbf{F} X(k_1)\right) \tag{6.20}$$

The first 3 elements of that vector represent the difference in control to be applied at the sample k_1, then the linear system is integrated to get the state vector $X(k_1 + 1)$ and its corresponding reference $r(k_1 + 1)$, so the procedure can be iterated.
Alternatively, if maximum and minimum TVC are imposed, the control law can be derived using quadratic programming theory.

6.3   Results

First, let's take a look at the results coming out from PD controller. Figures 6.2,6.3,6.4 show the integration results of the first launcher configuration, while figures 6.5,6.6,6.7 show the second. The

two configurations are computed and discussed in chapter 2.

The dots represent the points at which the trajectory is divided as explained in section 6.1. Table 6.2 shows the final orbit results of both configurations compared with the reference, this proves the feasibility of this kind of controller despite being very easy to implement. In the second configuration more than the first, the error due to a not perfect alignment during the coasting phase can be noticed as expressed in section 6.1. Despite this error, the altitude precision is in the order of 20 km, in line with the accuracy of an upper solid stage.

Configuration	Altitude	Flight Path Angle	Velocity
Units	Km	deg	Km/s
Reference	500	0	7.67
I Configuration	496	0.2	7.99
II Configuration	522	-0.8	8.14

Table 6.2: Final PD Control Result

Regarding the MPC, a first test has been performed in order to ensure the validity of the controller. The test wants the rocket to follow a linear trajectory with constant altitude imposed at 11 Km. Maximum TVC has been imposed to 7 degrees, time step to 0.1 seconds, and prediction horizon and control horizon has been fixed respectively at 20 and 10.

The results can be seen in figures 6.8,6.9,6.10.

As can be noticed, the β angle has some sort of random behavior and then it starts oscillating from the maximum to the minimum. Therefore the attitude of the rocket is uncontrolled making more and more rotations.

Those test must be intended for a preliminary assessment of the MPC algorithm explained in section 6.2. From the first simulations just shown, the need of a further investigation arises. Section 6.3.1 reports all the possible issues that may lead to the uncontrolled behavior of the launcher. Therefore, a future work on this topic must take those considerations well into account.
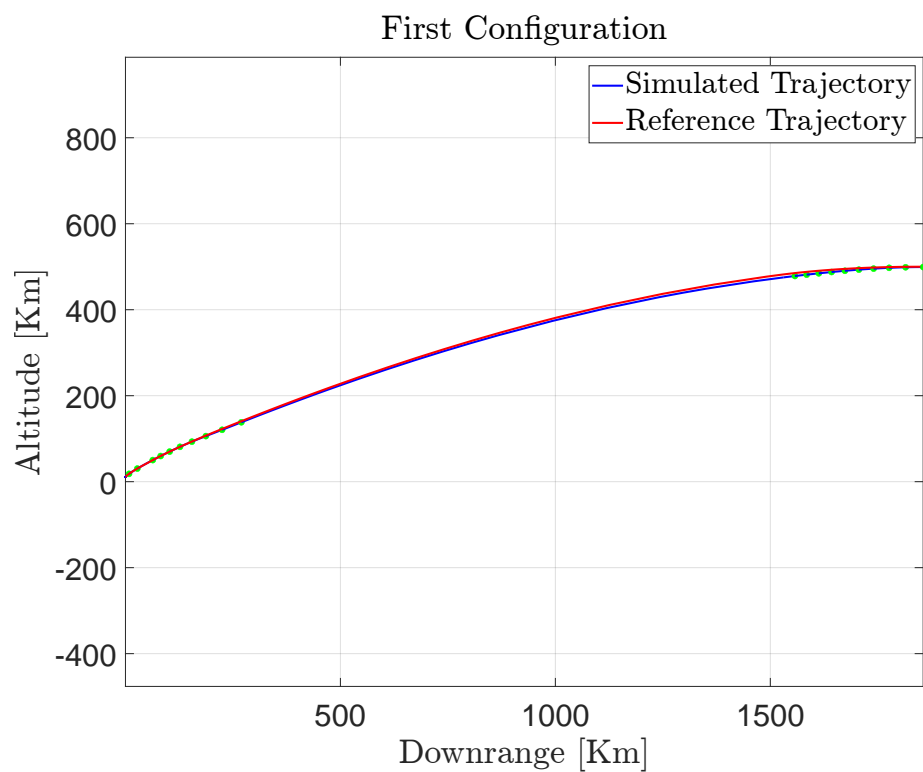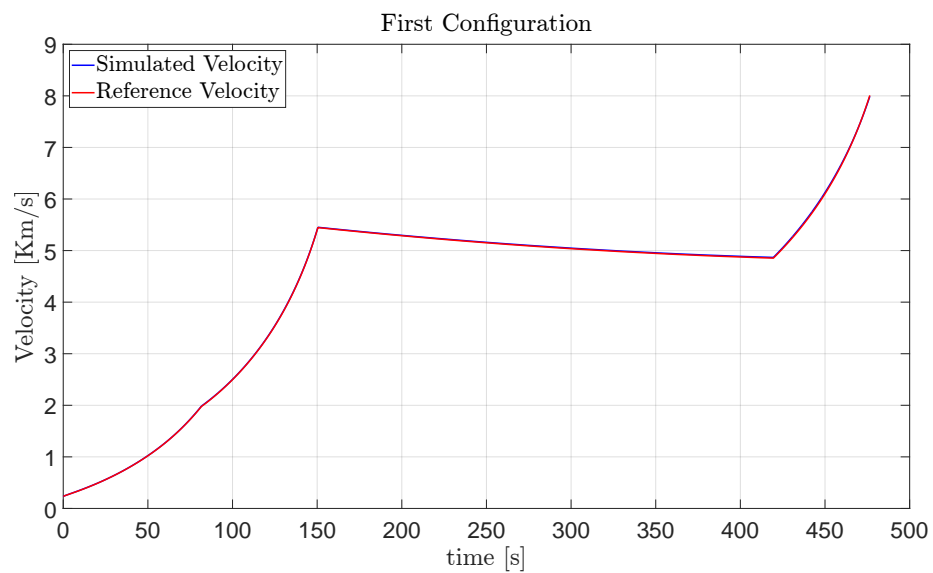
Figure 6.2: First Configuration Trajectory

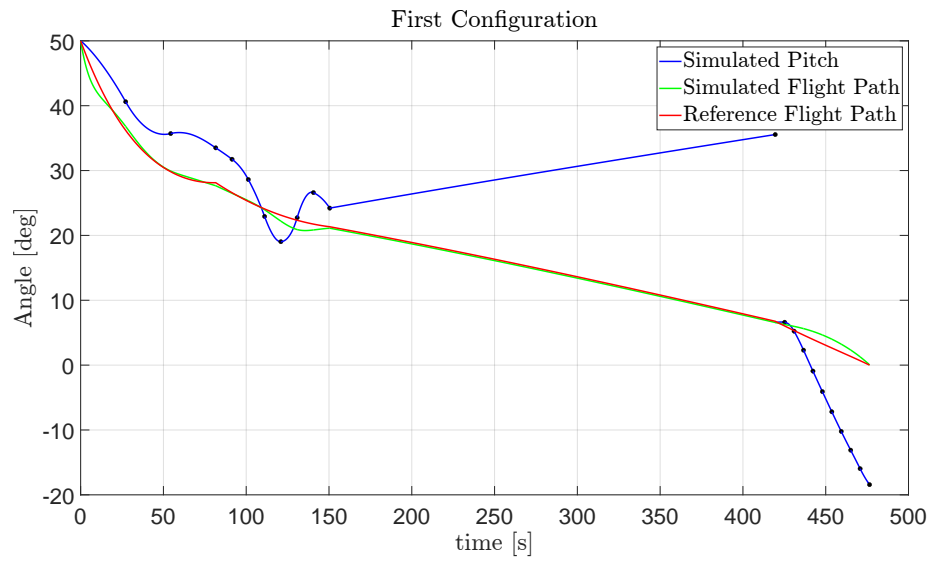Figure 6.3: First Configuration Velocity

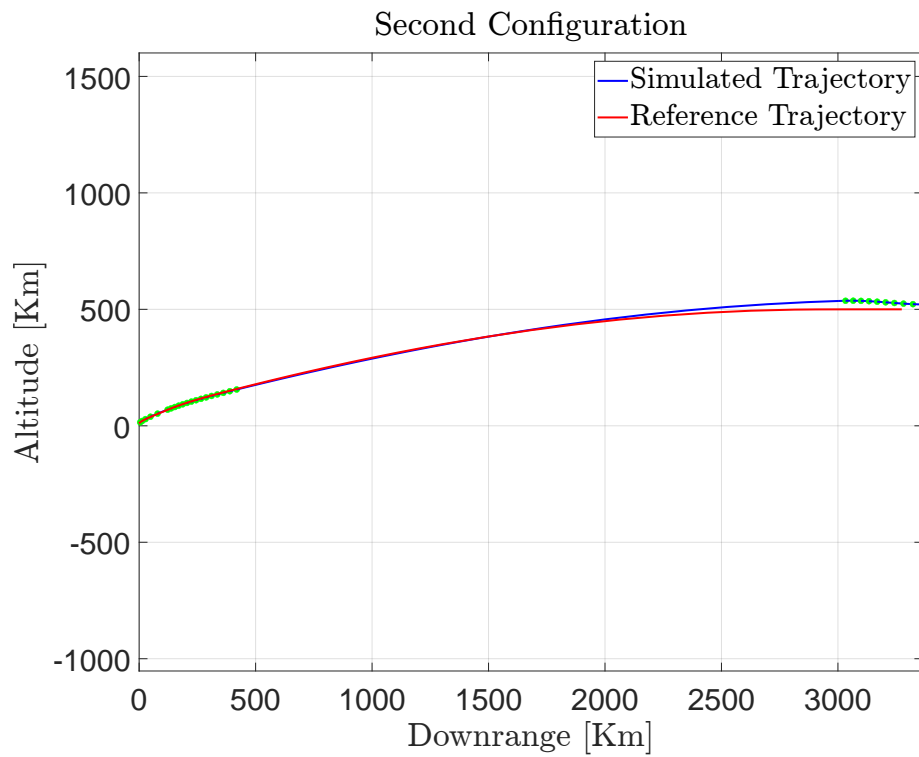Figure 6.4: First Configuration Angles

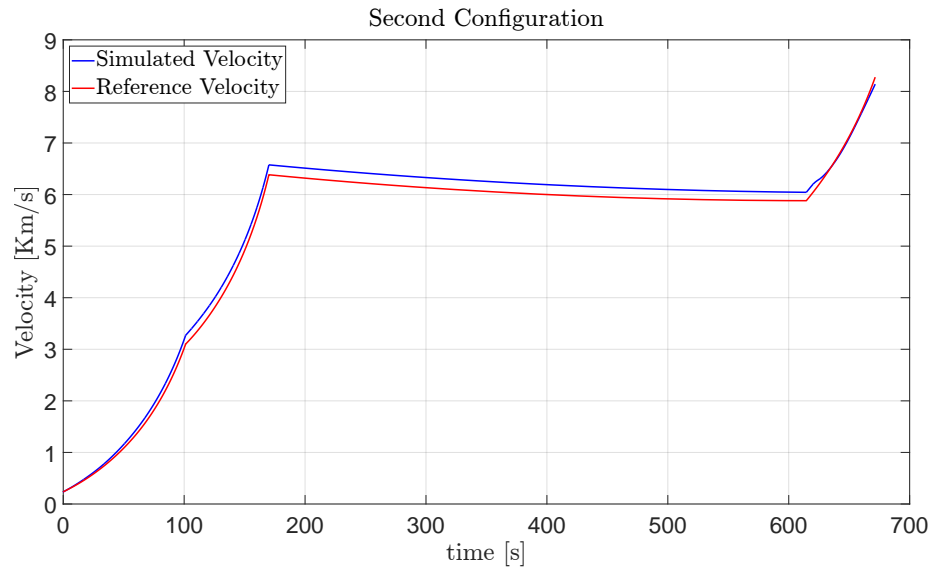## Second Configuration

Figure 6.5: Second Configuration Trajectory

Figure 6.6: Second Configuration Velocity
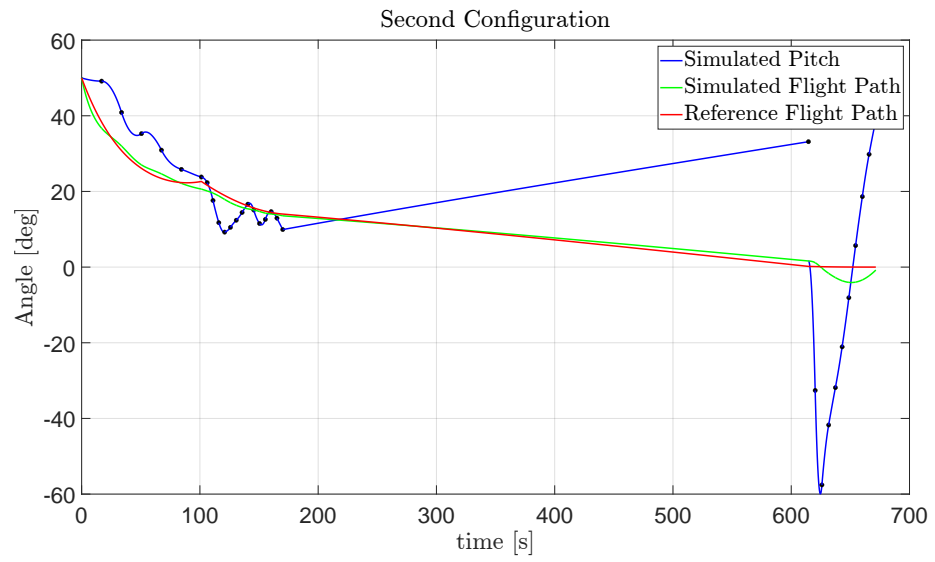
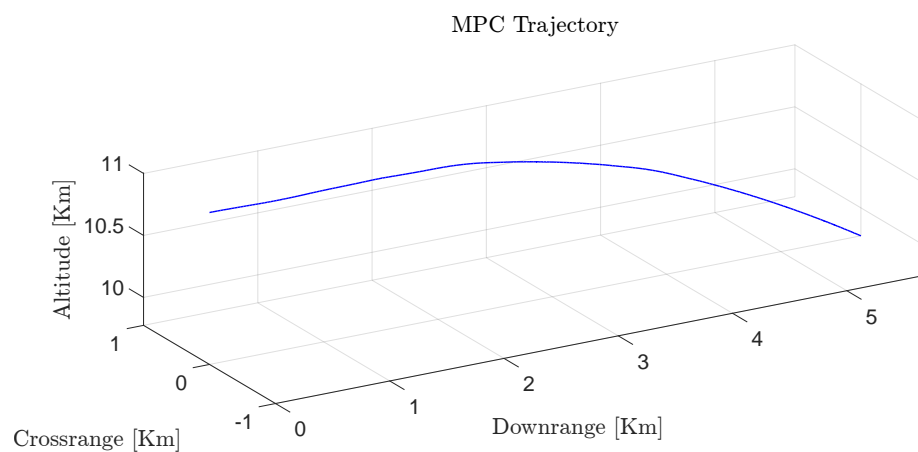Figure 6.7: Second Configuration Angles

106

MPC Trajectory

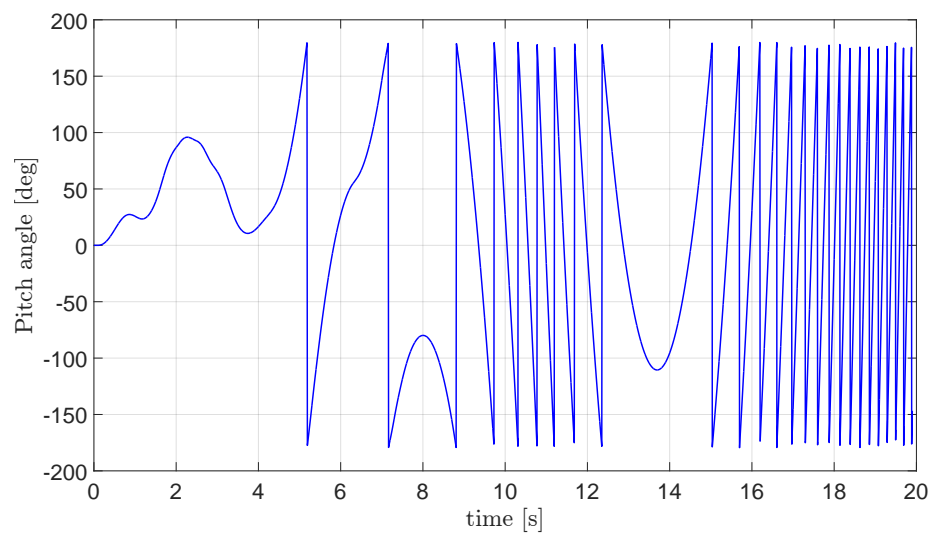Figure 6.8: MPC Test Trajectory
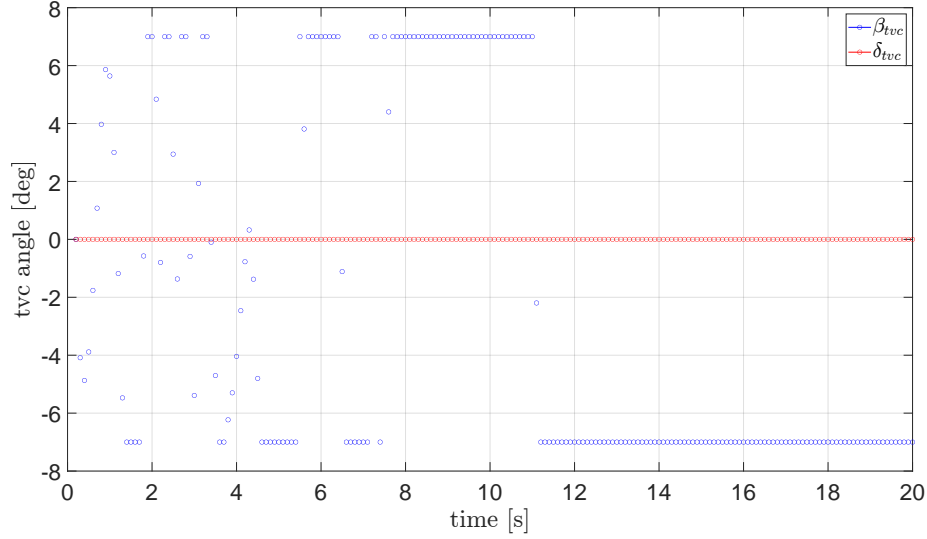

Figure 6.9: MPC Test Pitch

Figure 6.10: MPC Test TVC

6.3.1 Possible MPC Issues

The MPC still needs further investigations to become an applicable solution. The possible reasons could be the followings.

First, the continuous matrix $\mathbf{A}_c$ is singular, so there are problems in inverting the matrix during the solution and avoid the possibility of using other kind of laws such as LQR. The passage between continuous and discrete system makes the A matrix no more singular but it remains highly ill-conditioned.

Another possible problem regards the non controllability (yet observable) of the continuous dynamic system, a possible solution is a change of coordinates from cartesian to another type, maybe even reducing the number of degrees of freedom.

One final problem is the value of the Euler angles that must stay below certain threshold due to the hypothesis of small angles, the only way found so far is to put those angles as output values and limit them using QP. In this case not only the outputs are increasing, but moreover a reference value for those angles must be found that is not trivial since the standard reference comes from a simplified model without attitude. Furthermore in order to introduce boundaries of outputs a more complex procedure must be followed, and this lies beyond the purpose of this master thesis. Another possibility could be to give reference also from the attitude point of view and not only the trajectory, the reference could come from the usage of the PD controller just explained. In any case, there is plenty of work still to be done.

6.4   Main Budgets

The final budgets in terms of mass can be seen in table 6.3. What can be noticed is that the second configuration has almost twice the mass of the first one. This is not surprising because also the payload is doubled. However, thanks to the multiconfiguration staging process, those two payloads very different from each other, are being launched by the same 4 solid rocket motors, just used in different configurations.

Masses	$M_{payload}$	M_p	M_s	M_0	$M_0 + 20\%$margin
Units	Kg	Kg	Kg	Kg	Kg
I Configuration	10.6	531	51.3	593	711
II Configuration	20.1	963	90.2	1073	1288

Table 6.3: Final Launcher Budget

Another very interesting outcome, is shown in table 6.4. As explained, the staging design does not account for any kind of losses, therefore a big margin over the ΔV must be imposed. The simple 3DOF rocket model accounts only for few losses, so the final velocities are lower. Finally the 6DOF is the most accurate one among the ones developed in this master thesis, this means that the final velocity is the closest to the real one.

Velocities	$V_{orbital}$	ΔVMargin	$V_{staging}$	V_{3dof}	V_{6dof}
Units	Km/s	-	Km/s	Km/s	Km/s
I Configuration	7.166	1.22	9.292	8.009	7.991
II Configuration	7.166	1.22	9.292	8.276	8.143

Table 6.4: Final Velocity Budget

Chapter 7

Conclusions

During this work, a first iteration of an air to orbit launch vehicle design has been performed. This study has been done according to the Multidisciplinary approach explained in section 1.3. The outcome is the sizing of the system with a breakdown of masses that proves the feasibility of this concept. This output might be assumed as a starting point for further refinements in light of a potential small launcher implementation.

Despite having used simple models, the launcher has been designed from every meaningful point of view, from the propulsion hardware to the guidance control law, passing by the launch location and the re-entry effects. Through this design process the help given by the multidisciplinary approach has been very effective in building the design process shown in figure 1.5.
The multiconfiguration staging explained in chapter 2, has been proven to be very effective in increasing the payload range without a correspondingly increase in the costs. The next step is to go on with the same approach but using models much more refined capable of considering all the different losses.

Regarding the propulsion architecture, solid rocket motor technology has proved its effectiveness in terms of both reliability, simplicity and costs; therefore it is the perfect candidate to start a more detailed implementation. The hybrid rocket engine of the third stage is very interesting, the only major drawbacks of this solution is probably the low TRL of the technology. Future works should assess the validity of this solution computing the advantages in a more quantitative way.

The work on the launch zones was very effective as well, it provided 5 candidates based on safety and proximity of Italian airports. Further work must be able to estimate better both the falling ranges, and the threat given by the dead rocket bodies. Moreover, political agreement must be made concerning the deployment and flight of rockets above foreign territories.

A complete 6DOF has been implemented to further demonstrate the validity of design done in the previous chapters. Moreover, a very interesting linearization process has been performed and then verified with respect to other models. The full model has been used together with a simple PD control law implemented just for this purpose.

Finally, a Model Predictive Control law has been derived to implement an onboard controller capable of autonomously guiding the launch vehicle on its way to orbit. A preliminary test analysis on the algorithm has been done resulting in a few issues, which are discussed in details in section 6.3.1.

However, a first step towards the implementation of an embedded MPC controller has been done. The linear model has been derived and verified (5.8), the MPC algorithm has been modeled and tested (6.2), and finally some consideration regarding the results obtained have been pointed out in section 6.3.1.

7.1 Further Work

Despite having designed a small air launcher rocket from many points of view, there are still several open points to be addressed in a future work.

1. The missing RCS system and all the avionics in general.

2. A cost analysis to assess the position of this vehicle in the launch market, and to infer how many launch can be expected each year. This analysis can be a first step towards the industrial implementation point of view.

3. A global refinement of all the models used in the 6DOF rocket model, to improve the simulation results.

4. The addition of disturbances such as wind gusts, in this way the MPC controller can also prove its effectiveness.

5. All the interfaces between the launch vehicle and the carrier aircraft must be considered.

6. Proceed with the design of the HRE upper stage.

7. Assess the feasibility of the MPC controller, and proceed with the preliminary work done in this master thesis.

Bibliography

[1] Nanosat database https://www.nanosats.eu/.

[2] Janovsky R. Koelle D. E. *Development and transportation costs of space launch systems.* DGLR/CEAS European Air and Space Conference.

[3] Fleeman E. L. *Tactical Missile Design.* AIAA, 2006.

[4] Eurofighter https://www.eurofighter.com/the-aircraft.

[5] Sforza P. M. *Manned Spacecraft Design Principles.* University of Florida, 2016.

[6] Virgin Orbit. *LauncheOne Service Guide.* Launcher Manual.

[7] Orbital ATK. *Pegasus User's Guide Review.* Launcher Manual.

[8] Sutton P. G. *Rocket Propulsion Elements.* Wiley, 2010.

[9] Avio propulsion system https://www.avio.com/propulsion-system.

[10] ArianeSpace. *VEGA Payload User's Guide Version.* Launcher Manual.

[11] Nasa spaceflight https://www.nasaspaceflight.com/.

[12] Virgin orbit launcherone https://virginorbit.com/technology/.

[13] Nasa vcls https://www.nasa.gov/press-release/nasa-awards-venture-class-launch-services-contracts-for-cubesat-satellites.

[14] Firefly Aerospace. *Alpha Payload User's Guide Version 2.0.* Launcher Manual.

[15] RocketLab. *Electron Payload User's Guide Version 6.4.* Launcher Manual.

[16] Kroo I. M. Braun R. D., Moore A. A. *Collaborative Approach to Launch Vehicle Design.* Journal of Spacecraft and Rockets, 1997.

[17] Dépincé P. Chriette A. Balesdent M., Bérend N. *A survey of multidisciplinary design optimization methods in launch vehicle design.* Springer, 2011.

[18] Haftka R. T. Sobieszczanski-Sobieski J. *Multidisciplinary aerospace design optimization - Survey of recent developments.* AIAA 34th Aerospace Sciences Meeting and Exhibit, 1996.

[19] Castellini F. *Multidisciplinary Design Optimization for Expendable Launch Vehicles.* Ph.D. Thesis Politecnico di Milano, 2012.

[20] Vallado D. A. *Fundamentals of Astrodynamics and Applications.* Springer, 2007.

[21] ISIS Space. *CubeSats Deployer Brochure.* ISIS Space.

[22] Ruag https://www.ruag.com/en/products-services/space/launchers/launchers.

[23] Sarigul-Klijn M. Sarigul-Klijn N. *Air Launching Eart-to-Orbit Vehicles: Delta V gains from Launch Conditions and Vehicle Aerodynamics.* AIAA.

[24] Esa clean space $https://www.esa.int/safety_security/clean_space/green_technologies$.

[25] International Launch Services. *Proton Launch System Mission Planner's Guide.* Launcher Manual.

[26] Calabro M. Wingborg N. *Green Solid Propellant for Launchers.* Grail H2020.

[27] Gordon S. McBride B. J. *Computer Program for Calculation of Complex Chemical Equilibrium Compositions and Applications.* NASA Lewis Research Center, 1996.

[28] Leary J. P. Landsbaum E. M., Salinas M. P. *Specific Impulse Prediction of Solid-Propellant Motors.* The Aerospace Corporation, El Segundo, Calif., 2012.

[29] Humble R. W. *Space Propulsion Analysis and Design.* McGraw-Hill, 1995.

[30] Lee J. Rhee I., Lee C. *Optimal design for hybrid rocket engine for air launch vehicle.* Journal of Mechanical Science and Technology 22, 2008.

[31] Vieira R. de Souza Costa F. *Preliminary Analysis of Hybrid Rockets for Launching Nanosats into LEO.* Journal of the Brazilian Society of Mechanics, Science and Engineering, 2010.

[32] Cantwell B. Stevens J. Karabeyoglu A., Falconer T. *Design of an Orbital Hybrid Rocket Vehicle Launched from Canberra Air Platform.* 41st AIAA/ASME/SAE/ASEE Joint Propulsion Conference and Exhibit, 2005.

[33] Byun Y. Lee J., Noh K. *Preliminary Design of the Hybrid Air-launching Rocket for Nanosat.* Fifth International Conference on Computational Science and Applications, 2007.

[34] Mullens P. Ventura M. *The use of hydrogen peroxide for propulsion and power.* 35th AIAA/ASME/SAE/ASEE Joint Propulsion Conference and Exhibit, 1999.

[35] Krishnan S. George P. *Fuel Regression rate enhancement studies in HTPB/GOx Hybrid Rocket Motors.* AIAA, 1998.

[36] Waite M. J. Hertzelle W. S. *Design of a small H2O2/HTPB hybrid sounding rocket motor.* AIAA, 1996.

[37] Massimo P. Bisin R. Galfetti L. Paravan C., Lisi F. *Burning Behavior Investigation of a Vortex Flow Pancake Hybrid Rocket Engine.* AIAA Propulsion and Energy 2019 Forum, 2019.

[38] Hopkins Jr. J. P. Isakowitz S. J., Hopkins J. B. *International Reference Guide To Space Launch Systems.* AIAA.

[39] NASA. *Aerothermodynamic Course.* JPL TFAWS, 2019.

[40] Bourbigot S. Tranchard P. *High Temperature-Dependent Thermal Properties of a Carbon-Fiber Epoxy Composite.* University of Lille, Unité Matériaux et Transformation, 2017.

[41] Jablonski A. M. *Deorbiting of microsatellites in Low Earth Orbit (LEO).* Defence R and D Canada Ottawa, 2008.

[42] Crassidis J. L. Markley F. L. *Fundamentals of Spacecraft Attitude Determination and Control.* Springer, 2014.

[43] Abd El Rhman O. Dorrah H. T. Fawzy M., Aboelela M. A. S. *Design of Missile Control System Using Model Predictive Control.* The Online Journal on Computer Science and Information Technology (OJCSIT).

[44] Bemporad A. Pascucci C. A., Bennani S. *Model Predictive Control for Powered Descent Guidance and Control.* 2015 European Control Conference (ECC).

[45] Wang L. *Model Predictive Control System Design and Implementation using Matlab.* Springer, 2008.

[46] Diehl M. M. Rawlings J. B., Mayne D. Q. *Model Predictive Control: Theory, Computation, and Design.* Nob Hill Publishing, 2019.

Appendix A

Appendix

Equation (A.1) shows all the elements needed to compute the linear matrices for the state space reported in section 6.2.

$$
\begin{cases}
A_{\alpha x1} = N_{z0}\cos\theta\sin\psi + N_{y0}\sin\theta \\
A_{\alpha y1} = N_{z0}\cos\theta\cos\psi + N_{z/\alpha}\sin\theta - (T-D0)\sin\theta \\
A_{\alpha z1} = -N_{y0}\cos\theta\cos\psi - N_{y/\alpha}\cos\theta\sin\psi - (T-D0)\cos\theta\sin\psi \\
A_{\alpha x2} = -N_{z0}\cos\phi\cos\psi - N_{y0}\sin\phi\cos\theta + N_{z0}\sin\phi\sin\theta\sin\psi \\
A_{\alpha y2} = -N_{z/\alpha}\sin\phi\cos\theta + (T-D0)\sin\phi\cos\theta + N_{z0}\cos\phi\sin\psi + N_{z0}\sin\phi\sin\theta\cos\psi \\
A_{\alpha z2} = N_{y/\alpha}\cos\phi\cos\psi + (T-D0)\cos\phi\cos\psi - N_{y0}\cos\phi\sin\psi - N_{y0}\sin\phi\sin\theta\cos\psi + \\
\quad -N_{y/\alpha}\sin\phi\sin\theta\sin\psi - (T-D0)\sin\phi\sin\theta\sin\psi \\
A_{\alpha x3} = N_{y0}\cos\phi\cos\psi - N_{z0}\sin\phi\cos\psi - N_{z0}\cos\phi\sin\theta\sin\psi \\
A_{\alpha y3} = N_{z/\alpha}\cos\phi\cos\psi - (T-D0)\cos\phi\cos\psi + Nz0\sin\phi\sin\psi - N_{z0}\cos\phi\sin\theta\cos\psi \\
A_{\alpha z3} = N_{y/\alpha}\sin\phi\cos\psi + (T-D0)\sin\phi\cos\psi - N_{y0}\sin\phi\sin\psi + N_{z0}\cos\phi\sin\theta\cos\psi + \\
\quad +N_{y/\alpha}\cos\phi\sin\theta\sin\psi + (T-D0)\cos\phi\sin\theta\sin\psi \\
B_{\delta 1} = -T\cos\theta\cos\psi\alpha_z - T\cos\theta\sin\psi + T\sin\theta\alpha_x \\
B_{\beta 1} = T\cos\theta\cos\psi\alpha_y + T\cos\theta\sin\psi\alpha_x + T\sin\theta \\
B_{c1} = (T-D0)\cos\theta\cos\psi - N_{y0}\cos\theta\sin\psi + N_{z0}\sin\theta + mg_1 \\
B_{\delta 2} = T\cos\phi\cos\psi - T\sin\phi\cos\theta\alpha_x - T\cos\phi\sin\psi\alpha_z - T\sin\phi\sin\theta\cos\psi\alpha_z - T\sin\phi\sin\theta\sin\psi \\
B_{\beta 2} = -T\cos\phi\cos\psi\alpha_x - T\sin\phi\cos\theta + T\cos\phi\sin\psi\alpha_y + T\sin\phi\sin\theta\cos\psi\alpha_y + T\sin\phi\sin\theta\sin\psi\alpha_x \\
B_{c2} = N_{y0}\cos\phi\cos\psi - N_{z0}\sin\phi\cos\theta + (T-D0)\cos\phi\sin\psi + (T-D0)\sin\phi\sin\theta\cos\psi + \\
\quad -N_{y0}\sin\phi\sin\theta\sin\psi + mg_2 \\
B_{\delta 3} = T\cos\phi\cos\psi\alpha_x + T\sin\phi\cos\psi - T\sin\phi\sin\psi\alpha_z + T\cos\phi\sin\theta\cos\psi\alpha_z + T\cos\phi\sin\theta\sin\psi \\
B_{\beta 3} = T\cos\phi\cos\psi - T\sin\phi\cos\psi\alpha_x + T\sin\phi\sin\psi\alpha_y - T\cos\phi\sin\theta\cos\psi\alpha_y - T\cos\phi\sin\theta\sin\psi\alpha_x \\
B_{c3} = N_{z0}\cos\phi\cos\psi + N_{y0}\sin\phi\cos\psi + (T-D0)\sin\phi\sin\psi - (T-D0)\cos\phi\sin\theta\cos\psi + \\
\quad +N_{y0}\cos\phi\sin\theta\sin\psi + mg_3
\end{cases}
$$

$$(A.1)$$

Where g_1, g_2 and g_3 are the 3 component of the gravity force computed at each interval.

Figure A.1 shows the effect of tail wings on the ascent control given by the thrust vector control. As expected they provide a stabilizing effect reducing the amount of control needed, moreover it can be noticed that the difference between the control using wings with the one without, decreases with time. This is fully expected since the rocket is gaining altitude, consequently the air density is decreasing which means a lower aerodynamic effect of wings.
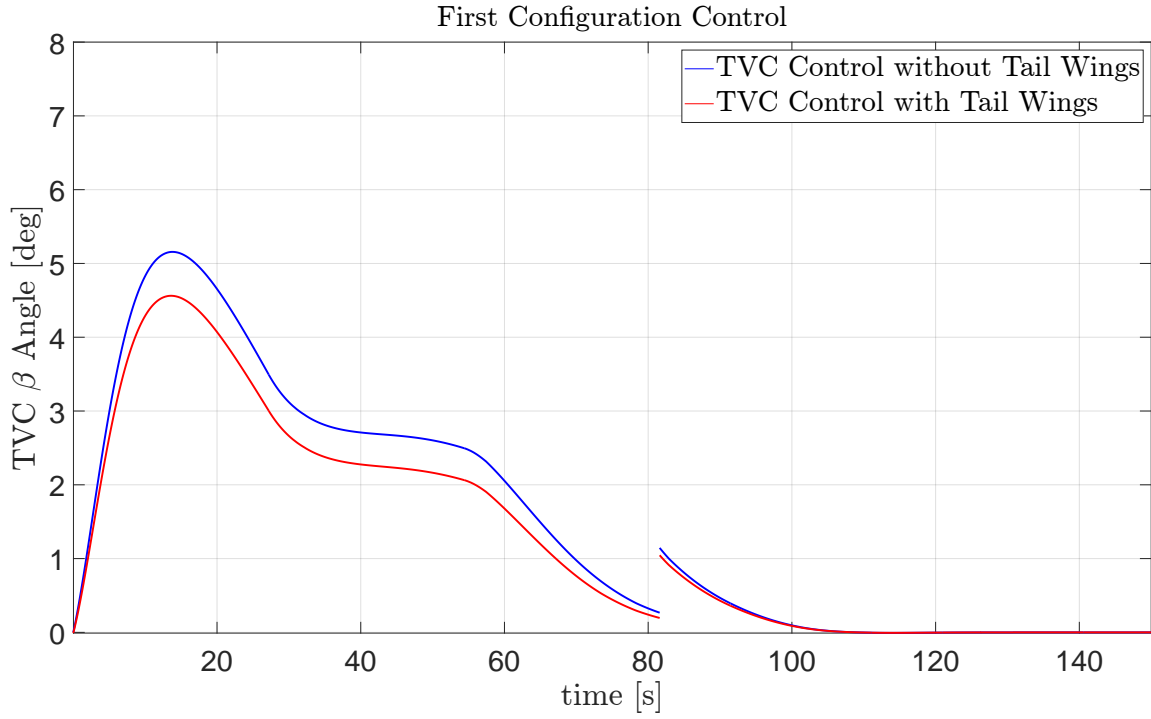

Figure A.1: Wings effects on control